AUTOMATIC RECOGNITION AND DEMODULATION OF DIGITALLY

MODULATED COMMUNICATIONS SIGNALS USING WAVELET-DOMAIN

SIGNATURES

by

KA MUN HO

A Dissertation submitted to the

Graduate School-New Brunswick

Rutgers, The State University of New Jersey

in partial fulfillment of the requirements

for the degree of

Doctor of Philosophy

Graduate Program in Electrical and Computer Engineering

written under the direction of

Professor David G. Daut

and approved by

_____

_____

_____

_____

_____

New Brunswick, New Jersey

January, 2010

ABSTRACT OF THE DISSERTATION

Automatic Recognition and Demodulation of Digitally Modulated Communications

Signals Using Wavelet-Domain Signatures

By KA MUN HO

Dissertation Director:
Professor David G. Daut

Abstract – Wavelet transform-based methodologies for both Automatic Modulation Recognition (AMR) and Demodulation of digitally modulated communications signals can be utilized in an enabling platform for the implementation of a new class of communications systems. In particular, such techniques could enable the development of agile radio transceivers for use in both commercial and military applications. Such radio transceivers would have the ability to transmit and receive signals using many different modulation schemes while employing a common receiver architecture based on a single demodulator.

In this dissertation, the development of AMR and Demodulation techniques are based on the relatively new mathematical theory of Wavelet Transforms (WTs). Information-bearing signals acquired by communications receivers are transformed into the wavelet-domain using the Continuous Wavelet Transform (CWT) and then applied to signal processing algorithms that also use the CWT in conjunction with pattern recognition techniques. In particular, the method of template-matching is used for both the AMR and Demodulation processes. Signal templates characterizing various modulated signals are

used for both processes. The signal templates are determined based on the signal features present in the fractal patterns of their corresponding scalograms for specific modulation schemes as they appear in the wavelet-domain. The algorithms developed in this work are capable of both classifying the method of modulation used in the acquired signal, as well as subsequently automatically demodulating the signal to recover the message.

The classes of digitally modulated signals considered in this work include variants of the Amplitude-, Frequency-, Phase-Shift Keying modulation families, i.e., ASK, FSK, and PSK, respectively, and multiple-level Quadrature Amplitude Modulation (M-ary QAM) families. The AMR and Demodulation performances are evaluated in the presence of Additive White Gaussian Noise (AWGN) over a wide range of Signal-to-Noise Ratio (SNR) values. Through extensive Monte Carlo computer simulations it is determined that the average correct classification rates using wavelet-based AMR for PSK, ASK, and QAM are over 98%, and over 90% for FSK signals, all at an SNR of 0 dB. The Bit Error Rate (BER) performance obtained using wavelet-based Demodulation is at least one order of magnitude better than the matched filter-based BER performance realized for the modulation schemes considered.

Acknowledgement

First, I would like to express my gratitude to my advisor Professor David G. Daut for his guidance and support throughout my Ph.D. studies at Rutgers, the State University of New Jersey. I have benefited from his knowledge and technical insight on digital communications. Most importantly, I have adapted my research skills, and style on technical presentation and writing technical documents from Prof. Daut.

I would like to express my gratitude to my Ph.D. committee members, Prof. Zoran Gajic, Prof. Sophocles Orfanidis, and Prof. Lawrence Rabiner. I would also like to thank Prof. Anant Madabushi for serving as the dissertation external committee member. Also, I have to thank Prof. Sigrid R. McAfee for her guidance on pursuing a Ph.D. degree in Electrical Engineering, and the way of solving engineering problems during my early years in graduate school.

I would like to extend my thanks to my colleague, Mr. Canute Vaz, for his helpful technical discussions on different topics in Electrical Engineering. I would also like to thank all of my friends for their accompaniment and providing me for the much needed distractions outside work.

Finally, I would like to thank my mother for her encouragement, love and friendship. She has made many sacrifices so as to provide me with the best education in the United States.

Dedication

To my mother

Table of Contents

Lists of Tables

List of Illustrations

Chapter 1

Introduction

A distinctive trend in the development of communications systems, for use in both commercial and military applications, is that the operating characteristics of such systems are becoming increasing stringent. In particular, systems are required to have the features of high reliability, portability, security, and also simultaneously consume ever smaller amounts of power. Communications engineers are required to design systems based on existing and emerging communications protocols and standards that cater to the different needs of customers while meeting these challenging requirements.

Typical contemporary communications systems are developed based on a wide range of wireless protocols and standards. For example, cellular phone systems may employ either Code Division Multiple Access (CDMA) or the Global System for Mobile communications (GSM), and personal wireless networks may follow either the IEEE 802.11 family of standards or the newly developed technology of Worldwide Interoperability for Microwave Access (WiMAX). With the variety of standards currently in use, there exist entire families of communications systems that are tailored specifically to each standard.

With consumers starting to use multiple communications devices, either in mobile, or in fixed locations, there is an implicit drawback to the current state of the art. The drawback is the lack of interoperability between such devices. In order to overcome this deficiency, a new paradigm is needed for the development of future communications systems that has a focus on the interoperability between different standards.

Such futuristic communications systems can be described as agile radio systems. Ideally, an agile radio should have the flexibility to transmit signals at different carrier frequencies and use different modulation schemes. In addition, the system should be able to correctly classify and appropriately demodulate signals in real-time. Automation of these functions is at the core of the agile nature of such radio systems.

With the use of the mathematical theory of Wavelet Transforms (WTs) the development of agile radio transceiver systems is possible. The development of such a system is the primary motivation of this dissertation with the focus on two of the core features of an agile transceiver, namely Automatic Modulation Recognition (AMR) and the subsequent Automatic Demodulation of communications signals.

Therefore, the focal points of this dissertation are:

1. The invention of WT-based techniques for the AMR of a select group of digitally modulated communications signals.

2. The invention of WT-based techniques for the Automatic Demodulation of digitally modulated communications signals subsequent to the AMR process.

1.1   Motivation

A typical contemporary communications receiver can be implemented by the means of three major sub-systems, as illustrated in Fig. 1.1.
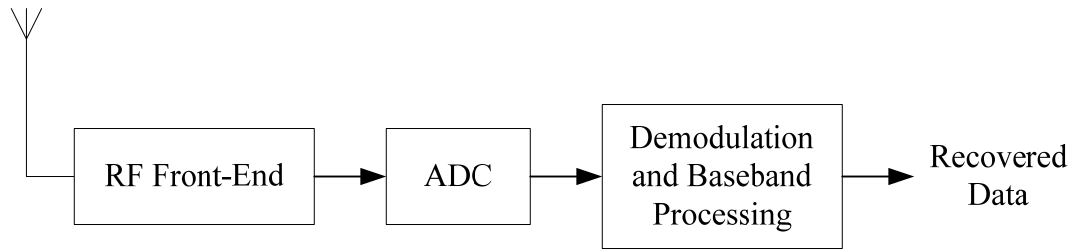
Fig. 1.1. Overall system-level description of a radio receiver [1].

1. **Radio Frequency (RF) front-end:** The RF front-end performs the down-conversion of the passband signal to an intermediate frequency for the ease of subsequent processing. It is composed of analog electronic sub-systems, such as mixer, local oscillators, band-pass filters, variable gain amplifiers and antennas.

2. **Mixed-signal stage:** This stage converts the downconverted signal output by the RF front-end to a digitized form. This stage is absent in analog receivers. The Analog-to-Digital Converter (ADC), in Fig. 1.1, converts the analog received signal into digitized form.

3. **Demodulation and baseband processing units:** The desired baseband data are recovered by a signal-specific demodulator, and any decoding of the recovered data is handled by a baseband processor.

Radio transmitters also use similar signal processing strategies as those in the receiver, except in reverse. First, baseband data are encoded, if needed, and the data are then used to modulate a carrier signal at an intermediate frequency. The modulated signal is then upconverted to the RF passband and transmitted.

A more detailed depiction of a modern radio transceiver system is provided in Fig. 1.2.
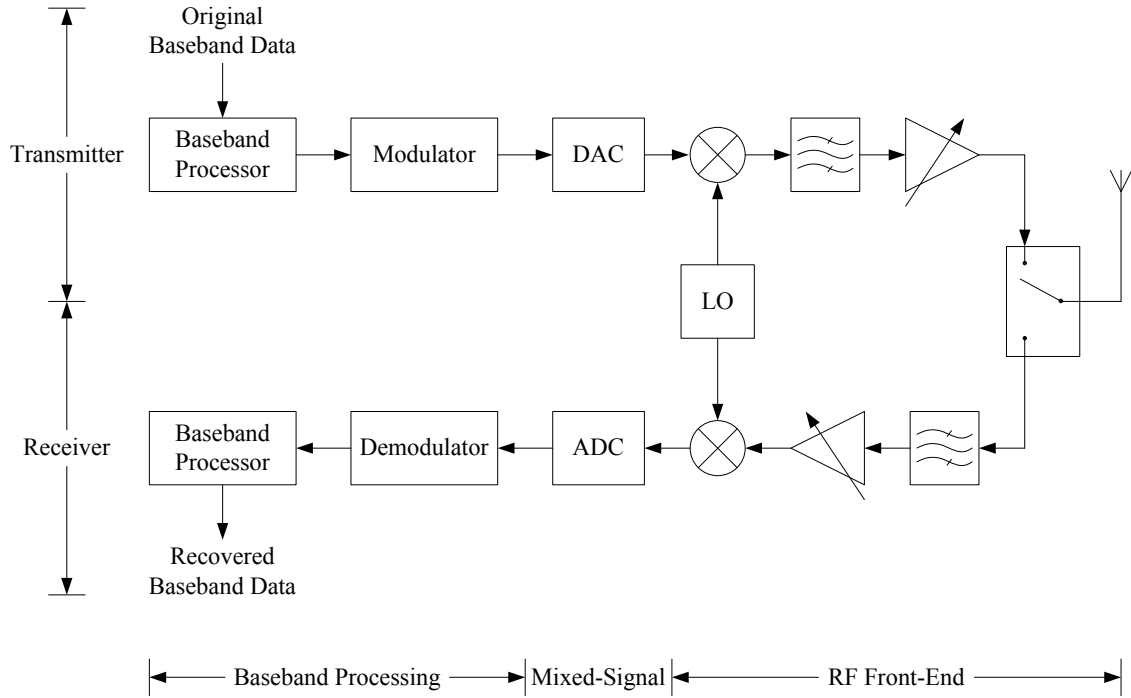
Fig. 1.2. Typical contemporary radio transceiver system [1].

Wireless communications systems are currently being developed based on advanced techniques such as Orthogonal Frequency Division Multiplexing (OFDM), Multiple-Input Multiple-Output (MIMO) system, and hybrid OFDM-MIMO techniques. Due to this trend, advanced concepts for high-speed communications, such as various time, frequency and spatial multiplexing techniques, are rapidly maturing.

The major limitation of communications systems based on advanced techniques as well as of basic systems, such as the system shown in Fig. 1.2, is the lack of interoperability between radios that implement different communications standards. One specific obstacle to interoperability between systems is the fact that different standards may use different modulation schemes.

The solution to this problem is to develop an agile radio system that has the ability to

automatically classify the modulation scheme used in a received signal and then automatically demodulate the signal. A system block diagram of an agile radio system that is composed of these core features is described in Fig. 1.3.
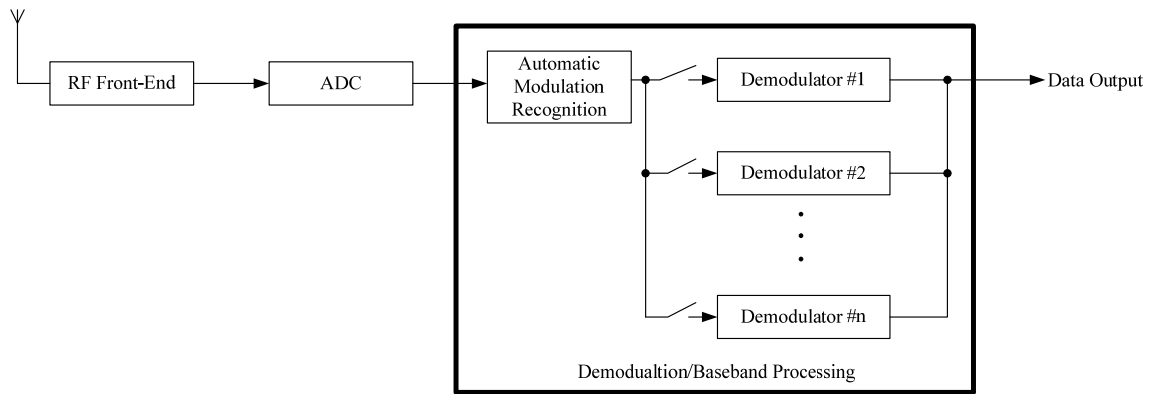
Fig. 1.3. A basic system block diagram of an agile radio receiver.

The AMR and demodulation processes of an agile radio receiver can be developed using the WT. In general, wavelets can be viewed as rapidly decaying oscillatory functions that can be used as basis functions to represent time-domain signals. They are especially useful in representing all types of practical signals that are aperiodic and have jump discontinuities.

Using Fourier Transform theory, a time-domain signal can be expressed in terms of sinusoidal basis functions in the spectral domain. The temporal detail of the signal, however, is lost during this process. On the other hand, the Short Time Fourier Transform (STFT) allows for the preservation of the temporal information of the signals by using windowing functions. In this case, however, the size of the window function is fixed and leads to an inherent problem of resolution: a narrow, highly localized, time-domain window of fixed size provides poorly localized spectral-domain resolution, and

conversely a poorly-localized temporal window provides highly localized spectral resolution. This drawback associated with fixed window sizes is especially problematic in the analysis of digitally modulated communications signals. An advantageous situation would be when the size of the window function can be altered to accommodate variations in the phase and frequency of a signal.

The WT provides the feature of flexible window functions. In the WT, a window function, i.e., a wavelet can be translated and dilated in time. The dilation of wavelets allows for the variation of the size of wavelet windows to a specific temporal resolution. The translated and dilated wavelets at different levels of resolution are cross-correlated with the signal, resulting in the desired wavelet coefficients. These wavelet coefficients implicitly contain the frequency information of the original signal, and explicitly preserve the temporal information of the signal.

From the perspective of fundamental system development, the WT can be used to develop a wavelet-based signal processing platform for agile radio systems. The agile nature of a receiver is established using a WT-based AMR process and a subsequent Automatic Demodulation process.

A system-level block diagram of such a Wavelet Platform is in Fig. 1.4. The Wavelet Platform in the figure consists of five major components:

1. **De-Noising:** WT-based de-noising methods have been well established. De-noising a corrupted received signal prior to processing it further would be a valuable feature included in the Wavelet Platform.

2. **Channel Estimation:** Electrical characterization of the medium through which a

signal is propagating is performed in this operation. In addition, channel estimation serves to restore signal features prior to WT-based AMR and demodulation processes in order to improve performance.

3. **Channel Equalization:** The mitigation of unwanted channel effects present in received signals is a desirable signal conditioning step before invoking the AMR process.

4. **AMR:** This is a core feature of the Wavelet Platform. This processor automatically identifies the modulation scheme of a received signal.

5. **Demodulation:** Automation demodulation is the second core feature of the Wavelet Platform. After the modulation scheme of the unknown received signal is recognized, the signal is then jointly and automatically demodulated appropriately to recover the transmitted information.
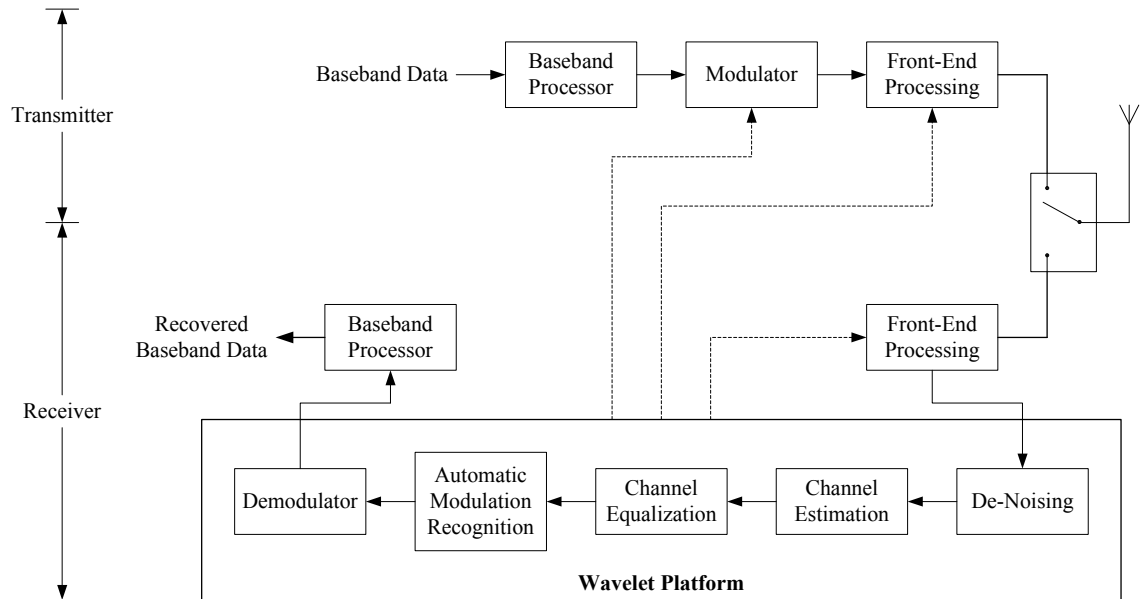
Fig. 1.4. System-level block diagram of an agile radio transceiver based on the Wavelet Platform [2].

In Fig. 1.4, both a transmitter and a receiver are shown as being part of an agile transceiver. Major sub-systems of the receiver are implemented in the context of the Wavelet Platform. In this transceiver, the transmitter operation is partially controlled by the Wavelet Platform. The dashed lines serve to indicate feedback provided by the Wavelet Platform to sub-systems in the transmitter. The information fed back can be used to alter transmission characteristics such as the modulation scheme, carrier frequency, etc., as needed. This functionality is yet another feature of agility possessed by the wavelet-based transceiver.

In brief, the intention of developing wavelet-based AMR and automatic Demodulation techniques is to advance the state of the art of communication systems by providing a fundamental step towards interoperability between communications standards through the use of wavelet transforms.

1.2   Objectives of the Dissertation

The primary objectives of this research work are:

1. To devise a technique for choosing a suitable wavelet(s) for use in both the AMR and Demodulation processes.

2. Invention of a technique for choosing wavelet-domain signatures that are needed for both the AMR and Demodulation processes.

3. Invention of techniques for AMR and automatic Demodulation using appropriate wavelet-domain signatures, and evaluation of the performance of these new techniques.

4. Compare the performance of the WT-based AMR and Demodulation

methodologies with results obtained using other methodologies that have been reported in the literature.

The WT-based AMR and Demodulation processes both use the Continuous Wavelet Transform (CWT).

Automatic Modulation Recognition

AMR is to be carried out with the use of WD signatures, or feature templates, which contain characteristic features of a particular modulation scheme expressed in the wavelet-domain. The received signal is transformed into the wavelet-domain using the CWT. The cross-correlations between the transformed received signal and the WD signatures are computed to obtained decision variables. The decision variables are used in decision-making operations comprising the AMR algorithm.

The AMR algorithm is developed using a hypothesis testing methodology. The efficacy of the AMR algorithm is validated using computer simulations. The simulations are Monte Carlo experiments conducted in a manner so as to provide statistically significant results.

Demodulation

WT-based Demodulation is developed based on the cross-correlations of WD signatures with a received signal whose modulation technique has been classified. Demodulation algorithms are specifically developed for each of the modulation schemes considered in this work. The BER performances of the demodulation algorithms are compared with the traditional matched filter-based BER performances for each modulation scheme. The received signals have been corrupted by Additive White Gaussian Noise (AWGN) of

varying power levels.

Modulation Schemes

The modulation schemes considered in this research work are presented below. Some of the current, planned, and future applications using the respective schemes are also described.

1. **M-ary Phase Shift Keying (M-PSK)**

Table 1.1 MPSK modulation schemes and major applications

(a)	BPSK	IEEE 802.11a [1] and ZigBEE standards [3].
(b)	QPSK	IEEE 802.11b systems [4].
(c)	$\pi/4$-QPSK	Bluetooth 2 [5].
(d)	8-PSK	Wireless communications systems applications.

2. **M-level Quadrature Amplitude Modulation (M-ary QAM)**

Table 1.2 M-QAM modulation schemes and major applications

(a)	16-QAM	Digital terrestrial television applications in the United Kingdom [7].
(b)	64-QAM	• Cable modems for high-speed internet access. • Digital Video Transmission Standard for cable television in the U.S. [8]. • Digital terrestrial television applications in the United Kingdom [7].
(c)	256-QAM	• Cable modems for high-speed internet access. • Digital Video Transmission Standard for cable television in the U.S. [8].

3. **Amplitude Shift Keying (ASK)**

   Binary ASK is used in applications such as the transmission of digital data over an optical fiber.

4. **Frequency Shift Keying (FSK)**

   Binary FSK is predominantly used in applications such as caller ID, fax services, and the transmission of telemetry data.

1.3 Major Contributions of the Dissertation

Among the many contributions of this research work, the following are considered to be the most significant:

1. Development of a technique for choosing the suitable wavelet(s) for both the WD AMR and the WD Demodulation processes.

2. Identification of WD signatures in digitally modulated communications signals for use in WD AMR and WD Demodulation processes.

3. Development of new techniques for signal classification and demodulation of digitally modulated communications signals using wavelet-domain signatures.

4. Introduction of a "moving origin" concept in order to recognize the different sizes of square constellations for M-ary QAM signals based on a blind identification process.

1.4 Organization of the Dissertation

This dissertation is composed of eight chapters. Chapter 1 introduces the framework of agile transceivers and the problems being addressed in this study.

Chapter 2 contains an overview of existing AMR methodologies that use techniques largely based on either a decision-theoretic approach, or a pattern recognition approach. A summary of AMR techniques that employ WTs is also provided. In the remainder of Chapter 2, an overview of demodulation techniques is provided, along with a survey of demodulation techniques that are augmented by the use of de-noising procedures in the wavelet-domain.

A brief primer on the CWT, along with descriptions of digital communications signals and WD signature models, is provided in Chapter 3. The wavelet-domain cross-correlation operation used in the AMR and demodulation algorithms is also introduced in Chapter 3.

The preliminary setups required for both the AMR and the Demodulation processes are described in Chapter 4. Several key parameters required for the AMR and Demodulation processes are investigated in this chapter, including: 1.) Selection of WD signatures; 2.) The length, or size, of the templates representing the WD signatures; and 3.) The suitable choice of wavelet(s) used to transform the received signals.

This research work has produced two distinct WT-based AMR methodologies. Each is based on a different type of template describing the communications signal features. The two WT-based AMR methodologies involve:

1. **Unique features templates**

   Templates that contain unique features of specific types of digitally modulated signals that arise due to the symbol transitions inherent in the modulated waveform structure.

2. **Common features templates**

   Templates that contain variations of the sinusoidal feature within a symbol period of different modulation schemes. The sinusoidal feature within a symbol is common in all modulation schemes arising from either the carrier, or variations in the carrier signal.

Two different AMR algorithms have been developed based on these two types of

templates.

AMR using unique features templates is considered in Chapter 5. In this chapter detailed design procedures for the AMR algorithm, results of computer simulation experiments, and comparisons of the results with the existing literature are provided.

In Chapter 6, AMR using common features templates is developed. The AMR algorithm based on the common features templates, the simulation results, and comparisons of results are described in detail.

In Chapter 7, the techniques used for automatic signal demodulation in the wavelet-domain are presented. The BER performances of the WT-based demodulation of the various modulation schemes are compared with the relevant matched filter-based BER performances.

Finally, in Chapter 8, the important features of the AMR and Demodulation processes invented in this dissertation are summarized; extensions of the work are identified for possible future investigation; and, the conclusions of this research work are provided.

Chapter 2

Literature Survey

In this chapter, a survey of the literature on AMR methodologies and demodulation techniques is presented. The survey is sub-divided into two main sections. The first section is on AMR, and consists of:

1. Decision-theoretic approaches,

2. Pattern recognition techniques, and

3. Methods that have already been developed using the wavelet transform.

The second section is a survey of the demodulation techniques that have been reported in the literature.

2.1   Automatic Modulation Recognition Techniques

Automatic Modulation Recognition techniques [9]-[64] have been explored in detail since the 1980s. Several techniques have been developed to perform signal identification. AMR techniques can be fundamentally classified into two main categories: techniques utilizing a decision-theoretic approach [9]-[35], and techniques utilizing pattern recognition approaches [36]-[47].

In order to augment, the AMR process, recently Support Vector Machines (SVMs) and Artificial Neural Networks (ANNs) have been used with various decision-theoretic and pattern recognition approaches to improve the overall modulation recognition process.

Both SVMs and ANNs also have been used in conjunction with wavelet transform-based techniques for the purpose of modulation classification.

Most of the work reported in the literature is largely theoretical. In most cases, however, the realization of the techniques in a hardware format for use in communications systems is either absent, or minimally developed. Techniques for AMR are challenging since there is no *a priori* information about the signals and other parameters at the receiver such as the signal power, carrier frequency, carrier phase, Signal-to-Noise Ratio (SNR), synchronization, etc.

The remainder of this section contains a survey of existing methods for AMR. In particular, the decision-theoretic approach, the pattern recognition approach, wavelet-based techniques, and recent trends in AMR research will be presented.

2.1.1   Techniques Based on the Decision-Theoretic Approach

In this popular approach, decision theory is applied to the problem of AMR. Specifically, upon reception, several statistical parameters, e.g., variance, mean, average power, of a signal are computed by the communications receivers. The same statistical parameters are also computed beforehand for the ideal cases of several modulation types. The statistics of the received signal are then correlated with those of the ideal cases, and decisions as to which modulation scheme is active are then made. Some of the work reported in the literature makes use of likelihood functions in conjunction with specific statistical parameters to distinguish between modulation schemes.

In the literature, both analog and digital modulation schemes are reported to have been identified successfully by the use of decision-theoretic approaches. Depending on the AMR techniques used, different signal parameters and decision variables are extracted in order to perform modulation type classification. The variety of approaches in the literature includes:

- Statistical parameters with new 4th order cumulants [18]

- Constellation rotation of the received symbols and a 4th order cumulant of a 1-D distribution of the signal's in-phase component [21]

- Combination of high-order mixed moments [22]

- The ratio of the power of the primary spectral line to the rest of the lines in the Power Spectral Density (PSD), the number of notable spectral lines in the PSD, the ratio of the Cyclic Spectral Density (CSD) function maximum modulus at two different cyclic frequencies, the number of notable spectral lines in the CSD [23]

- Envelope features based on the 2nd and 4th-order moments of the signal envelope [24]

- The ratio of the variance to mean square of the normalized instantaneous envelope of the signal [25]

- Bayesian likelihood function [25]

- Two-element antenna with maximum likelihood function [27]

- The maximum value of power spectral density of the normalized-centered instantaneous amplitude, standard deviation of the absolute value of the

centered non-linear component of the instantaneous phase in the non-weak intervals of a signal segment, the standard deviation of the direct (not absolute) value of the centered non-linear component of the instantaneous phase, the standard deviation of the absolute value of the normalized instantaneous amplitude; and the standard deviation of the absolute value of the normalized instantaneous frequency over different symbol periods are used in [32].

2.1.2 Techniques Based on the Pattern Recognition Approach

In this section, several studies on AMR using pattern recognition approaches that have been reported in the literature are presented. The most common and direct is the use of histograms to count the number of occurrences of the instantaneous amplitude, instantaneous frequency, and instantaneous phase of a received signal [45]-[46]. In these studies, the communications signals considered were Amplitude Modulation (AM), BASK, BFSK, 4-FSK, BPSK, QPSK, and 8-PSK. Another study reported in the literature utilized the amplitude histogram, the signal bandwidth, and the relationship between spectral components [46]. All of these parameters were obtained from the instantaneous amplitude of the Intermediate Frequency (IF) signal spectrum.

A survey paper published in 2000 reported that using of statistical parameters together with a pattern recognition approach can be applied to AMR [42]. The specific statistical features considered in that study were:

- Kurtosis of the signal envelope

- Variance of the derivative of the Power Spectral Density (PSD) of the signal

- Mean of the absolute value of the signal frequency.

The digitally modulated communications signals considered in that study were ASK, FSK, 4-Differential Phase Shift Keying (4-DPSK) and 16-QAM. Furthermore, a classifier based on fuzzy logic was also utilized to distinguish between the various signals. The rate of correct classification was reported to be 90% at SNR = 5 dB, but rapidly reduced to 0% at SNR = 0 dB.

2.1.3   The Use of Artificial Neural Networks and Support Vector Machines for Modulation Recognition

In recent years, newer methods for modulation classification based on a combination of the decision-theoretic approach and other computational techniques such as SVMs [11]-[13] and ANNs [14]-[16] have been developed. These new methods provide higher accuracy of classification when communications signals are subject to noise and channel impairments. The ANNs and SVM techniques have also been used in conjunction with WTs [49], [56].

SVM is a mathematical technique which maps the input data, which are the statistical parameters of the received signals in this case, to a higher-dimensional space. With the use of an appropriate kernel function, the two sets of data points are separated by a hyperplane. By separating the data representing the statistical parameters of the received signal, modulation classification can be carried out. ANNs are a rather new technique used in applications requiring computational decision-making. Multiple input stimuli are provided to an ANN and are propagated through an interconnected network of nodes. Each node has the ability to assign a weight to each input signal. However, ANNs also

have the ability to adaptively change these weights based on the specific decision-making mathematical model chosen for the ANN. Using signal parameters obtained from either the decision-theoretic, or pattern recognition-based methods, ANNs can be used for modulation classification. In addition, the adaptive learning ability of ANNs is especially useful for the classification of communications signals that are subject to noise and channel impairments.

In [56], an ANN and the WT were used in order to increase the detection probability of a code acquisition system. The WT was used to extract the structural parameters, i.e., signal power and phase of the received signal. The Morlet wavelet family was used in this method. Specifically, the Back Propagation (BP) ANN was used for template matching in conjunction with the structural parameters to achieve signal identification. The rate of correct classification was reported to be approximately 94%, however, the specific details about the noise scenarios applied to the test signals were omitted. Another study employed neural networks and the DWT to obtain the Shannon entropy of the input signals [55]. The calculated entropy was used to train the BP ANN. The signal was processed using three different signal processing techniques, such as Fast Fourier Transform (FFT), power spectral density estimator, and entropy in the WD. These techniques were used in conjunction with the ANN in order to perform modulation recognition. It was concluded, however, that the use of entropy for modulation classification was an unsuitable method when compared to other methods.

In [49], an SVM-based modulation classification method was developed. In that method, the Haar wavelet was used as the kernel function. BPSK, QPSK, and AM signals, corrupted by additive band-limited Gaussian noise, were used as test signals in the

reported work. The rate of correct classification was 84% in the presence of band-limited Gaussian noise.

2.1.4   Wavelet Transform-Based Techniques

WTs have been used for signal identification in a wide variety of areas, such as, medical applications, manufacturing processing, fault detection in a power system, and image processing. There are also a few publications that have used WT for AMR [48]-[64].

One popular WT-based approach involves computing the histogram of the wavelet coefficients of the received signals and then counting the number of peaks in the histogram in order to distinguish between PSK and FSK [54]; QPSK and GMSK [48], [61]; and M-QAM and M-ASK [50].

In [54], the method used to distinguish PSK and FSK signals is to determine the number of distinct histogram ordinate levels reached by the histogram data peaks. The distinct levels are used as thresholds in a subsequent decision-making step. Hence, the number M of distinct levels is used to identify the M-ary modulated signals. Fig. 2.1 shows the histogram for BPSK, QPSK, BFSK and 4-FSK signals. The dotted horizontal lines in Fig. 2.1 indicate the thresholds for the various M-ary modulation schemes. The success rate of modulation classification was reported to be 100% at an SNR of 13 dB, 99% at an SNR of 10 dB, and 97% at an SNR of 8 dB.
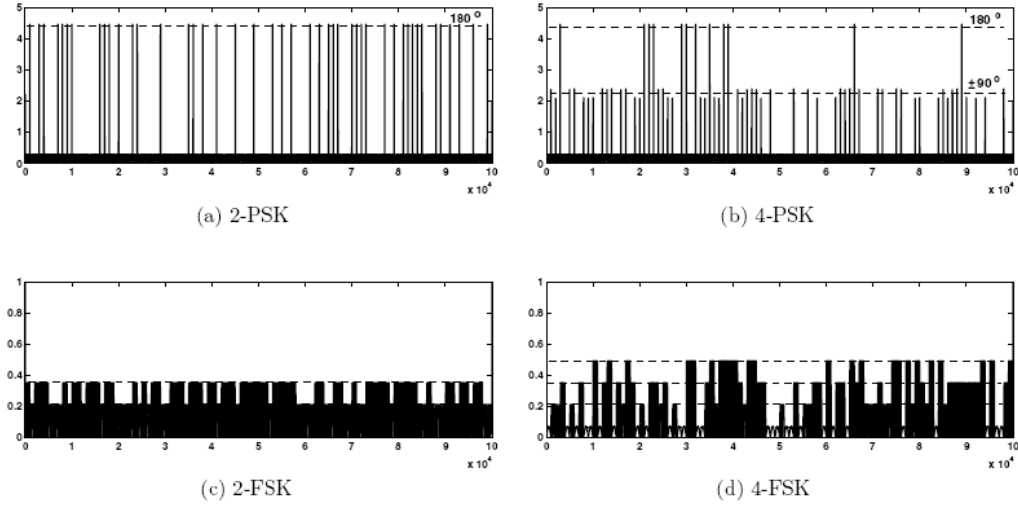
Fig. 2.1. DWT of different modulated signals [54].

QPSK and GMSK modulation schemes are commonly used in CDMA and GSM technologies. One method [48] used to distinguish such signals first computes the Discrete Wavelet Transform (DWT) of the received signal, and then the DWT coefficients are used to construct histograms. Again, by identifying the number of peaks in the histograms corresponding to the received signal, the modulation scheme used can be recognized. In [61], Ho, et al., presented an improved method of identifying GMSK and QPSK signals by correlating the histogram amplitudes of the signals with a Gaussian distribution.

Most WT-based AMR methods use the Haar Wavelet for the extraction of wavelet coefficients to be used in computing either the desired histograms, or other statistical parameters as needed [49] [50] [58]-[62]. Other wavelets, such as the Daubechies (db) family, and the complex Shannon wavelet, may also be used to obtain the wavelet coefficients of a signal that will be used for AMR. In [53], Ou, et al., proposed a modified

Haar wavelet as the mother wavelet to extract the wavelet coefficients used to compute the histogram.

Other methods in conjunction with the WT-based methods have also been introduced for use in AMR. WT-based methods have also been combined with SVMs [49] and ANNs [55]-[56]. In these cases, statistical parameters, such as the variance of the received signal, and also the normalization of the signals, are computed for use as decision metrics in the AMR process [58] [59] [62].

In [51], Chen, et al., proposed an algorithm which could identify signals in either the inter-class, or intra-class by combining both WT and likelihood functions, which is known as the decision-theoretic approach in the literature. The success rate of this method is above 90% with a Carrier-to-Noise Ratio (CNR) of 13 dB and above.

Most of the literature involving the WT for AMR employs the Haar, Daubechies, complex Shannon and Morlet wavelets. Most studies are based on the computation of the histogram for the wavelet coefficients so as to identifying the number of peaks. However, the drawback of this method is that only intra-class signals can be identified. Methods for the identification of inter-class signals are still underdeveloped.

2.2 Techniques for Demodulation of Digital Data

Traditionally, demodulation techniques are based on the concept of matched filtering [66]-[67] applied to the detection of digitally modulated communications signals. Matched filtering methods are based on the cross-correlation of the basis functions with the received communications signals in order to detect the presence, or absence, of the

basis function contained in the unknown signal. Using a subsequent Bayesian detector, the baseband data bit sequence can be recovered.

Only one technique involving the use of WT in improving the demodulation of communications signal has been developed. The approach used is to de-noise received signals prior to demodulation using a standard matched filtering-based method [68]-[69]. In the work reported in [68], the signal was corrupted by AWGN resulting in SNR values in the range of -3 dB to 3 dB, and the Haar wavelet was used in implementing the DWT. It was determined that wavelet de-noising requires multiple samples per symbol to be effective.

In [69], the use of different wavelets for signal decomposition employing the DWT was presented. Both soft- and hard-thresholding were applied to the wavelet coefficients of noisy communications signal prior to invoking the matched filter-based demodulation method. PSK signal families were considered in this study. Signals were corrupted by AWGN yielding SNR values in the range of -5 dB to 10 dB. The results show that the use of wavelet-domain thresholding significantly improves the overall BER performance of matched filter-based demodulation of PSK signals.

Chapter 3

Mathematical Preliminaries

Descriptions of the underlying theories of the CWT and the DWT are presented in Section 3.1. Emphasis in the presentations, however, is on the CWT since that is the transform used throughout this dissertation. In general terms, the CWT is defined as the cross-correlation of a wavelet and a function of interest, while the DWT may be described in terms of the filter theory approach of Multiresolution Analysis (MRA).

In Section 3.2, the time-domain mathematical models of the communications signals investigated in this dissertation are presented. The WD AMR process developed in this dissertation involves the cross-correlation of WD signatures and communications signals. The cross-correlation operation in the WD is presented in Section 3.3.

3.1   An Overview of the Wavelet Transform

A brief introduction to the mathematical concept of the WT [65], [70]-[73] is presented in this section. WTs can be essentially implemented using either the CWT or the DWT [76]-[80]. The CWT is especially useful for the characterization (analysis) of signals, while the DWT is used in signal and image processing for reconstruction and synthesis [79]. In this dissertation, the CWT is used for both the AMR and the Demodulation processes.

Wavelets can be generally viewed as rapidly decaying oscillatory functions that may be used as basis functions to represent signals. They are especially useful in representing all types of signals that appear in practice with characteristics that are aperiodic and/or have jump discontinuities. Some wavelets are compactly supported, i.e., localized in time, such

as the cubic B-spline wavelet [73]. Others, such as the Morlet wavelet, which is constructed by modulating a sinusoidal function by a Gaussian function, are not [71].

Using Fourier transform theory, a time-domain signal can be expressed in terms of sinusoidal functions (a continuous-time basis set) in the spectral domain. In this process, however, the temporal detail of the signal is lost. By definition, Fourier transforms use the entire time signal to produce the frequency-domain description of the signal. In the case of transient signal analysis, the Short-Time Fourier Transform (STFT) [74] allows for the preservation of the temporal information of the signal by using windowing functions.

A carefully chosen user-defined window function is first multiplied with the signal function, and then the Fourier transform of the resultant product function is taken. By translating the window along the signal function in time, and then computing the Fourier transform of each "windowed signal", the STFT technique provides the ability to capture the spectral content of the signal without losing the temporal content.

The fact that the window must be of fixed size, however, leads to an inherent problem of resolution: a narrow, highly-localized, time-domain window of fixed size provides poorly localized spectral-domain resolution, and conversely a broad, or non-localized, temporal window provides highly localized spectral resolution. This drawback associated with fixed window sizes is especially problematic in the analysis of digitally modulated communications signals. An advantageous situation would be when the size of the window function can be altered to accommodate variations of phase and frequency that are characteristic of a digitally modulated communications signal.

In order to overcome this problem, WTs may be used instead. In the WT, a window function, i.e., a wavelet can be translated and dilated in time. The dilation of wavelets allows for the variation in the size of wavelet windows so as to achieve a specific temporal resolution. The translated and dilated wavelets at different level of resolution are cross-correlated with the signal, resulting in the desired wavelet coefficients. These wavelet coefficients implicitly contain the frequency information of the original signal, and explicitly preserve the temporal information of the signal.

3.1.1   Review of the Continuous Wavelet Transform

In contrast with the Fourier transform and the STFT, the window functions of wavelet transforms have the properties that the function $\psi(t)$ averages to zero over all time and has finite energy [65], i.e., $\int_{-\infty}^{\infty} \psi(t)\, dt = 0$ and $\int_{-\infty}^{\infty} |\psi(t)|^2\, dt < \infty$, respectively.

It follows that window functions so described, allow for not only temporal translation but also for time dilation. In other words, the width of the windows can be varied to achieve a required resolution in either the temporal or spectral domains. Such window functions are called wavelets. Transforming, that is comparing translated and scaled (dilated) wavelets with the original signal yields correlation coefficients. In this way, at different scales, correlation coefficients contain the frequency content of the original signal while automatically preserving the temporal information of the signal.

The CWT, for a given wavelet $\psi(t)$, is formally defined as

$$W(a,b) = \int\limits_{-\infty}^{\infty} f(t)\psi_{a,b}^*(t)\,dt \tag{3.1}$$

where $\psi_{a,b}(t) \equiv \dfrac{1}{\sqrt{|a|}}\psi\left(\dfrac{t-b}{a}\right)$, $f(t)$ is the function to be transformed, a is the scale, or

dilation, variable and b is the translation variable.
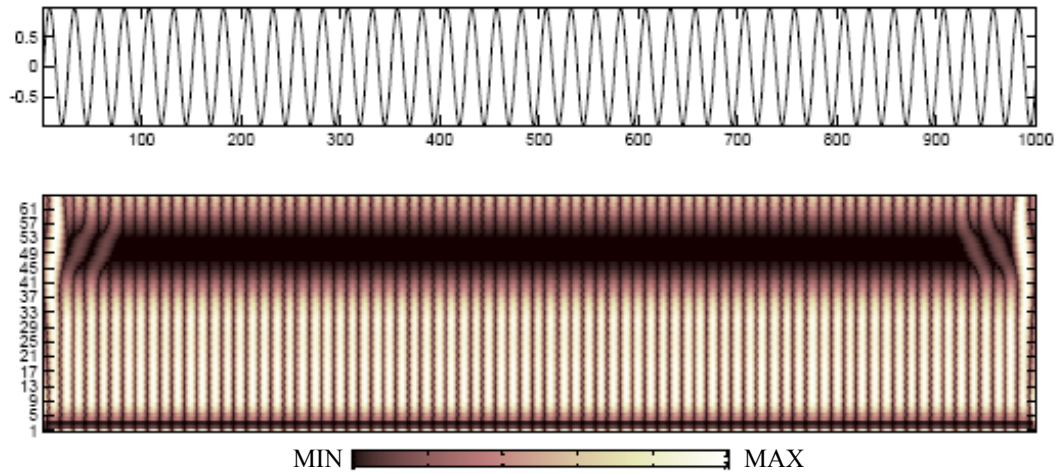
Fig. 3.1. (Top) A time-domain sinusoidal signal, (Bottom) The corresponding WD

scalogram of the sinusoidal signal.

In Fig. 3.1, an example is shown of a sinusoidal signal in both the time-domain and the

wavelet-domain. The abscissa, for both time- and wavelet-domains, represents the time

axis of the signal. The ordinate of the time-domain plot represents the amplitude of the

signal. On the other hand, the ordinate of the wavelet-domain scalogram represents the

different scales, or dilations, of the wavelet function, $\psi(t)$, that is used to compute the

CWT. In other words, the different scales also denote as the different window sizes of the

wavelet that is cross-correlated with the time-domain signal. The combination of all the

cross-correlation values (also known as the wavelet coefficients) for the different dilations of the wavelet function, $\psi(t)$, makes up the scalogram. The different scales are defined as the levels of resolution. The term levels of resolution is used in the remainder of the dissertation.

On examining the fractal patterns of the segments appearing in the scalograms, it is seen that structural details are present in two-dimensions (translation and scale) when one-dimensional time-domain modulated signals are transformed into the WD. At some levels of resolution in the WD, the signals are represented richly. While at other levels of resolution the representation of the signal energy content is very weak. In the WD scalogram shown in Fig. 3.1 (Bottom), the darker areas represent smaller cross-correlation values obtained when the windowed time-domain signal is compared with a wavelet of choice. The lighter areas in the scalogram represent larger magnitude wavelet coefficients obtained with the windowed signal and the choice of wavelet. This particular characteristic of the scalogram data is utilized advantageously in the WD AMR process.

Wavelets that are used for the CWT are typically required to satisfy the following properties [83]:

i. **Admissibility:** Wavelets are required to be square integrable functions and must not have a non-zero component at zero frequency. It is important that this property be satisfied in order for the inverse CWT to be defined.

    Mathematically, this condition is described as

$$c_\psi = \int_{-\infty}^{\infty} \frac{|\Psi(\omega)|^2}{|\omega|} d\omega < +\infty \qquad (3.2)$$

where $\Psi(\omega)$ is the Fourier transform of the wavelet $\psi(t)$, and c_ψ is the admissibility constant.

ii. **Regularity:** This condition ensures that the wavelet transform coefficients, obtained using (3.1), decrease quickly in magnitude as the dilation changes. By doing this, the wavelets can be very highly localized in time without causing an unbounded time-bandwidth product.

Therefore, if a wavelet satisfies the condition that

$$M_p = \int_{-\infty}^{\infty} t^p \psi(t) dt = 0 \quad \text{for} \quad p = 0, 1, 2, \cdots, n \qquad (3.3)$$

where M_p is the pth moment of the wavelet, then the wavelet is said to be of order n.

iii. **Linear Transformations:** The wavelet transform, $W_f(a,b)$, must satisfy the following conditions:

a) Superposition: $W_{f_1+f_2}(a,b) = W_{f_1}(a,b) + W_{f_2}(a,b)$ (3.4a)

b) Translation: $W_{f(t-t_0)}(a,b) = W_{f(t)}(a, b-t_0)$ (3.4b)

c) Rescaling: $W_{m^{1/2}f(mt)}(a,b) = W_{f(t)}(ma, mb)$. (3.4c)

By using the CWT, a broad class of communications signals can be expressed in terms of wavelets belonging to different wavelet families. The results of such CWT operations are wavelet coefficients that are specific to each combination of signal and wavelet. More

precisely, the wavelet coefficients may be obtained for different scales and translations of the wavelet. By identifying the changes in the wavelet coefficients of a communications signal, the characteristic amplitude, phase and frequency fluctuations inherent in a communications signal can be identified.

3.1.2   Review of Multiresolution Analysis and the Discrete Wavelet Transform

The Digital Signal Processing (DSP) technique of MRA is based on the use of orthonormal wavelet bases for signal analysis [70], [82]. In this technique, a sampled signal is passed through a series of Finite Impulse Response (FIR) filters in the manner depicted in Fig. 3.2.
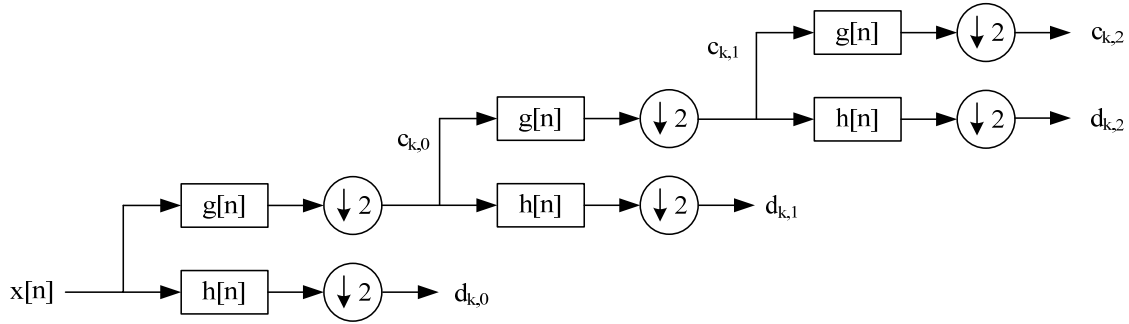
Fig. 3.2. A three-level filter bank illustrative of the MRA process.

The impulse responses of low-pass and high-pass filters are denoted by h[n] and g[n], respectively. The output of the high-pass filters provides the detail coefficients, $d_{k,j}$, and the output of the low-pass filters provide the approximation coefficients, $c_{k,j}$. With the requirement that the input signal be represented by 2^n samples, the output of each filter is down-sampled by a factor of 2 and the process is continued for as many user-defined levels as desired in order to obtain the required decomposition of the original signal.

In order to use MRA to implement the DWT technique a scaling function, $\phi(t)$, is

defined as [77]

$$\phi(t) = \sqrt{2} \sum_{m=0}^{N} h(N-m)\phi(2t-m) \tag{3.5}$$

where $N+1$ is the order of the filter and m indexes into the set of filter coefficients

under consideration. The mother wavelet, $\psi(t)$, can then be described in terms of the

scaling function, and the filter coefficients according to

$$\psi(t) = \sqrt{2} \sum_{m=0}^{N} g'(m)\phi(2t-m) = \sqrt{2} \sum_{m=0}^{N} -(-1)^m h'(N-m)\phi(2t-m). \tag{3.6}$$

In this MRA approach of implementing the DWT both the detail and approximation

coefficients of an input signal can be computed at different levels of resolution, as

illustrated in Fig. 3.2. Practically, the DWT can be used for the compression of data

prior to transmission through a noisy channel, for the de-noising of signals acquired by a

communications receiver, reconstruction of time-domain signals described in the

wavelet-domain, etc. [83]

As mentioned earlier, in developing the WD AMR process in this dissertation, it has

been found that the CWT is more suitable than the DWT. In the case of CWT, the signal

is represented by wavelet coefficients at different levels of resolution, which preserves

most of the signal contents. The CWT is also particularly useful for capturing the jump

discontinuities present in a signal, which often occurs in digitally modulated

communications signals. On the other hand, the DWT performs a decimation of the

wavelet-coefficients that is attractive for use in decomposition of a signal. This is

particularly useful in de-noising operations performed on a noisy signal, however, it

doesn't help to preserve the signal contents that would be needed for signal classification. Hence, subsequent attention is focused on the CWT.

3.2   Digital Communications Signal Models

Four different families of digital modulation schemes are considered in this dissertation. Specifically, binary and quaternary ASK and FSK signals, M-ary PSK signals for M = 2, 4, and 8, and multiple-level QAM signals for M = 4, 16, 64, and 256 are investigated in conjunction with developing classification strategies for WD AMR.

The time-domain ASK signals are defined as

$$
s_i(t) = \begin{cases} A_i \sqrt{\dfrac{2E_b}{T_b}} \cos(2\pi f_c t), & 0 \le t \le T_b \\ 0, & \text{otherwise} \end{cases}
\tag{3.7}
$$

where $i = 1, 2, 3, 4, \ldots$. The variable A_i represents the different levels of amplitude in ASK signals such that $\{A_i\} \in \mathbb{R}$. In the case of BASK, two amplitudes, A_1 and A_2, denote data symbols '0' and '1', respectively. In the case of 4-ASK signals, the four amplitudes, A_1, A_2, A_3, and A_4, correspond to the data symbols '00', '01', '10', and '11.' The parameter E_b denotes the energy per symbol, T_b denotes the temporal duration of the symbol, and the carrier frequency is denoted by f_c.

The time-domain FSK signals used are defined as [84]

$$
s_i(t) = \begin{cases} \sqrt{\dfrac{2E_b}{T_b}} \cos(2\pi f_i t), & 0 \le t \le T_b \\ 0, & \text{otherwise} \end{cases}
\tag{3.8}
$$

where $i = 1, 2, 3, 4, ...$ The parameter f_i denotes the different carrier frequencies that are required for different orders of FSK signals. For example, f_1 and f_2 denote the carrier frequencies the used to represent the data symbols '0' and '1' in a BFSK signal, respectively, etc.

Time-domain M-ary PSK signals are defined as [84]

$$s_i(t) = \begin{cases} \sqrt{\dfrac{2E_b}{T_b}} \cos\left[2\pi f_c t + \dfrac{2\pi}{M}(i-1)\right], & 0 \le t \le T_b \\ 0, & \text{otherwise} \end{cases} \tag{3.9}$$

where $i = 1, ..., M$. The parameter M represents the order of the PSK signals, e.g., $M = 2$ for BPSK signals, $M = 4$ for QPSK signals, etc. In the case when $i = 1$ and 2, the corresponding data symbols are '0' and '1' in a BPSK signal. In the case when $i = 1, 2, 3,$ and 4 the data symbols are denoted as '00,' '01,' '10' and '11' in a QPSK signal, respectively. The M-QAM signals are defined as [84]

$$s_k = \sqrt{\dfrac{2E_b}{T_b}} a_k \cos(2\pi f_c t) - \sqrt{\dfrac{2E_b}{T_b}} b_k \sin(2\pi f_c t), \qquad 0 \le t \le T_b \tag{3.10}$$

where $k = 0, \pm 1, \pm 2, ...$, and the quantities a_k and b_k represent the discrete amplitudes for the in-phase and quadrature carriers, respectively.

3.3   Wavelet-Domain Cross-Correlation Operation

In this section the concept of the cross-correlation operation in the wavelet-domain is explained.   The WD AMR process developed in this dissertation uses WD cross-correlation coefficients in several decision making algorithms.

In the time-domain, the cross-correlation of two functions $x(t)$ and $y(t)$ is described as [79]

$$R_{x,y}(\tau) = \int_{-\infty}^{\infty} x(t) y^*(t-\tau) dt.$$ (3.11)

A signal, $s(t)$, transformed into the wavelet-domain by means of the CWT is described as a cross-correlation between the signal and a wavelet, that is

$$W_s(a,b) = \int_0^T s(t) \psi_{a,b}^*(t) dt$$ (3.12)

where $\psi_{a,b}(t) \equiv \dfrac{1}{\sqrt{|a|}} \psi\left(\dfrac{t-b}{a}\right)$ is the wavelet, a is the scale variable, and b is the translation variable.

Using (3.12), the two functions $x(t)$ and $y(t)$ can be described in the wavelet-domain as

$$W_x(a,b) = \int_0^T x(t) \psi_{a,b}^*(t) dt$$ (3.13)

and

$$W_y(a,b) = \int_0^T y(t) \psi_{a,b}^*(t) dt.$$ (3.14)

The CWT representation of these two wavelet-domain functions can be expressed in discrete-time notation as

$$\{W_x(a,b)\}[n] = \sum_{n=1}^{N} x[n] \bullet \psi_{a,b}^*[n]$$ (3.15)

and

$$\{W_y(a,b)\}[n] = \sum_{n=1}^{N} y[n] \bullet \psi_{a,b}^*[n].$$ (3.16)

The cross-correlation between two functions defined in the wavelet-domain can, therefore, be expressed as

$$W_{R_{x,y}(a,b)} = \left(\{W_x(a,b)\}[n_a,n_b] \right) \otimes \left(\{W_y(a,b)\}[n_a,n_b] \right) . \tag{3.17}$$

The quantity n_a denotes the scale variable in the scalogram, i.e., $n_a \in \{1,2,...,N_a\}$, where N_a is the maximum number of resolution levels computed. The quantity n_b denotes the translation variable in the scalogram, i.e., $n_b \in \{0,1,...,N_b\}$, where N_b is the maximum duration of the signal. Note that in Eqn. (3.17) the symbol $\otimes$ denotes the correlation operator. Eqn. (3.17) can also be expressed as

$$W_{R_{x,y}(a,b)} = \sum_{n_a} \sum_{n_b} \left(\{W_x(a,b)\}[n_a,n_b] \right) \cdot \left(\{W_y(a,b)\}[n_a,n_b] \right). \tag{3.18}$$

Chapter 4

Setup for the Automatic Modulation Recognition Process

The Wavelet-Domain (WD) Automatic Modulation Recognition (AMR) process developed in this dissertation is based on cross-correlating the Continuous Wavelet Transform (CWT) of a digitally modulated signal of unknown modulation scheme, taken to be at the input to a receiver, with a set of WD signatures that are locally stored templates within a communications receiver. Therefore, in order to develop such a WD AMR process, it is required to properly identify the WD signatures, or templates. At the outset, a suitable wavelet must also be chosen in order to construct the templates for use in the WD AMR process and also for performing the CWT of the received signal.

The methodologies to construct the templates are based on specific distinguishing features of digitally modulated communications signals in both the time- and wavelet-domains. Different temporal lengths of the WD signature templates are investigated in order to enhance the cross-correlation operation used in conjunction with the decision making algorithms. One immediate benefit of small WD signature lengths is a reduction in the computational effort of the cross-correlation operations.

The choice of wavelet is arrived at based on the sensitivity of different candidate wavelets to variations in the amplitude, frequency, and phase of a digitally modulated signal. In this dissertation, the choice of a best-matched wavelet is selected based on the largest cross-correlation result from among different WD signatures corresponding to a total of 65 candidate wavelets. A matrix is formed using the cross-correlation values of WD signatures for different signal features using various candidate wavelets. The values

are hard-thresholded in order to eliminate candidate wavelets which are not sensitive to a particular distinguishing signal feature.

In this chapter, the main topics that are discussed include:

1. Techniques for template selection in the WD.

2. Variations in the temporal length, or size, of templates representing WD signatures.

3. Choice of candidate wavelets based on cross-correlation values.

4.1 Template Selection for the Wavelet-Domain Automatic Modulation Recognition Process

To develop the WD AMR process, it is necessary to properly identify the WD signatures, or templates, that will be used in the AMR process. As seen from the definitions of the digitally modulated signals given in Chapter 3, each of the digital modulation schemes contain different types of features which can be extracted to serve as the WD signatures for the WD AMR process. These features arise due to baseband symbol transitions, and are seen to be variations in amplitude, frequency, and phase, of a carrier signal.

Figs. 4.1-4.3 illustrate BASK, BFSK, and BPSK signals with frame lengths that are 8 data-bearing symbols long in the time-domain, respectively. Symbol transitions, i.e., the variations of amplitude, frequency, and phase, are enclosed in the boxes. In this dissertation, such carrier transitions that arise between different symbols are used to define the **unique features templates**.
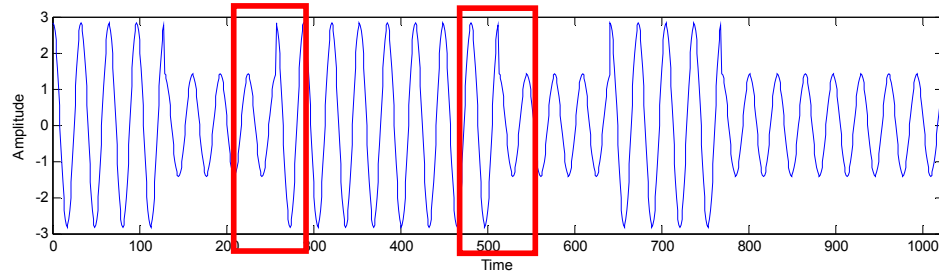
Fig. 4.1. Time-domain BASK signal with transitions contained within the box.
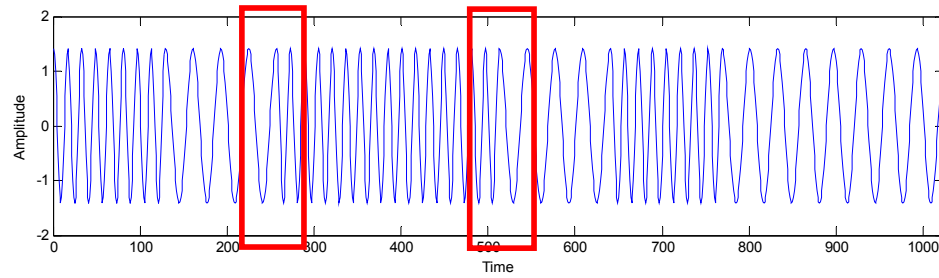
Fig. 4.2. Time-domain BFSK signal with transitions contained within the box.
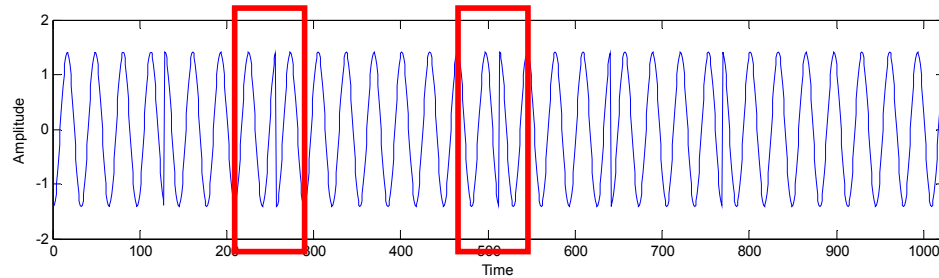
Fig. 4.3. Time-domain BPSK signal with transitions contained within the box.

The wavelet-domain scalograms of the signals shown in Figs. 4.1-4.3 are provided in Figs. 4.4-4.6, respectively with regions of the binary data transitions contained within the box.
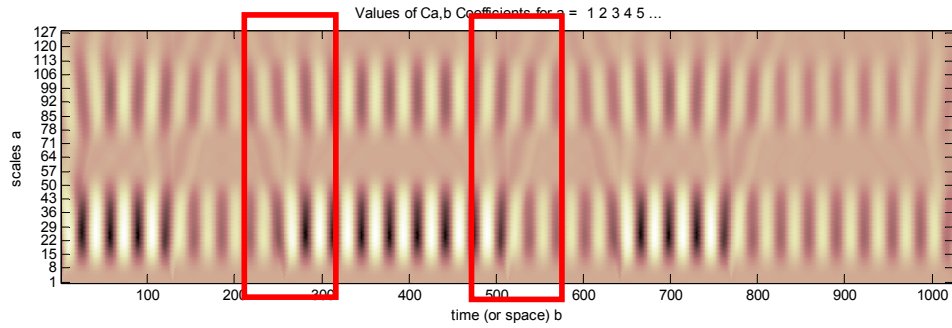
Fig. 4.4. Wavelet-domain scalogram of the BASK signal.
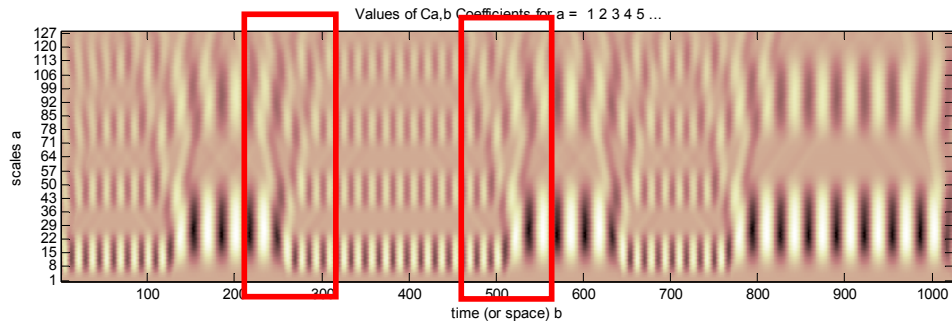
Fig. 4.5. Wavelet-domain scalogram of the BFSK signal.
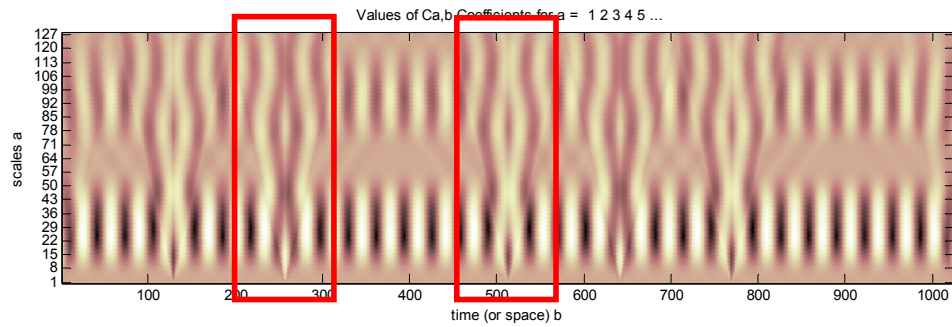
Fig. 4.6. Wavelet-domain scalogram of the BPSK signal.

The WD representations of the unique features of BASK, BFSK, and BPSK signals, which arise due to symbol transitions, are seen in Figs. 4.4-4.6. These features are stored as templates representing the WD signatures of various modulation types for use in the WD AMR process. While it is observed that the unique features are present in both the time- and wavelet-domain templates, only WD signatures are used for the development

of the AMR process in this dissertation. The wavelet coefficients, which are represented as fractal patterns in the WD scalogram, implicitly contain frequency information while explicitly exhibiting the temporal information of the unique features.

As described in Chapter 3, the scalogram contains the wavelet coefficients generated by the signal and the choice of wavelet at different levels of resolution. In Fig. 4.4-4.6, the abscissa refers to the time location of the signal in the WD, and the ordinate represents the different levels of resolution. The darker areas represent the smaller valued wavelet coefficients that are produced by the smaller amount of cross-correlation that exists between the wavelet and the signal. On the other hand, the lighter areas represent the larger valued wavelet coefficients that denote the presence of larger amounts of cross-correlation between the wavelet and the signal at a specific scale (resolution). It is observed from the figures that for each symbol transition occurring in the communications signal, the WD scalograms contain correponding unique signatures. These unique signatures are highlighted within the box. These signatures are used to develop the WD AMR and the WD Demodulation processes.

A second set of templates can also be identified by observing the time- and wavelet-domain illustrations of three different types of modulation schemes in Figs. 4.1-4.6. In comparing any two different symbols within a digitally modulated communications signal, it is seen that the sinusoidal carrier that present in both symbols is a common feature. The templates that are constructed based on the sinusoidal carrier, rather than on the transitions, are defined as **common features templates** in this dissertation.

Figs. 4.7-4.9 depict the common features of different modulation schemes in the time-domain. Each symbol is separated by a dashed line and the common features are enclosed in the boxes.
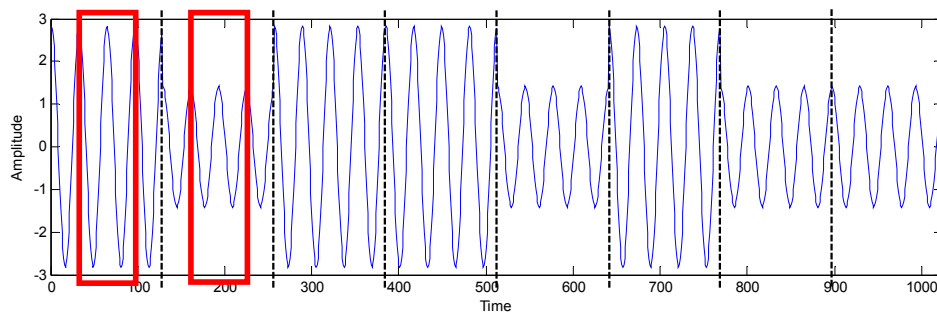
Fig. 4.7. Time-domain BASK signal with common features contained within the boxes.
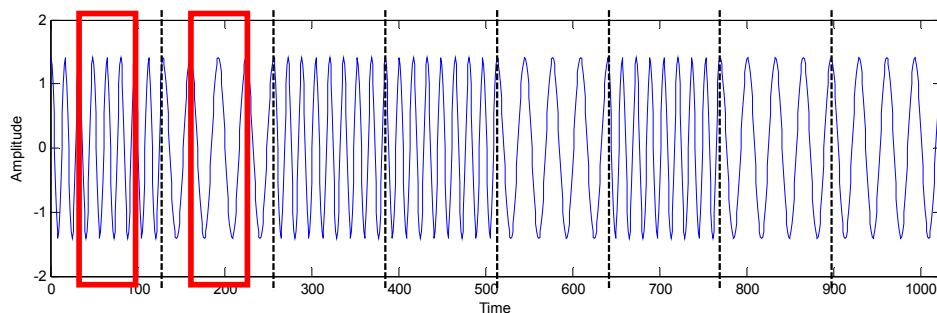
Fig. 4.8. Time-domain BFSK signal with common features contained within the boxes.
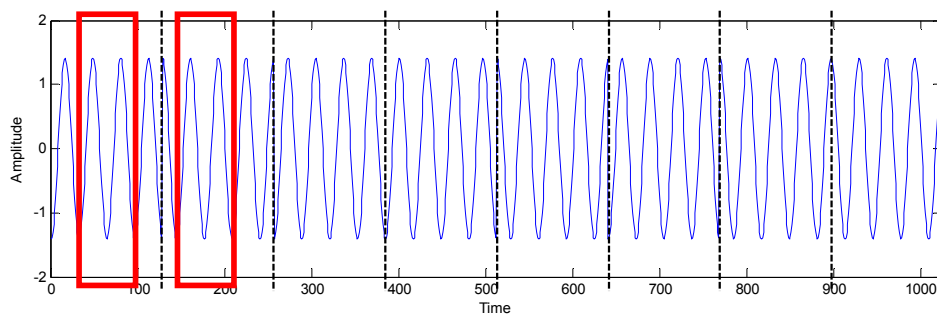
Fig. 4.9. Time-domain BPSK signal with common features contained within the boxes.

From Figs. 4.7-4.9, it is observed that all three digitally modulated signals contain the same common feature within different symbols, neglecting any variations in amplitude. This common feature is the sinusoidal carrier. An exception to this rule is in the case of BFSK, where another feature arises due to the variation frequency. Specifically, in BFSK signals there may be two different carrier frequencies within a modulated signal according to the definition of the modulation scheme and the actual data pattern. Since the method used in extracting the common features templates is the same (i.e., windowing the sinusoidal carrier within a symbol to obtain a template), the BFSK templates with different carrier frequencies are also grouped within the category of common features templates.

The WD scalograms of the signals shown in Figs. 4.7-4.9, i.e., the plots that have common features highlighted, are shown in Figs. 4.10-4.12, respectively. As seen in these figures, the scalograms depict details of the time-domain signal structure at different levels of resolution in the WD. In Figs. 4.10-4.12, the WD common features templates for the three modulation schemes are the contents of the boxes. Unlike the unique features templates representing symbol transitions, the common features templates capture the modulation characteristics within a symbol period as shown in boxes within these figures. The vertical dotted lines represent the symbol period boundaries within a finite duration of an overall communications signal.
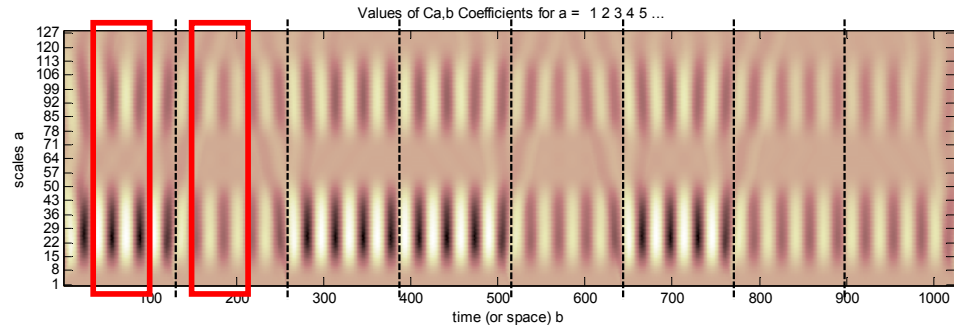
Fig. 4.10. Wavelet-domain scalogram of the BASK signal with the common features templates highlighted.
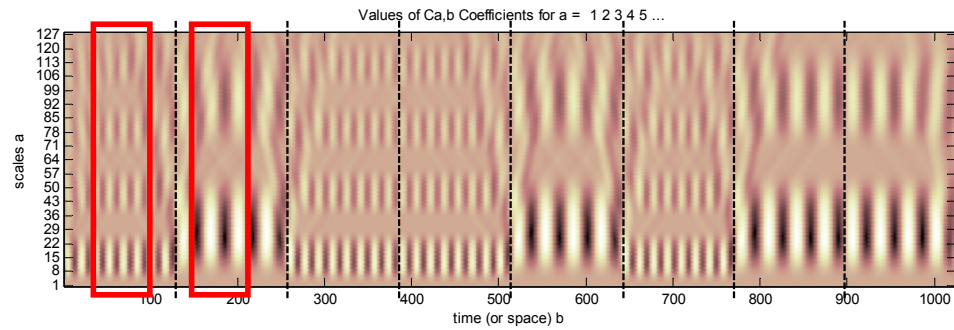
Fig. 4.11. Wavelet-domain scalogram of the BFSK signal with the common features templates highlighted.
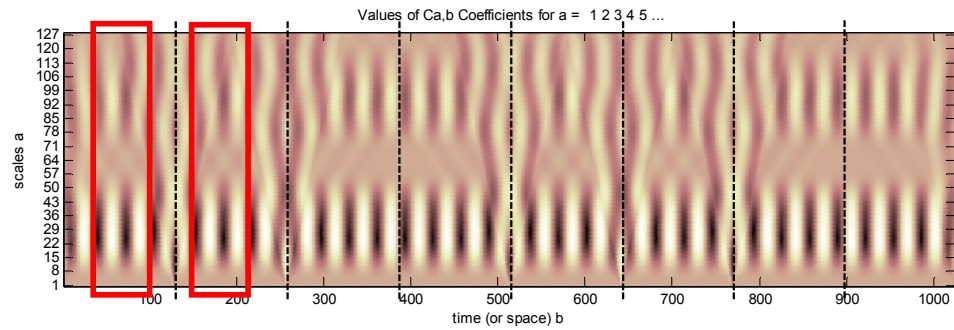
Fig. 4.12. Wavelet-domain scalogram of the BPSK signal with the common features templates highlighted.

From the various characteristics seen in Figs. 4.1-4.12, two distinct categories of templates can be constructed, and therefore, two distinct WD AMR algorithms will be developed. The two WD AMR algorithms are:

1. WD AMR process employing the unique features templates.
2. WD AMR process using the common features templates.

The observations that have been made thus far are based only on binary digitally modulated communications signals. The same concepts, however, can be used in order to construct the two categories of templates for signals associated with higher-order modulation schemes. For example, unique features templates can also be extracted based on the symbol transitions present in QPSK signals. Fig. 4.13 illustrates all of the possible unique features in the WD for a QPSK signal. By the definition of a QPSK signal described in (3.9), the signal is constructed based on different phase variations of symbols corresponding to different data bits. Therefore, the unique features templates are constructed based on symbol transitions, which arise from the QPSK signal phase variations. There are a total of 16 unique features templates extracted for use in both the WD AMR and Demodulation processes.

In Fig. 4.13, it is observed that each unique feature, arising due to symbol transitions, is different from all of the other features. Therefore, it is anticipated that using these unique features templates within the WD AMR process would result in a high rate of correct classification for QPSK modulated signals. Furthermore, due to their uniqueness, these templates can also be used advantageously to develop a robust WD Demodulation algorithm.
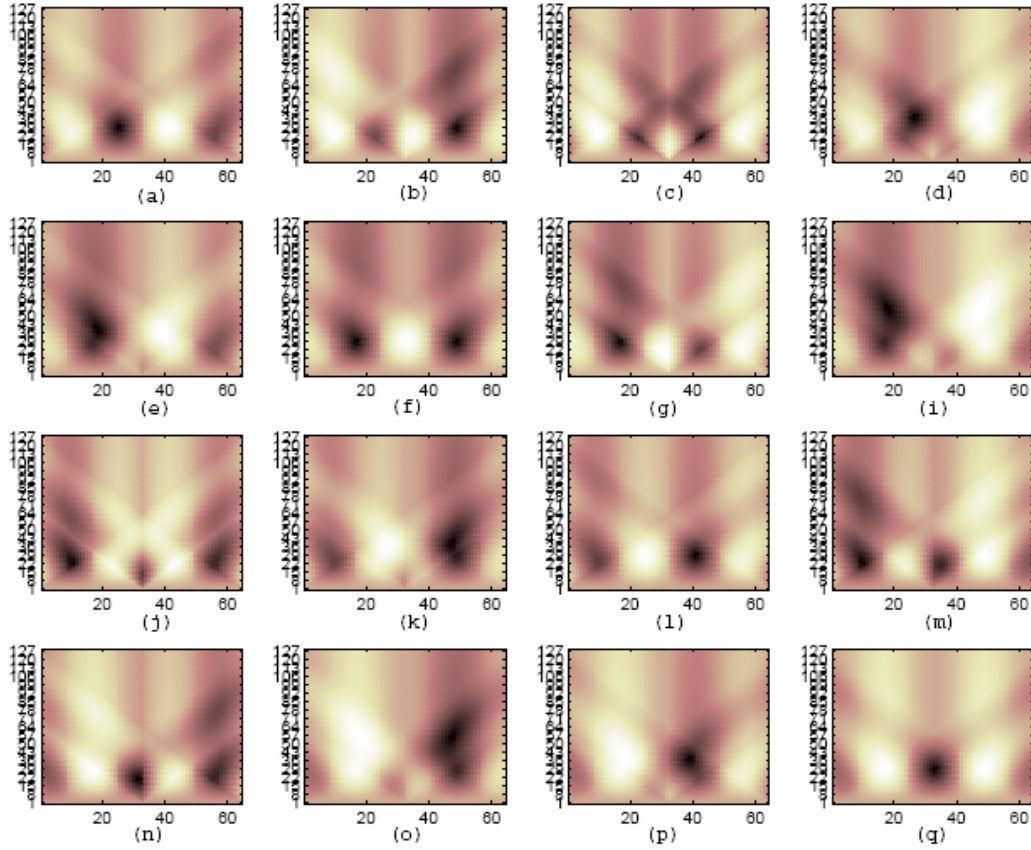
Fig. 4.13. (a-q) WD scalograms of the unique features corresponding to all sixteen symbol transitions in a QPSK signal.

As can be seen in the case of QPSK, the number of WD signatures required for the WD AMR process increases for more complex modulation schemes. However, on the other hand, the common features within the symbols of a QPSK signal are the same as those for a BPSK signal, as illustrated in Fig. 4.14. Therefore, the same set of common features templates, along with an appropiate hypothesis test, can be used to achieve classification of a signal with unknown modulation type with reduced complexity. In the case of 4-FSK there are four distinct common features due to the four different carrier frequencies that are used to represent the baseband symbols. This can be seen in Fig. 4.15.
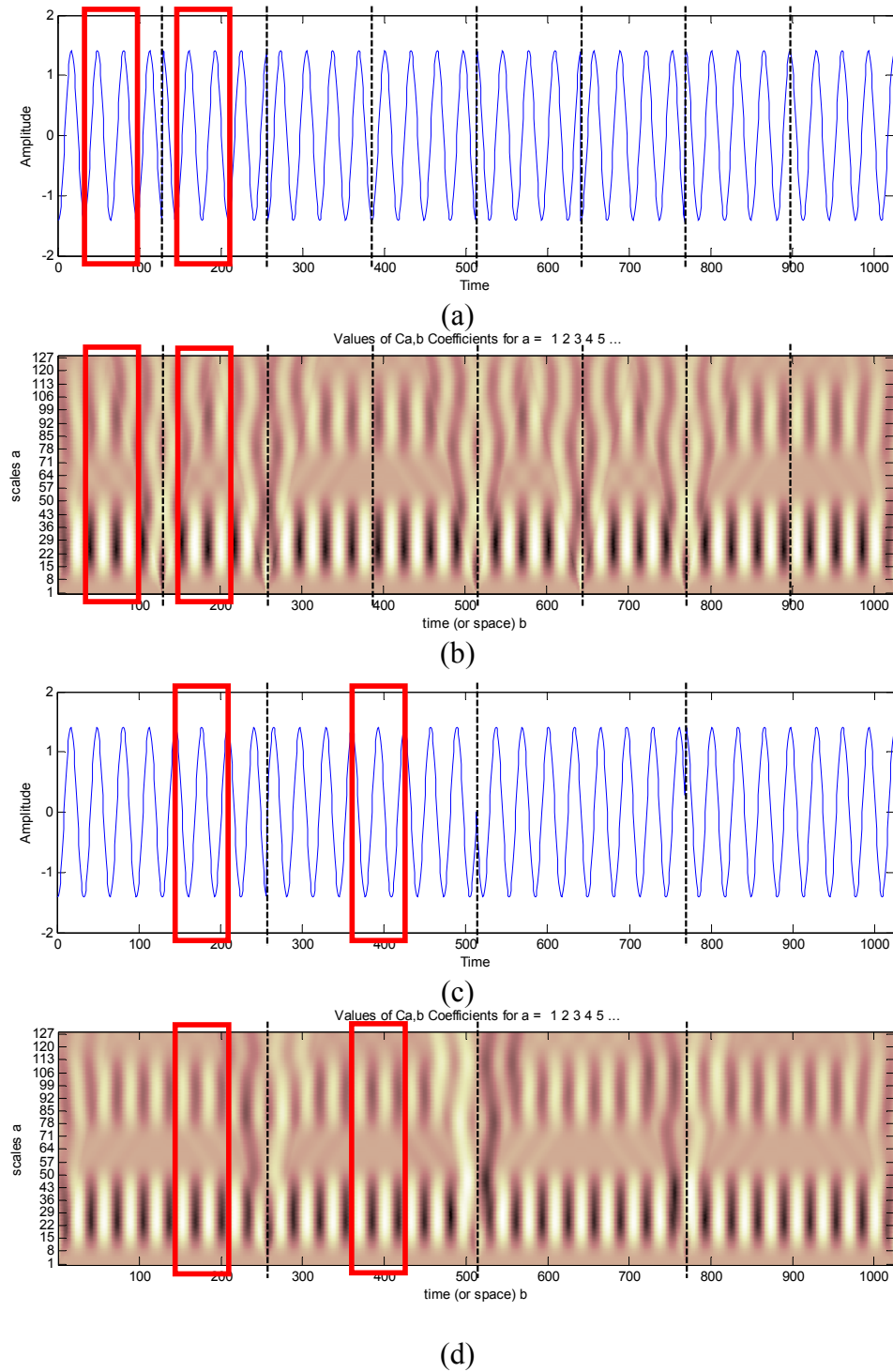
Fig. 4.14. (a) Time-domain BPSK signal, (b) WD scalogram for the BPSK signal, (c) Time-domain QPSK signal, and (d) WD scalogram of the QPSK signal.
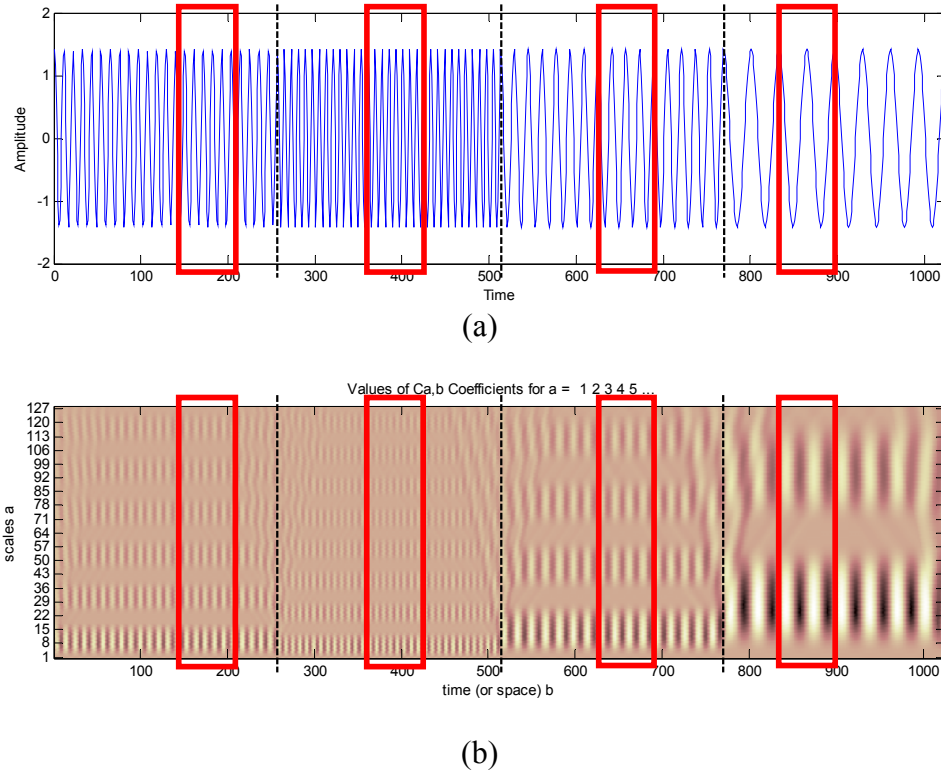
Fig. 4.15. (a) Time domain 4-FSK signal, and (b) WD scalogram of the 4-FSK signal.

Note again that higher-order ASK and PSK signals contain the same common features, and therefore, the same set of common features templates are used in the WD AMR process for these modulation schemes.

To summarize, two categories of templates have been identified to represent WD signatures for use in the development of WD AMR. The templates in the first category are called **unique features templates**, which contain carrier transition features specific to different modulation schemes. The templates belonging to the second category are called **common features templates** due to the fact that these templates represent the common features of a sinusoidal carrier that are present in different baseband symbols.

Chapter 5 will be focused on the development of a WD AMR algorithm using the unique features templates, while Chapter 6 will describe a WD AMR algorithm using the common features templates.

4.2   Mathematical Models of the Templates for Wavelet-Domain Signatures

WD signatures of specific time-domain features of digitally modulated signals are used for the AMR process in this dissertation. Details of the templates describing the WD signatures were described in Section 4.1. There are two categories of templates for the WD signatures, namely, the unique features templates and the common features templates. Time-domain analytical representations of the templates are presented as follows.

1. **Unique Features Templates**

   These templates are described based on symbol transitions that occur within a digitally modulated communications signal. Two unique features templates can be extracted from each of the 3 binary digitally modulated signals. The piece-wise continuous models of these templates are defined according to the following:

   i. For BASK signals, the two templates are defined as

   $$p_{BASK,1}(t) = \begin{cases} A_1 \cos(2\pi f_c t), & t_1 < t \leq t_2 \\ A_2 \cos(2\pi f_c t), & t_3 < t \leq t_4 \end{cases} \qquad (4.1a)$$

$$p_{BASK,2}(t) = \begin{cases} A_2 \cos(2\pi f_c t), & t_1 < t \le t_2 \\ A_1 \cos(2\pi f_c t), & t_3 < t \le t_4 \end{cases}. \tag{4.1b}$$

ii. For BFSK signals, the two templates are defined as

$$p_{BFSK,1}(t) = \begin{cases} \cos(2\pi f_1 t), & t_1 < t \le t_2 \\ \cos(2\pi f_2 t), & t_3 < t \le t_4 \end{cases} \tag{4.2a}$$

$$p_{BFSK,2}(t) = \begin{cases} \cos(2\pi f_2 t), & t_1 < t \le t_2 \\ \cos(2\pi f_1 t), & t_3 < t \le t_4 \end{cases}. \tag{4.2b}$$

iii. For BPSK signals, the two templates are defined as

$$p_{BPSK,1}(t) = \begin{cases} \cos(2\pi f_c t), & t_1 < t \le t_2 \\ \cos(2\pi f_c t + \pi), & t_3 < t \le t_4 \end{cases} \tag{4.3a}$$

$$p_{BPSK,2}(t) = \begin{cases} \cos(2\pi f_c t + \pi), & t_1 < t \le t_2 \\ \cos(2\pi f_c t), & t_3 < t \le t_4 \end{cases}. \tag{4.3b}$$

In (4.1)-(4.3), A_i represents the amplitudes, f_i represents the symbol frequencies and f_c denotes the carrier frequency of the modulated signals. The time instant t_i represents the locations of the template boundaries within the communications signal under consideration, as illustrated in Fig. 4.16.
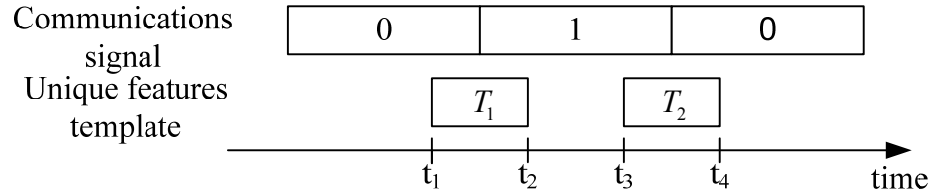
Fig. 4.16. Illustration of time-domain unique features templates.

As seen in Fig. 4.16, a communications signal having a frame length of 3 symbols is shown with both of the possible symbol transitions present, i.e., "0"

to "1" and "1" to "0." The two unique features templates, T_1 and T_2, can be described based on the mathematical models presented in (4.1)-(4.3).

2. **Common Features Templates**

This set of templates is described with the sinusoidal carrier being a common feature within all symbols of the digital modulation schemes. A fixed template size is extracted at various temporal locations within a symbol period. The analytical models of the templates are defined as follows.

   i. **Common Features Templates with Variation of Phase**

Depending upon the temporal location of the template extracted, the template is described generally as

$$p(t) = \cos(2\pi f_c t + \theta), \qquad t_1 < t \le t_2. \tag{4.4}$$

The phase variable, θ, represents the shifting of the templates within a symbol period as needed. A graphical representation of this concept is shown in Fig. 4.17. In this figure, the time duration of Template T_1 is from t_1 to t_2 and Template T_2 is from t_1' to t_2'.
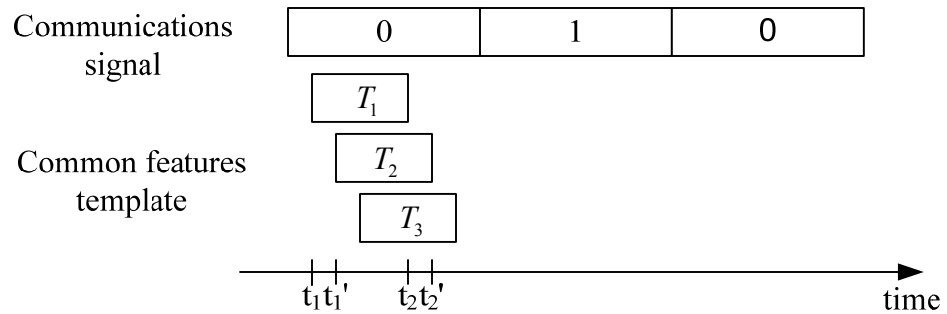
Fig. 4.17. Illustration of common features templates at different locations within a symbol.

ii. Common Features Templates with Different Frequencies

In an M-ary FSK signal, different carrier frequencies are used to represent different data symbols within the modulated signal. Therefore, another common features template can be defined according to

$$p(t) = \cos(2\pi f_i t), \quad t_1 < t \leq t_2 \tag{4.5}$$

where f_i is the active carrier frequency in the specified symbol time slot.

4.3   Determining the Length of the Templates for Wavelet-Domain Signatures

In the AMR process that is developed in this dissertation, a wavelet-transformed received signal of finite time duration is cross-correlated with WD signatures, which are also of finite time duration. The WD signatures may be either unique features templates or common features templates. In the WD cross-correlation operation, templates of finite length, are slid across the communications signal, and then compared to it via correlation in order to determine if the wavelet-transformed signal contains any features that are similar to the WD signatures represented by the templates.

When unique features templates are used, these WD templates must be perfectly aligned with the carrier transitions corresponding to each baseband symbol in the cross-correlation operations. In order to ensure such alignment the duration, or length, of each template must be a perfect divisor of the duration of each signal segment corresponding

to a data symbol. Once again, it is noted that both the template and the signal referred to here are expressed in the WD and are represented using two-dimensional scalograms.

The word "duration," in this context, refers to the time duration (finite length) of the templates in both the WD and the time-domain. Due to the nature of the CWT, the transformed signal maintains the same location on the time axis as the time-domain signal.

Fig. 4.18 illustrates the process of the sliding cross-correlation operation between a template and a communications signal. In this process, the template is cross-correlated with the first signal segment and the cross-correlation values between the two in each section of the signal are computed. A signal segment shown in Fig. 4.18 represents a data symbol period within the received signal. The template is then slid so as to be aligned with the next signal segment, and the two are cross-correlated. The process is continued until the template has been cross-correlated with all segments of the signal.
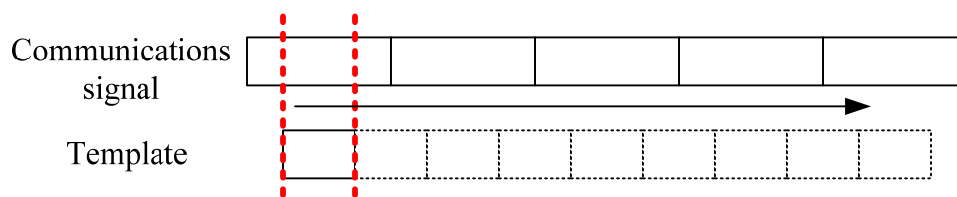
Fig. 4.18. Illustration of the sliding cross-correlation process between a template and a communications signal.

In this example, the carrier in each signal segment, representing a baseband data symbol, is composed of 128 samples/symbol. Due to the number of samples contained in a symbol, the maximum template length is 128 samples. The possible lengths of templates are 128, 64, 32, 16, 8, 4, and 2 samples. The length of the templates representing the WD

signatures, however, cannot be too short due to the loss of resolution in the WD scalogram. The loss of resolution directly affects the performance of the WD AMR process. A graphical representation of the sliding process with different template lengths is shown in Fig. 4.19. For the sake of illustration, only templates of size 128, 64, and 32 samples are used.
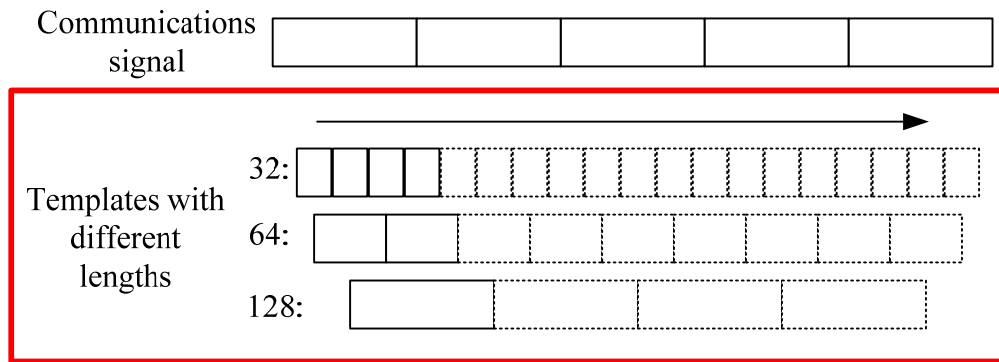
Fig. 4.19. Graphical representation of the cross-correlation operation using different template lengths.

The scalogram of a BPSK test signal with a frame length of 40 symbols, is shown in Fig. 4.20. The test signal is used to demonstrate the cross-correlation operation with different lengths for the unique features templates, as described in Fig. 4.21. As seen in Figs. 4.22-24, the cross-correlation results of the unique features templates with lengths of 32, 64, and 128 samples when compared with the BPSK test signal are shown. It is observed that that the longer the length of the template, the fewer the number of cross-correlation peaks that are computed and available for decision making.
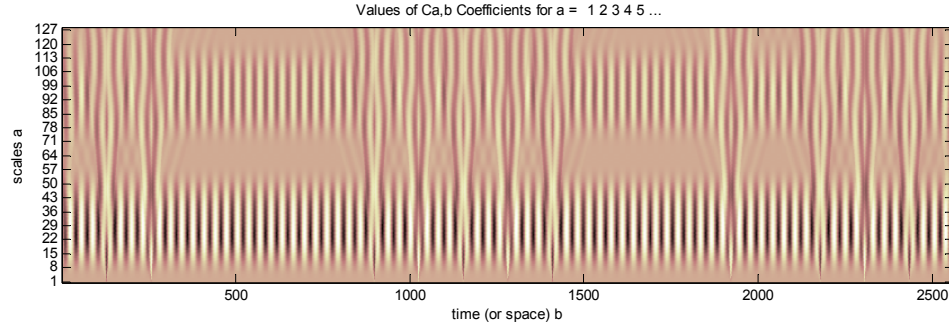
Fig. 4.20. Scalogram of a BPSK test signal.

The choice of template length for both the WD AMR and Demodulation processes is 64 samples. The particular choice of 64 samples in a template maintains the required resolution in the WD scalogram. Furthermore, using 64 samples does not increase the computational effort in performing the cross-correlation operation as compared to when templates consist of 128 samples. Another possible effect due to the different template lengths is that of the WD AMR system robustness in the presence of AWGN. More samples in a template (longer in length) may result in a higher possibility of error since the WD AMR and the WD Demodulation processes are based on a cross-correlation operations with the received, noisy signal and noise-free templates. A detail explanation concerning the effect of noise is presented in Chapter 7.

(a)　　　　　　　　(b)　　　　　　　　(c)
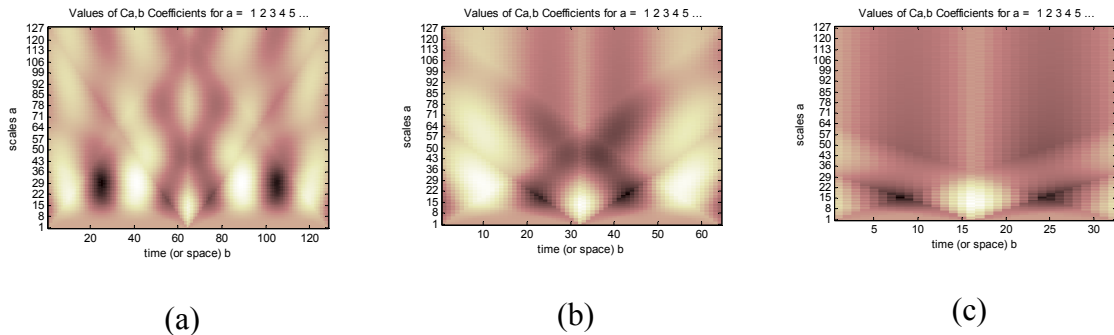
Fig. 4.21. WD unique features Template 1 with length of (a) 128 samples, (b) 64 samples, and (c) 32 samples.
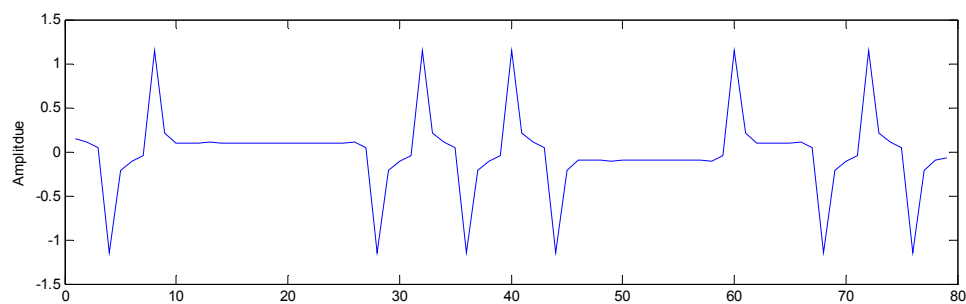
Fig. 4.22. Cross-correlation results using a unique features template that is 32 samples in length.
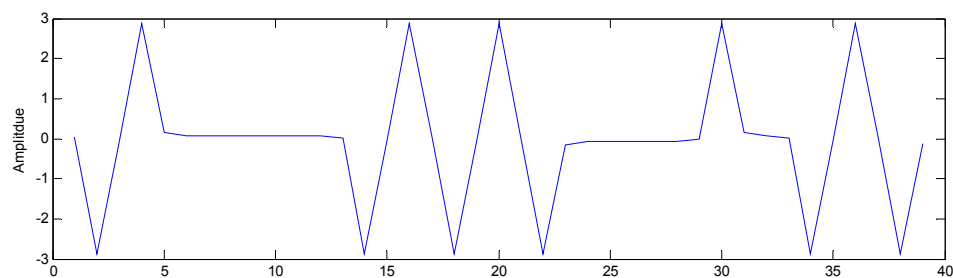
Fig. 4.23. Cross-correlation results using a unique features template that is 64 samples in length.
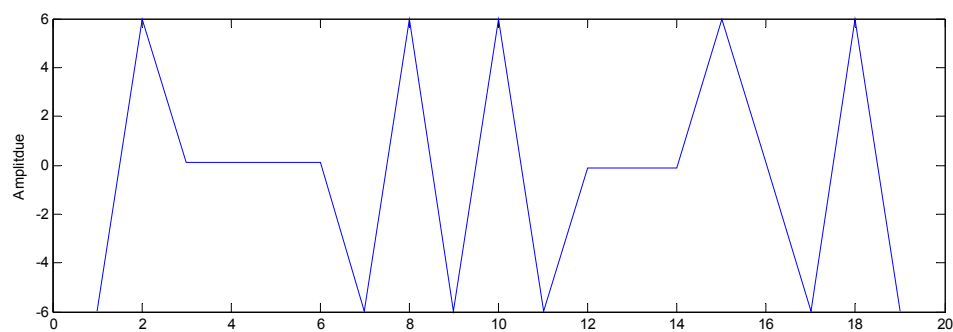
Fig. 4.24. Cross-correlation results using a unique features template that is 128 samples in length.

4.4   Selection of Wavelets to be Used for Automatic Modulation Recognition

Sixty-five wavelets are considered in this dissertation for possible use in constructing an AMR processor. In order to find the most suitable wavelet, or wavelets, for use in the WD AMR process, custom matrix images are generated. The images are based on the auto- and cross-correlation data of the unique features templates and the common features templates that had been constructed using the 65 different candidate wavelets.

The candidate wavelets considered in this study include:

1. Haar wavelet

2. Mexican wavelet

3. Morlet wavelet

4. Meyer wavelet

5. Discrete Meyer wavelet

6. The family of Daubechies wavelets (db1-db10)

7. Symlets (sym2-sym8)

8. Coiflets (coif1-coif5)

9. Biorthogonal spline wavelets (bior1.1, 1.3, 1.5, 2.2, 2.4, 2.6, 2.8, 3.1, 3.3, 3.5, 3.7, 3.9, 4.4, 5.5, 6.8)

10. Reverse biorthogonal spline wavelets (rbio1.1, 1.3, 1.5, 2.2, 2.4, 2.6, 2.8, 3.1, 3.3, 3.5, 3.7, 3.9, 4.4, 5.5, 6.8)

11. The Gaussian wavelet family (gaus1-gaus8)

Since there are two categories of templates representing the WD signatures, i.e., unique features templates and common features templates, two sets of matrix images are developed to aid in the determination of the suitable choice of wavelet(s) for the WD AMR process.

To summarize, the goals of this section are:

1. From the auto-correlations of all templates, to identify the wavelet(s) that produces large magnitude results for all three modulation schemes (i.e. BASK, BFSK, and BPSK).

2. To verify that the cross-correlations of all templates, i.e., the WD signatures between the three modulation schemes are weak. This verification would support the creation of an AMR process based on WD signatures.

4.4.1 Selection of Wavelets Using Unique Features Templates

Each of the binary digital modulation schemes, i.e., BASK, BFSK, and BPSK, produce two unique features templates. For the purpose of clarity, the unique features template for the transition from symbol '0' to symbol '1' is denoted as "Template 1," and "Template 2" is used to denote transitions from symbol '1' to symbol '0'. This nomenclature is used for the unique features templates for all three binary modulation schemes.

The matrix image created in this section contains the cross-correlation values between all unique features templates for all three modulation schemes. The matrix image is used to help identify the most suitable wavelet(s) for WD AMR. Note that either Template 1, or Template 2 for each of the modulation schemes could be used in this procedure. Of

course, two such cross-correlation studies may be performed; one with Template 1s for the various modulation schemes, and the other using Template 2. However, both studies would be redundant because the desired wavelet(s) can be identified from just one matrix image.

The procedure for constructing the matrix image is described as follows:

Step 1: Express BASK, BFSK, and BPSK test signals in the WD using each of the 65 wavelets.

Step 2: Extract the unique features templates from each of the WD scalograms. (This step results in 65 versions of Template 1 and 65 versions of Template 2, although use of only Template 1 is sufficient).

Step 3: Cross-correlate all 65 **BASK** Template 1s with all 65 **BASK** Template 1s.

Step 4: Cross-correlate all 65 **BASK** Template 1s with all 65 **BFSK** Template 1s.

Step 5: Cross-correlate all 65 **BASK** Template 1s with all 65 **BPSK** Template 1s.

Step 6: Repeat Steps 3-5 using BFSK Template 1s instead of BASK Template 1s.

Step 7: Repeat Steps 3-5 using BPSK Template 1s instead of BASK Template 1s. (Steps 3-7 result in a total of 9 sets of auto- and cross-correlation results.)

Step 8: Arrange all 9 sets of results into a matrix, as shown in Fig. 4.25.

BASK $\otimes$ BASK	BASK $\otimes$ BFSK	BASK $\otimes$ BPSK
BFSK $\otimes$ BASK	BFSK $\otimes$ BFSK	BFSK $\otimes$ BPSK
BPSK $\otimes$ BASK	BPSK $\otimes$ BASK	BPSK $\otimes$ BPSK

Fig. 4.25. Cross-correlation values arranged in sub-matrices within the matrix image.

Within the matrix image illustrated in Fig. 4.25, there are 9 sub-matrices. These sub-matrices are arranged in the typical manner wherein the diagonals of each sub-matrix contain the auto-correlations of each template with itself. An example of the arrangement of the data in the sub-matrices is illustrated in Fig. 4.26 in which 65 wavelets are considered.
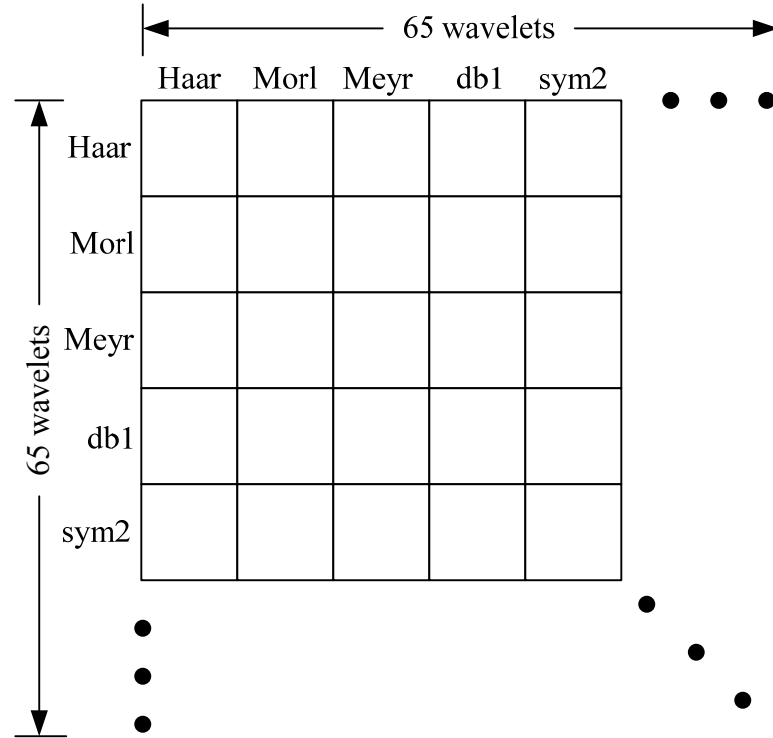
Fig. 4.26. An example of the construction of the sub-matrices.

As seen in Fig. 4.26, each cell in the sub-matrix contains the cross-correlation data of the templates with specific candidate wavelets according to the header of each row and column.

In this study only Template 1 has been used for all 3 modulation schemes. The auto- and cross-correlations of all 65 Template 1s for all 3 modulation schemes are arranged in the matrix image shown in Fig. 4.27.

In order to determine the most suitable wavelet(s) from examination of the matrix image, the data are subjected to hard-thresholding. The first threshold value used is $\Delta = 0$. Since negative cross-correlation coefficients in this case imply that the two templates are

reverse in shape, such data are discarded. The matrix image in Fig. 4.27 illustrates the effect of this thresholding.
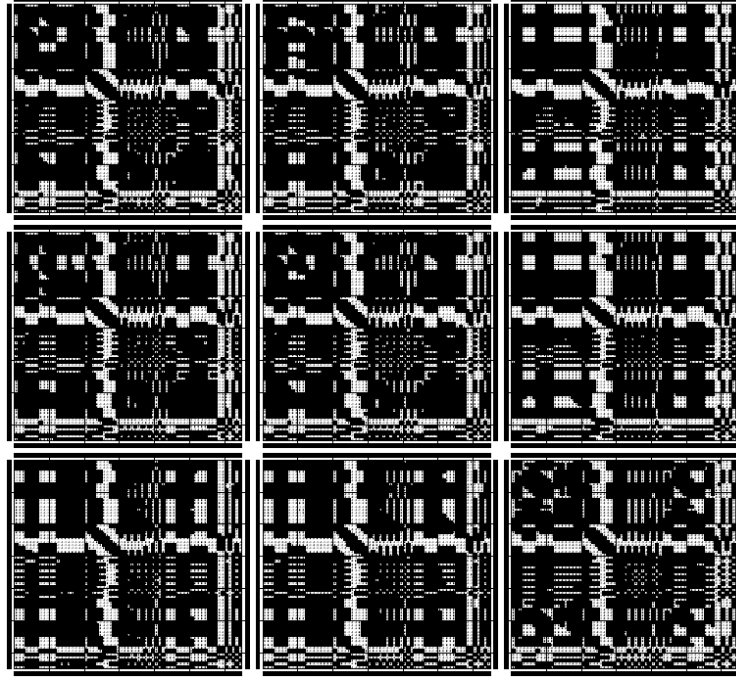
Fig. 4.27. Matrix image with a threshold value $\Delta = 0$.

In the matrix image shown in Fig. 4.27, white spots incidate a cross-correlation value that has been discarded. Conversely, black spots indcate a value that has been retained. It had been observed that the largest cross-correlation value from among the remaining data has a magnitude approximately equal to 11. Therefore, the data are subjected to three heuristic thresholds. The thresholds are $\Delta = 1$, 2, and 2.5. The results of thresholding are illustrated in Figs. 4.28-4.30 for the three different threshold values.
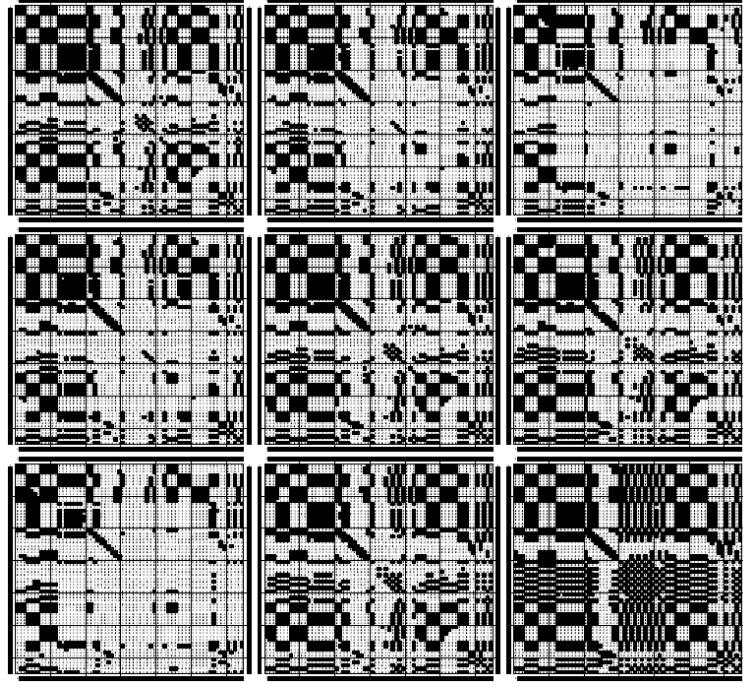
Fig. 4.28. Matrix image with a threshold value of Δ = 1.

In Fig. 4.28, the threshold value Δ = 1, is seen to be too low. This observation is made because there are still too many large-valued cross-correlation data remaining. Due to this, it is not possible to identify the desired wavelets, i.e., wavelets that produce Template 1s that result in large magnitude correlation values for all of the three modulation schemes.

A higher threshold value must, therefore, be applied. Next, the threshold value Δ = 2 is used, and the resulting matrix image is shown in Fig. 4.29. In this image a suitable wavelet is identifiable. The chosen wavelet is the Reverse Biorthogonal Spline 1.3 (rbio 1.3). The auto- and cross-correlation values corresponding to the templates based on this wavelet are shown within the circles that are included in Fig. 4.29.

The solid circles indicate the auto-correlation values corresponding to the Template 1s based on the rbio1.3 wavelet. The dotted circles indicate the locations of the cross-correlation values of the templates that are based on rbio1.3. This observation is critical for the AMR process since it implies that Template 1, based on rbio1.3, of one modulation scheme will not strongly correlate with a unique feature of another modulation scheme.
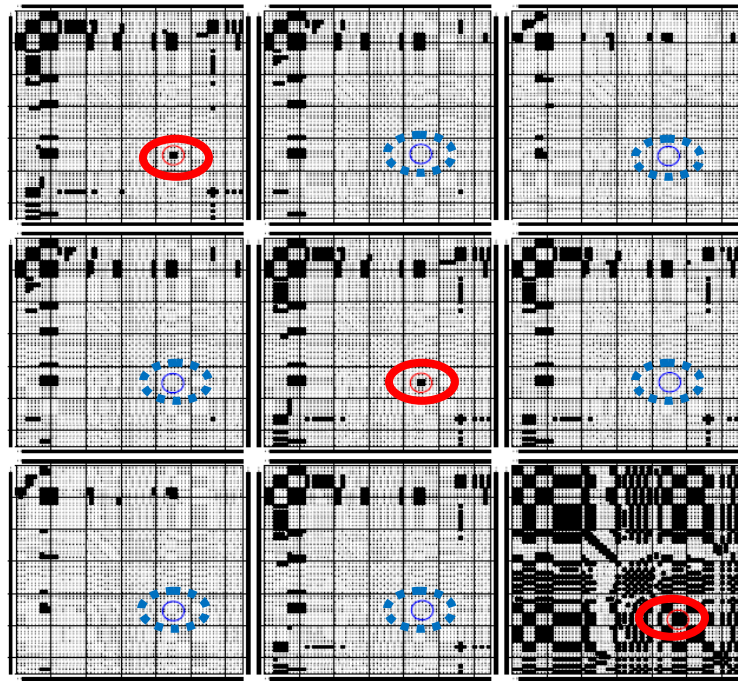
Fig. 4.29. Matrix image with a threshold value of $\Delta = 2$.

For the sake of completeness, an even higher threshold value $\Delta = 2.5$ is also used. The resulting matrix image is provided in Fig. 4.30. It is seen that most results have been discarded, and hence, no common wavelet(s) can be identified with this large of a threshold.
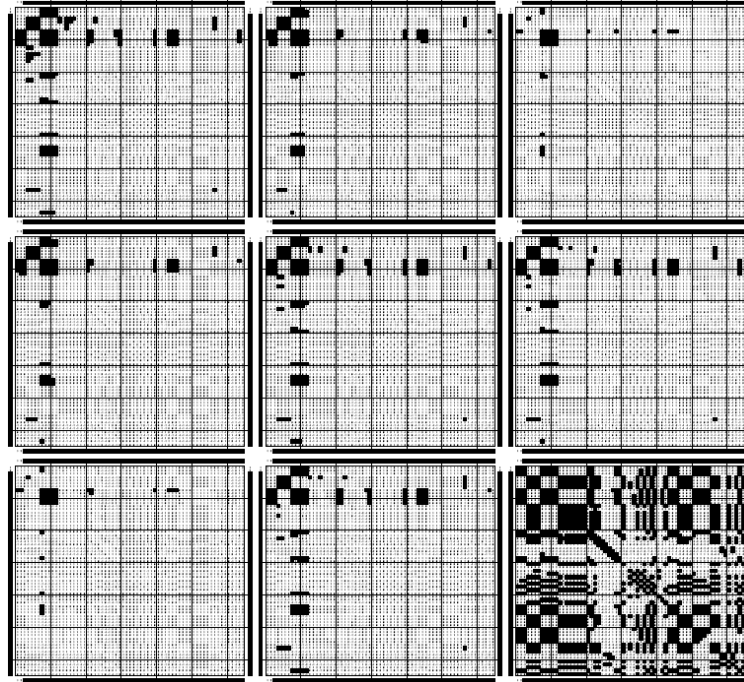
Fig. 4.30. Matrix image with a threshold value of $\Delta = 2.5$.

4.4.2 Selection of Wavelets Using Common Features Templates

The exact procedure used in Section 4.4.1 is now applied to determine the most suitable wavelet(s) on which the common features templates can be based. The only difference in this case is that the common features templates are used instead of the unique features templates.

The common features templates to be used for the creation of the matrix image in this case are highlighted in boxes in as shown Fig. 4.31. Once again the dotted vertical lines in Fig. 4.31 indicate the symbol boundaries in the modulated signals.
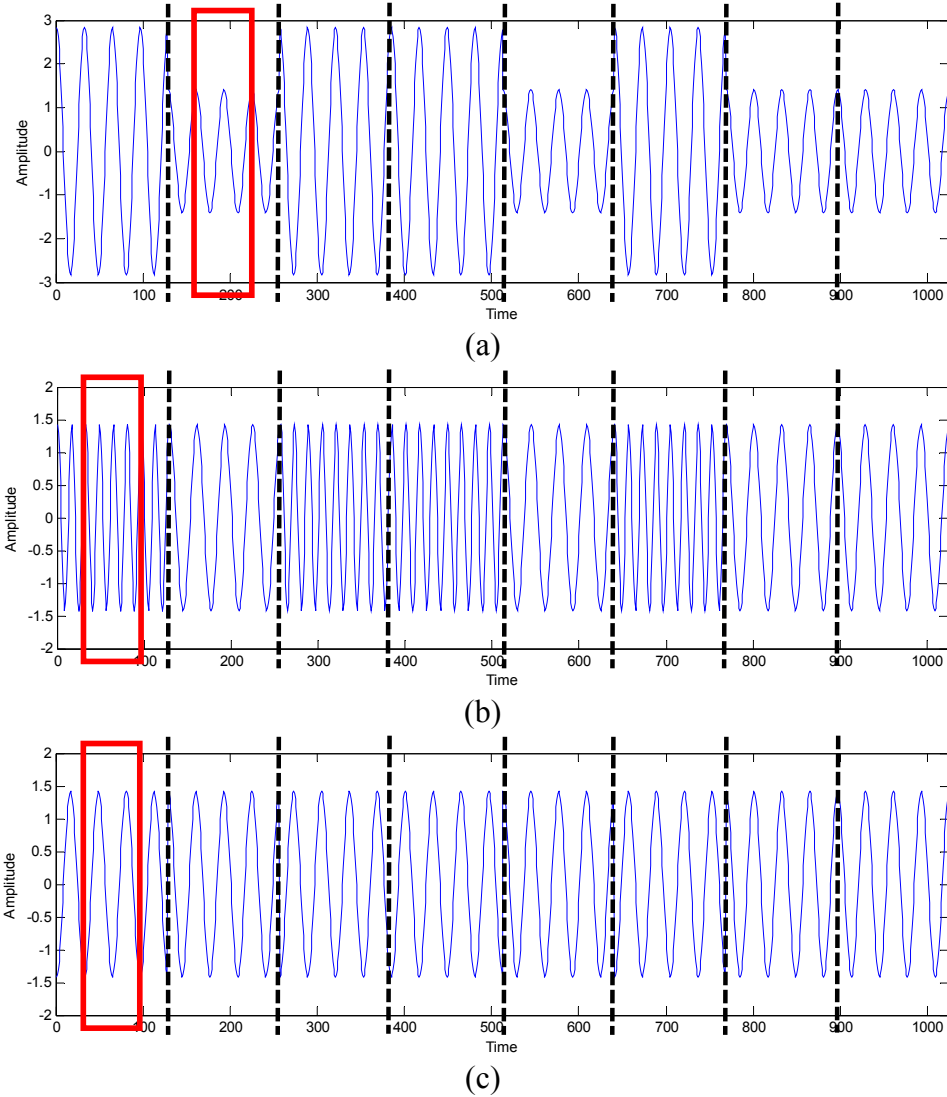
Fig. 4.31. Common feature templates highlighted in boxes in (a) BASK signal, (b) BFSK signal, and (c) BPSK signal.

The arrangement of the sub-matrices within the master matrix image is the same as that described in Fig. 4.25.

In the matrix image shown in Fig. 4.32, the largest cross-correlation result has a magnitude approximately equal to 14. The first heuristic threshold value of $\Delta = 1$ is selected, and the data that are lower than this threshold are discarded. From the large

number of white spots present in Fig. 4.32, it is seen that most of the data are, in fact, discarded. Hence, a suitable wavelet can be immediately identified.

The solid circles on the major diagonal of the matrix image indicate the auto-correlation values of the various templates in the WD that are large in magnitude for all 3 modulation schemes. The dotted circles indicate the locations of cross-correlation values corresponding to the same wavelet. It is seen that the values in these locations have been discarded during thresholding. This implies that the candidate wavelet is not sensitive enough when templates of common features representing one of the distinct variations, e.g., amplitude, frequency or phase, based on the candidate wavelet are cross-correlated with templates corresponding to any of the other distinctive features using the same wavelet. It is observed that the most suitable wavelet to be utilized in the WD AMR process is once again the rbio1.3 wavelet. This is the same wavelet identified in the case of the unique features templates as described in Section 4.4.1.
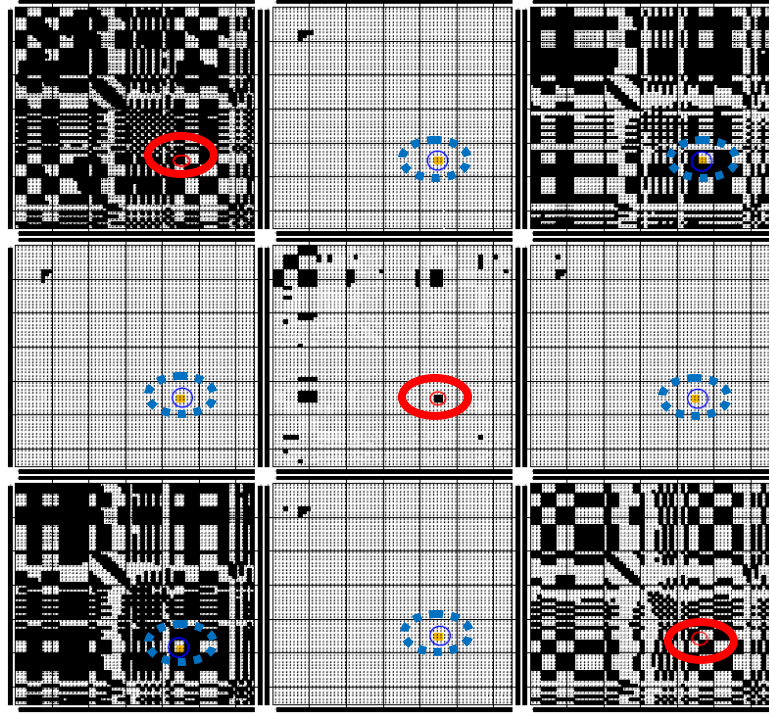
Fig. 4.32. Matrix image based on the common features templates, with a threshold value

of $\Delta = 1$.

4.5   Discussion of Methodologies

In this chapter, three important preliminary steps have been described that are required for the development of the WD AMR process.

The first step is the definition of WD templates based on the features contained within a binary digitally modulated communications signal. Specifically, two categories of templates are defined for each modulation scheme: unique features templates and common features templates.

For higher-order modulation schemes, it is must be noted that the number of unique feature templates that are required for AMR can be very large. This is due to the fact that

higher-order modulation schemes contain more unique features, due to an increased number of possible symbol transitions, when compared to lower-order modulation schemes. Table 4.1 shows the number of unique features templates that must be extracted from different modulation schemes for the subsequent use in the WD AMR process.

Table 4.1 Number of unique features templates needed for different modulation schemes.

Modulation Scheme	Number of Unique Features Templates Needed
BASK	2
4-ASK	16
BFSK	2
4-FSK	16
BPSK	2
QPSK	16
8-PSK	64
4-QAM	16
16-QAM	256
64-QAM	4096
256-QAM	65536

From Table 4.1, it is easily seen that as the order of the digital modulation scheme increases, the number of unique features templates required for the WD AMR process also increases rapidly. Therefore, it can be concluded that the computational effort for classifying the correct type of modulation scheme will also be significantly increased.

Due to this observation, the unique features templates will only be used for developing a WD AMR process for classifying binary digitally modulated communications signals.

On the other hand, the common features templates do not suffer from such a disadvantage because a minimum of 2 templates to a maximum of only 28 templates are needed to adequately represent all of the digital modulation schemes considered in this study. The common features templates are, therefore, used to develop a WD AMR process for all of the modulation schemes listed in Table 4.1.

In the second preliminary step, WD templates having lengths of 32, 64, and 128 samples were studied. As shown in Figs. 4.22-4.24, it was observed that those templates composed of 64 and 128 samples demonstrate stronger cross-correlation results between the templates and the test communications signals. Due to this observation, the WD templates that are 32 samples in length are discarded. Therefore, templates that are either 64, or 128 samples in length can be used in developing the WD AMR process since such templates produce the required resolution in the WD cross-correlation operations. It will be seen in Chapters 5 and 6 that using templates that are $N/2$ samples in length is sufficient for very high correct classification rates to be achieved by the AMR process. Here, N is the number of samples in each signal segment that represents a data symbol. This is also the case in WD Demodulation, which is described in Chapter 7.

In the third, and final, preliminary step, matrix images that contain the cross-correlation results of WD templates for BASK, BFSK, and BPSK signals, based on different wavelets, were created. Two studies were conducted: one using the unique features templates and the other using the common features templates. On subjecting the data in

the matrix images to hard-thresholding with different heuristic threshold values, it has been found that the most suitable wavelet for developing the WD AMR process is the rbio1.3 wavelet.

In Chapters 5 and 6, two fundamental WD AMR algorithms are developed, using the rbio 1.3 wavelet, based on the unique features templates and the common features templates, respectively.

Chapter 5

Automatic Modulation Recognition Process Using Unique Features Templates

AMR can be described as blind identification of the modulation scheme used to format digital data embedded in a received signal. In this dissertation, the main focus is on developing a methodology for AMR using WTs in conjunction with pattern recognition. The WD AMR method employs the concept of template matching for modulation identification prior to signal demodulation in order to recover the original data bit sequences over a wide range of SNR values.

The WD AMR process described in this chapter involves the use of unique features templates that have been developed in Chapter 4. The unique features templates represent signal features that distinguish the transitions from data symbol '0' to data symbol '1' and vice versa. The transitions are indicated by a change in the amplitude, frequency and/or phase of a digitally modulated signal. It was identified in Chapter 4 that this set of templates is suitable for blind identification of binary digitally modulated communications signals acquired by a communications receiver. The specific modulation schemes considered here are BASK, BFSK, and BPSK.

5.1   Development of the Automatic Modulation Recognition Process Using Unique Features Templates

Prior to developing the WD AMR process using unique features templates, the templates and the wavelet were identified. As demonstrated in Chapter 4, the rbio1.3 wavelet has

been identified as the most suitable wavelet for the extraction of both the unique features and the common features templates. In this chapter, the focus is on the development of a WD AMR process that makes use of the unique features templates for binary communications signal since large numbers of unique features templates are required in the case of higher-order digitally modulated communications signals.

Each of the binary digitally modulated signals considered in this dissertation require two unique features templates, which are expressed in the WD and are based on the symbol transitions that are present within a signal. Unique features templates, in both time- and wavelet-domains, are illustrated graphically in Figs. 5.1-5.3. There are a total of six unique features templates needed to represent all three binary digital modulation schemes.

(a)

(b)

(c)

(d)
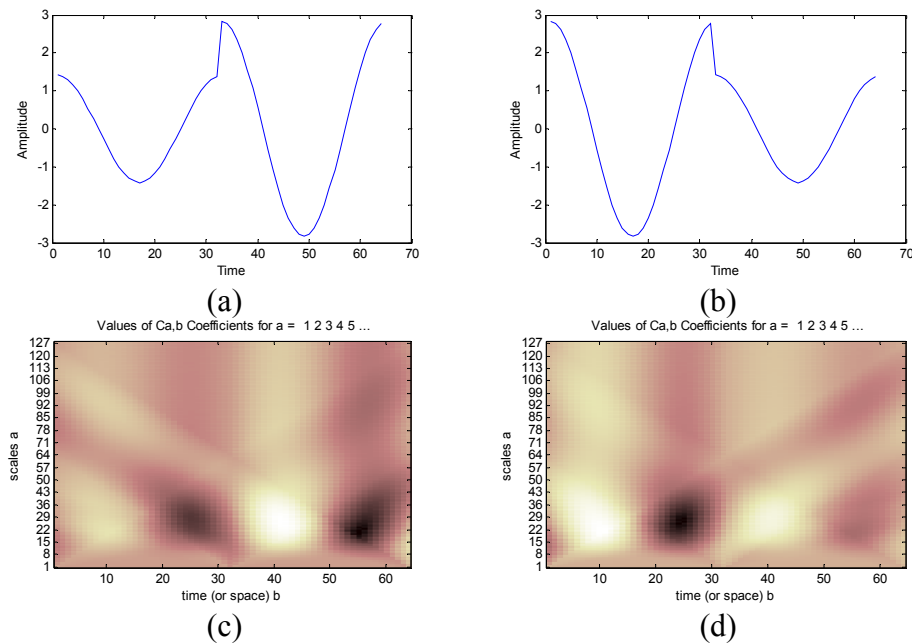
Fig. 5.1. Unique features templates for BASK signal (a-b) in time-domain, (c-d) in wavelet-domain.
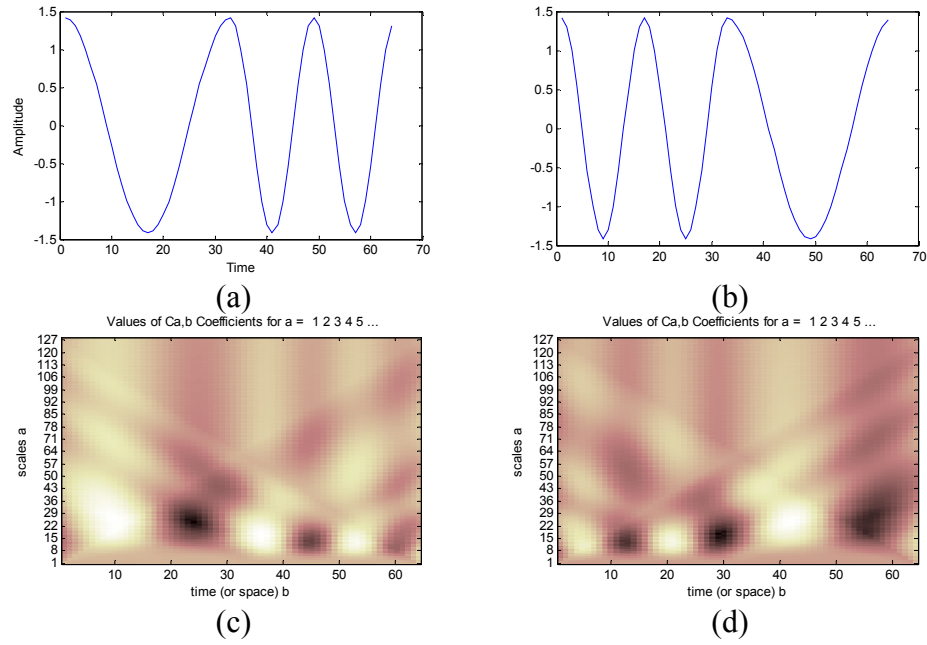
Fig. 5.2. Unique features templates for BFSK signal (a-b) in time-domain, (c-d) in wavelet-domain.
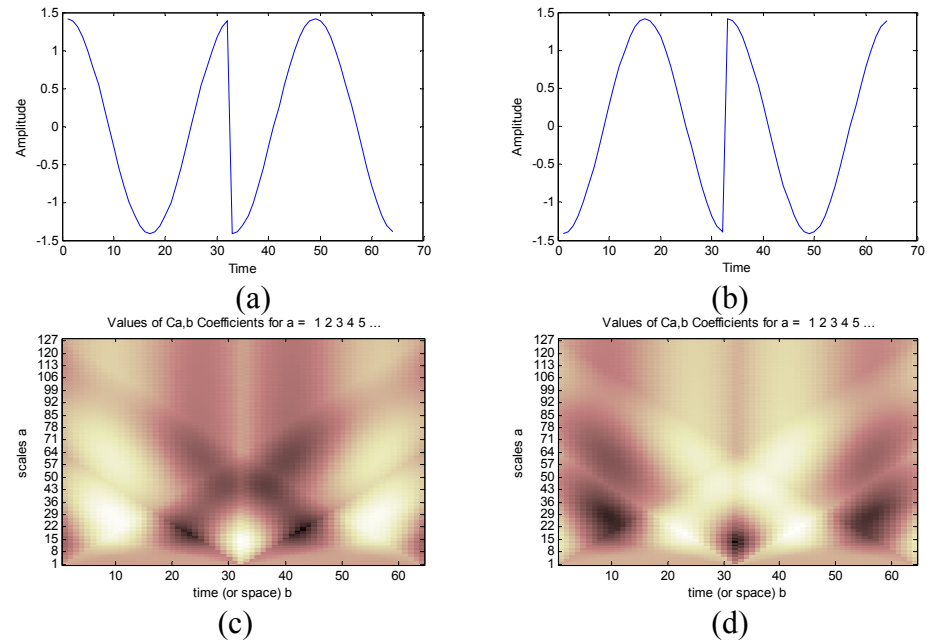
Fig. 5.3. Unique features templates for BPSK signal (a-b) in time-domain, (c-d) in wavelet-domain.

The noise-free WD unique features templates seen in Figs. 5.1-5.3 are based on representing the corresponding time-domain functions in the wavelet-domain using the rbio1.3 wavelet. These templates are stored for use in the WD AMR process. The WD AMR process using unique features templates is implemented according to the following algorithm:

Step 1:   Compute the CWT of the received binary digitally modulated signal up to 128 levels of resolution using the rbio1.3 wavelet.

Step 2:   Cross-correlate the WD signal obtained in Step 1 with each of the six unique features templates separately. Each template is to be cross-correlated with the signal at every baseband symbol location.

Step 3:   Select the cross-correlation values obtained using the two BASK templates. Compare the two values, one for each template, obtained at each symbol location, and select the larger value. Next, create a new record of all values selected in this manner, which is called the "time-and-merged" operation for the AMR process. This operation is depicted pictorially in Fig. 5.4.

Step 4:   Repeat Step 3 using the BFSK templates, and then repeat Step 3 again using the BPSK templates.

Step 5:   Compare data elements in each of the sets of cross-correlation values obtained with various templates. Select the largest values to form the "time-and-merged" cross-correlation results. Record the template type to which the value belongs, i.e., whether BASK, BFSK or BPSK.

Step 6:   Decide upon the specific modulation scheme employed by the received communications signal to be the same as the template type that was selected most often in Step 5, i.e., classification of the modulation type is accomplished via a majority vote procedure.

The algorithm described above is illustrated in the form of a block diagram in Fig. 5.5.

Fig. 5.4. Example of a "time-and-merged" operation in the WD AMR process.

Digitized
Received Signal

Fig. 5.5. Block diagram of the WD AMR process using unique features templates.

An important procedure in the WD AMR process is the "time-and-merged" operation described in Step 3 of the algorithm which is illustrated pictorially in Fig. 5.4. For the example illustrated in the figure, a BASK test signal having a frame length of 8 symbols is cross-correlated with the two BASK unique features templates at various data symbol locations. Then, the cross-correlation values obtained using both templates at each symbol period are compared. The cross-correlation result having the largest value is

selected. This resulting set of data are termed the "time-and-merged" cross-correlation values. These values are used in the WD AMR process for identification of the unknown modulation scheme of a received signal. In Fig. 5.4, L denotes a small cross-correlation value, and H represents a large cross-correlation value.

An example of recognition of a BASK signal is illustrated in Fig. 5.6. In the figure, the top row is representative of a BASK signal having a random data bit sequence. The BASK signal is input to a communications receiver that is initially unaware of the actual modulation type. The received BASK signal is a noisy digitally modulated signal that is transformed into the wavelet-domain using the rbio 1.3 wavelet. Hence, in actuality, the BASK signal in the top row of Fig. 5.6 is a WD scalogram.

In the WD AMR process illustrated in Fig. 5.5, the received signal is transformed and cross-correlated with 6 unique features templates (2 templates for each of the 3 binary modulation schemes). Consequently, 3 sets of "time-and-merged" cross-correlation results are generated. In Fig. 5.6, the following notations are used:

H   High cross-correlation value

L   Low cross-correlation value

M_A Intermediate cross-correlation value within the BASK template dataset

M_F Intermediate cross-correlation value within the BFSK template dataset

M_P Intermediate cross-correlation value within the BPSK template dataset.

The "time-and-merged" results are then used in the decision making operation in the AMR process.

BASK Signal bit sequence	1	1	0	1	1	0	0	1

Cross-correlation with BASK Template 1	M_A	**H**	L	M_A	**H**	M_A	L
Cross-correlation with BASK Template 2	M_A	L	**H**	M_A	L	M_A	**H**
Cross-correlation with BFSK Template 1	M_F	M_{F1}	M_F	**H**	M_F	M_F	M_F
Cross-correlation with BFSK Template 2	M_F	M_{F2}	M_F	L	M_F	M_F	M_F
Cross-correlation with BPSK Template 1	**H**	M_P	M_P	M_P	M_P	L	M_P
Cross-correlation with BPSK Template 2	L	M_P	M_P	M_P	M_P	**H**	M_P
BASK "time-and-merged" cross-correlation results	M_A	**H**	**H**	M_A	**H**	M_A	**H**
BFSK "time-and-merged" cross-correlation results	M_F	M_F	M_F	**H**	M_F	M_F	M_F
BPSK "time-and-merged" cross-correlation results	**H**	M_P	M_P	M_P	M_P	**H**	M_P
	BPSK	**BASK**	**BASK**	BFSK	**BASK**	BPSK	**BASK**

Fig. 5.6. Example of WD AMR process using the unique features templates.

The "time-and-merged" results for the example are highlighted in the box shown in Fig. 5.6. For each symbol period, the three "time-and-merged" data results are compared. The template having the best match to a candidate modulation type is identified based on the largest value contained in the "time-and-merged" data. The classification of the unknown modulation scheme is then accomplished via a majority vote of all the element-wise template identifications previously made. In the example of Fig. 5.6, BASK templates are

identified as being present in the received signal most often. Therefore, the modulation scheme employed by the received test signal is recognized to be that of BASK.

5.2   Simulation Experiment and Results

All of the binary digitally modulated test signals used in this study have been corrupted by zero-mean AWGN during transmission to produce received signals with SNR values in the range of -5 dB to 10 dB. The rates of correct classification produced by the WD AMR algorithm based on the unique features templates have been obtained using 20,000 Monte Carlo trials, where each simulation experiment employs 50 bits per frame. Each test signal used in the 20,000 trials randomly employs one among the BASK, BFSK, or BPSK modulation schemes.

The signals are oversampled by a factor of sixteen over the Nyquist rate corresponding to the carrier frequency. Oversampling is used because more signal content can be represented in the WD scalogram, which can then enhance the WD AMR process. Perfect symbol timing with no timing offset is also assumed throughout this dissertation.

All simulations have been performed using MATLAB. The results of the simulations are provided in Tables 5.1-5.4, which contain the rates of correct classification of signals with unknown modulation schemes corrupted by AWGN resulting in SNR values of 10 dB, 5 dB, 0 dB, and -5 dB.

Table 5.1 Rates of correct classification for SNR = 10 dB [85]

		Signal classified as (%)		
		BASK	BFSK	BPSK
T_X Signal	BASK	100	0	0
	BFSK	0.37	99.63	0
	BPSK	0.27	0	99.73

Table 5.2 Rates of correct classification for SNR = 5 dB [85]

		Signal classified as (%)		
		BASK	BFSK	BPSK
T_X Signal	BASK	100	0	0
	BFSK	0.85	98.70	0.45
	BPSK	0.27	0	99.73

Table 5.3 Rates of correct classification for SNR = 0 dB [85]

		Signal classified as (%)		
		BASK	BFSK	BPSK
T_X Signal	BASK	100	0	0
	BFSK	3.48	94.08	2.44
	BPSK	0.27	0	99.73

Table 5.4 Rates of correct classification for SNR = -5 dB [85]

		Signal classified as (%)		
		BASK	BFSK	BPSK
T_X Signal	BASK	100	0	0
	BFSK	34.39	54.0	11.61
	BPSK	0.27	0	99.73

5.3   Comparison of Results

In order to provide a point of reference to assess the quality of the results obtained in this research, several prior works using both WT-based and non-WT-based AMR methods have been surveyed. The best results obtained in these studies, as reported in the literature, are presented in Tables 5.5-5.7 for convenient comparison. In the tables, the symbol * denotes a WT-based method.

It must be pointed out that a direct comparison of the results obtained in this research with the results published in prior studies is not possible. This is due to the fact that the various studies do not necessarily make the same general *a priori* assumptions, do not use the same SNR values, and do not use the same Monte Carlo simulation parameters, such as number of symbols per transmission, etc.

Table 5.5 Survey of the literature for BASK classification [85]

AMR method devised by	Correct classification at highest SNR (%)	Correct classification at lowest SNR (%)
Hossen, et al. [38]	82.5 at 5 dB	97.5 at 3 dB
Azzouz, et al. [32]	100 at 20 dB	98.25 at 10 dB
Lopatka, et al. [42]	100 at 30 dB	~92 at 0 dB
Yang, et al. [15]	-	97.5 at 10 dB
This work	**100 at 10 dB**	**100 at -5 dB**

Table 5.6 Survey of the literature for BFSK classification [85]

AMR method devised by	Correct classification at highest SNR (%)	Correct classification at lowest SNR (%)
Azzouz, et al. [32]	100 at 20 dB	91.25 at 10 dB
Ho, et al. [58]*	-	100 at 13 dB
Jin, et al. [54]*	100 at 13 dB	95.3 at 8 dB
Ou, et al. [53]*	100 at 20 dB	~54 at -5 dB
Hossen, et al. [38]	100 at 5 dB	75 at 3 dB
This work	**99.3 at 10 dB**	**~54 at -5 dB**

Table 5.7 Survey of the literature for BPSK classification [85]

AMR method devised by	Correct classification at highest SNR (%)	Correct classification at lowest SNR (%)
Azzouz, et al. [32]	90.75 at 20 dB	96.25 at 10 dB
Dobre, et al. [9]	-	100 at 2 dB
Ho, et al. [58]*	-	98 at 13 dB
Jin, et al. [54]*	100 at 13 dB	99.5 at 8 dB
Ou, et al. [53]*	100 at 20 dB	~54 at -5 dB
Hossen, et al. [38]	100 at 5dB	87.5 at 3dB
This work	**99.7 at 10 dB**	**99.7 at -5 dB**

Two prior WT-based AMR studies involve computing the histogram of the CWT coefficients of the received signals and then counting the number of peaks in the histogram in order to classify the received signal as either BPSK or BFSK [53], [58]. The rates of correct classification for BPSK signals is 98% and for BFSK signals is 100% at an SNR = 13 dB in [58]. For the classification rates reported in [53], both BPSK and BFSK modulation were recognized at a rate of 100% at SNR = 20 dB. However, a rate of only 54% was achieved at SNR = -5 dB for both modulation types. In this work, the rates of correct classification are 100%, 99.3%, and 99.7% at SNR = 10 dB, for BASK, BFSK and BPSK signals, respectively. In the case of SNR = -5 dB, the rates of correct classification are 100% for BASK signals, 54% for BFSK signals, and 99.7% for BPSK signals.

5.4   Conclusions

It is observed from Tables 5.5-5.7 that the rates of correct classification of binary digitally modulated signals realized by the WD AMR process are equal to or better than the rates reported in the literature, especially when compared the WT-based AMR methods.

It has been determined via extensive computer simulations that the rate of correct classification for BASK signals is 100% and for BPSK signals the rate is 99.7% over the range of SNR values considered. The rates of correct classification for BFSK signals are 99.6%, 98.7%, 94.0% and 54% for SNR = 10 dB, 5 dB, 0 dB and -5 dB, respectively.

For the WD AMR process devised in this chapter, there are two important procedural factors that might have a substantial impact on the performance of the AMR process.

The first factor affecting the AMR performance is the number of baseband data symbols that comprise each transmitted signal. As described in Section 5.1, classification of unknown modulation schemes is accomplished based on the "time-and-merged" cross-correlation data via majority vote. Due to this procedure, it is reasonable that longer baseband data symbol sequences in each transmission interval, or frame, may provide better classification rates. Conversely, baseband data sequences of reduced lengths could result in poorer rates of correct classification than those obtained in this study. This hypothesis has been tested using computer simulations. The results reported in Table 5.8 show the rates of correct classification for BPSK signals having baseband symbol sequences of different lengths. The signals have been corrupted by AWGN such that SNR = 0 dB. These results confirm the prediction in that lower rates of correct

classification are obtained with WD AMR using the unique features templates consisting
of baseband symbol sequences of shorter length.

Table 5.8 Rates of correct classification for different baseband symbol sequence lengths
using BPSK signals

Length of the data words (bits)	Correct classification rate at 0 dB
50	99.73%
20	94.34%
10	82.56%

The second factor affecting the performance of the WD AMR process is the choice of
wavelet used. After computing the cross-correlation matrix for the unique features
templates using 65 different wavelets in order to determine the suitable wavelet(s) in
Chapter 4, it was observed that certain wavelets are more sensitive to the unique features
of a particular modulation schemes compared to other modulation schemes. This
observation raises the possibility that better rates of classification for BFSK signals than
those obtained in this study might be attainable using a different wavelet. The choice of
wavelet is determined based on the techniques devised in Chapter 4. From the matrix in
Fig. 4.29, the center sub-matrix represents the cross-correlation values of BFSK
templates expressed in 65 different versions. It is observed that the darker spots within
the sub-matrix show larger cross-correlation value. Some of darker spots only occur
within the sub-matrix, therefore, these spots, which correspond to specific wavelets, can
possibly be used to develop an WD AMR procedure to improve the classification rates

for BFSK signals. This is due to the sensitivity of the specific wavelet to the modulation

characteristics contained within a communications signal.

Chapter 6

Automatic Modulation Recognition Process Using Common Features Templates

The AMR algorithm developed in this chapter is based on the common features templates that have been constructed in the WD. The detailed procedure for the construction of the templates has been provided in Chapter 4. The templates are used in the cross-correlation operations within the AMR process to obtain decision variables. The digitally modulated signals considered in this chapter include M-ary ASK and M-ary FSK for M = 2 and 4; MPSK for M = 2, 4, and 8; and M-ary QAM for M = 4, 16, 64, and 256. The communications signals are corrupted with AWGN in the range of SNR from -5 dB to 10 dB.

In Section 6.1, several preliminary methodologies required for the WD AMR process using the common features templates are described. The WD AMR algorithm is then developed in Section 6.2. The WD AMR process is verified and evaluated. The results are presented in Section 6.3. Comparisons of the rates of correct modulation classification obtained in this study are made with results found in the literature. The comparisons are presented in Section 6.4.

6.1   Development of the Automatic Modulation Recognition Process Using Common Features Templates

As described in Chapter 5, the communications signal is first transformed into the WD using the CWT. The resulting CWT expression of the signal is then cross-correlated with

templates representing WD signatures of the candidate modulated signals. In this second WD AMR algorithm developed within this dissertation, the common features templates are used. Whereas, the unique features templates were used in the WD AMR algorithm presented in Chapter 5.

Recall from Chapter 4, that the common features templates are constructed based on the sinusoidal feature inherent in all of the digitally modulated communications signals considered in this study. In general, the sinusoidal feature is defined as

$$s(t) = \cos(2\pi f_c t) \tag{6.1}$$

where f_c is used to denoted the carrier frequency of the signal.

As mentioned in both Chapters 3 and 4, the sinusoidal features can be extracted at different temporal locations within a data symbol period of a communications signal. A common features template can also be subjected to a time-shift, which would correspond to a phase shift of the carrier signal. Therefore, in general, a common features template, $p(t)$, can be defined as

$$p(t) = \cos(2\pi f_c t + \theta) \qquad T_1 < t < T_2 \tag{6.2}$$

where θ represents the different phase shifts of the sinusoidal carrier, while T_1 and T_2 represent the beginning time and ending time of the template.

It has also been noted in Chapter 4 that temporal shifts of a signal in the time-domain correspond exactly to shifts indicated by the translation variable, b, in the wavelet-domain. Therefore, the phase-shifting operation in the time-domain has the time-shift effect that is desired in the wavelet-domain.

The various common features templates used in the development of the WD AMR process are described for the cases of $\theta = 0$, $\pi/2$, and $5\pi/4$, denoted as Template 1, Template 2, and Template 3, respectively in Fig. 6.1. The common features templates are also expressed in terms of the I (cosine) and Q (sine) signal basis functions, as depicted in Fig. 6.1. Template 1 is based on a cosine carrier with no phase shift. Template 2 is based on the sine carrier that is phase offset by $\pi/2$ radians. Template 3 is based on the cosine carrier basis function having a phase shift of $5\pi/4$ radians.
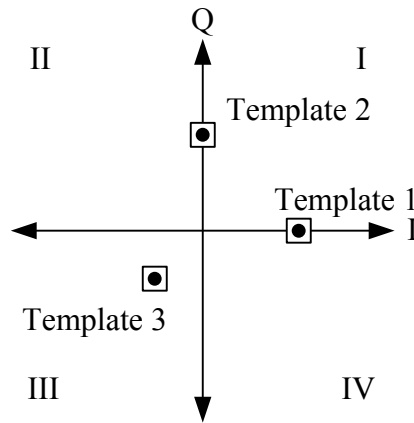
Fig. 6.1. Signal space representation of the three common features templates.

The mathematical models of the communications signals were described in Chapter 3. Template 1 and Template 2 are chosen because the communications signals considered in this work can be described mathematically using either one, or a combination, of the I and Q basis functions. For classification of more complex modulation schemes, a third template must be used. Therefore, Template 3 is introduced for classifying signals such as 8-PSK or 4-QAM.

The WD scalograms of the three common feature templates, T_1, T_2 and T_3, are illustrated in Fig. 6.2.

In Fig. 6.2 (a) the wavelet-domain representation for Template 1 of a sinusoidal carrier of finite duration with no phase shift is illustrated. The WD representation for Template 2 consisting of a phase shift of $\pi/2$ radians is shown in Fig. 6.2 (b). Fig. 6.2 (c) illustrates the WD representation for Template 3 corresponding to a sinusoidal carrier with a phase shift of $5\pi/4$ radians.

(a) $\theta = 0$ (b) $\theta = \pi/2$ (c) $\theta = 5\pi/4$
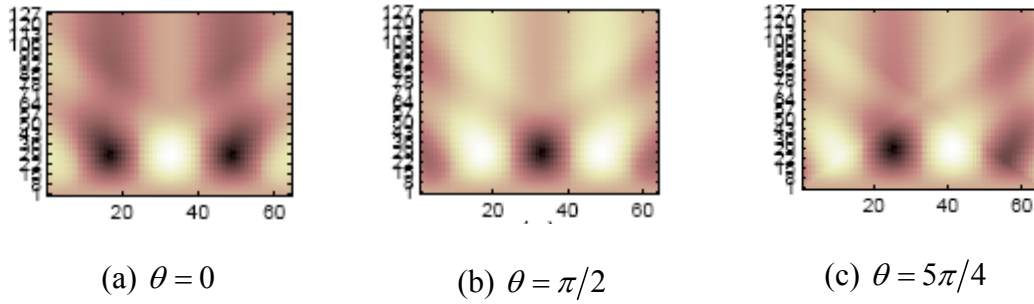
Fig. 6.2. The three common features templates used for the AMR process.

In developing the WD AMR algorithm, the cross-correlation values between the templates and the signal are first investigated. A sinusoidal function having phase shifts in increments of 10° is cross-correlated with Template 1 and Template 2. The signals with different phase shifts can be expressed in term of a signal constellation along a unit circle. Several observations are made based on the cross-correlation values with such sinusoidal signals and the templates.

The cross-correlation results obtained for Template 1 and Template 2 when compared to several sinusoidal functions are computed. The cross-correlation data involving Template 1 and Template 2 are tabulated in Tables 6.1 and 6.2, respectively. The first observation

is that when the signal constellation is within a ±90° swept region about the templates, the cross-correlation value is always positive. With this useful information, the quadrant of the signal location can be determined based on the cross-correlation results obtained with Template 1 and Template 2, as demonstrated in Table 6.3.

Table 6.1 Cross-correlation values of Template 1 and a sinusoidal function with different phase shifts

Phase (°)	Cross-correlation values	Phase (°)	Cross-correlation values	Phase (°)	Cross-correlation values	Phase (°)	Cross-correlation values
0	2.679502	90	0.013226	180	-2.81634	270	0.01876
10	2.697878	100	-0.12014	190	-2.63368	280	0.45944
20	2.520234	110	-0.48417	200	-2.6308	290	0.892583
30	2.273196	120	-0.81969	210	-2.21035	300	1.347197
40	2.050102	130	-1.15634	220	-2.02175	310	1.691355
50	1.732157	140	-1.7986	230	-1.68892	320	2.065244
60	1.336044	150	-1.94411	240	-1.35842	330	2.266879
70	0.903582	160	-2.35955	250	-0.81165	340	2.502652
80	0.451969	170	-2.74354	260	-0.4357	350	2.659614

Table 6.2 Cross-correlation values of Template 2 and a sinusoidal function with different

phase shifts

Phase (°)	Cross-correlation values	Phase (°)	Cross-correlation values	Phase (°)	Cross-correlation values	Phase (°)	Cross-correlation values
0	0.00129	90	2.815686	180	-0.09995	270	-2.70652
10	0.34639	100	2.503755	190	-0.57392	280	-2.52334
20	0.889756	110	2.255107	200	-0.82939	290	-2.4098
30	1.306933	120	2.066662	210	-1.30233	300	-2.11353
40	1.916086	130	1.799082	220	-1.68042	310	-1.86032
50	2.088706	140	1.505474	230	-1.98736	320	-1.46584
60	2.210679	150	0.901692	240	-2.24363	330	-0.77707
70	2.619054	160	0.386802	250	-2.60393	340	-0.35054
80	2.706011	170	0.088836	260	-2.62592	350	-0.11447

Table 6.3 Identification of signal space quadrant using the cross-correlation results of

Template 1 and Template 2

Quadrant	Cross-correlation with Template 1	Cross-correlation with Template 2
I	+	+
II	-	+
III	-	-
IV	+	-

In Figs. 6.3-6.13, the cross-correlation data obtained using a test signal compared with

each of the three common features templates are plotted. Based on observations about the

characteristics associated with from each set of cross-correlation data, the discrimination

of different modulation schemes can be achieved. All the cross-correlation data are normalized to have a dynamic range of -3 to 3. The modulation classification parameters, according to the test signal cross-correlation data, include the dynamic range of the cross-correlation data, as well as the number of distinct levels contained within the set of cross-correlation data. These parameters are used to develop both the WD AMR process and the subsequent WD Demodulation process.

As seen in Figs. 6.3 and 6.4, the cross-correlation results with Template 2 are zero. This is due to the fact that the template and the signals are orthogonal to each other. From the results shown for BASK, the cross-correlation results for Templates 1 and 3 produce a single constant envelope, while the results for 4-ASK contain multi-level data. These observations can be used, in part, for developing the WD AMR algorithm.
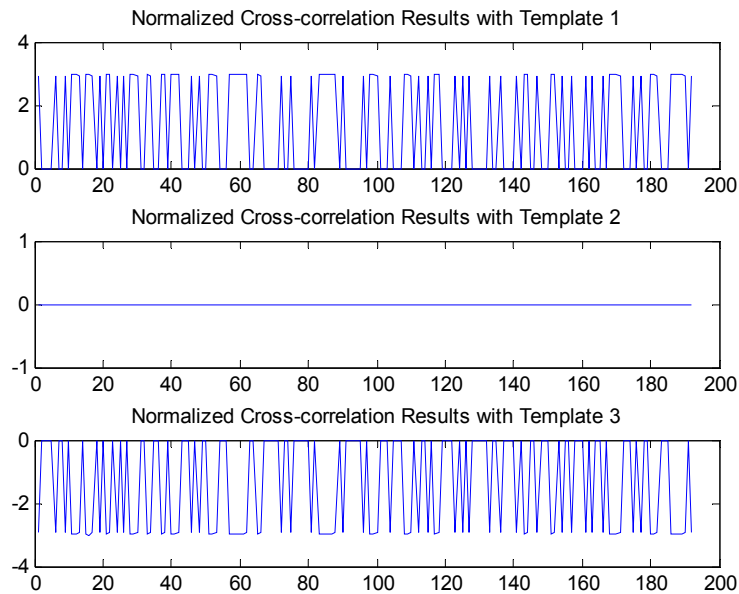
Fig. 6.3. Results of cross-correlation between BASK test signals and the common features templates.
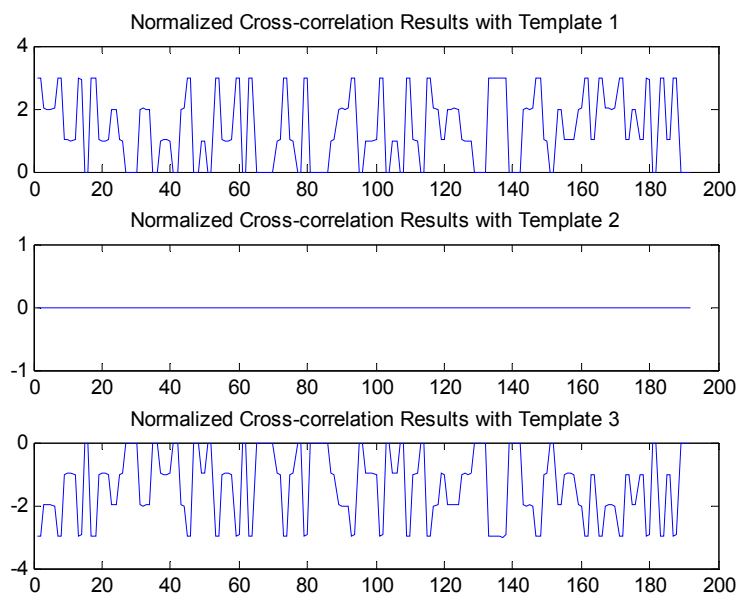
Fig. 6.4. Results of cross-correlation between 4-ASK test signals and the common

features templates.
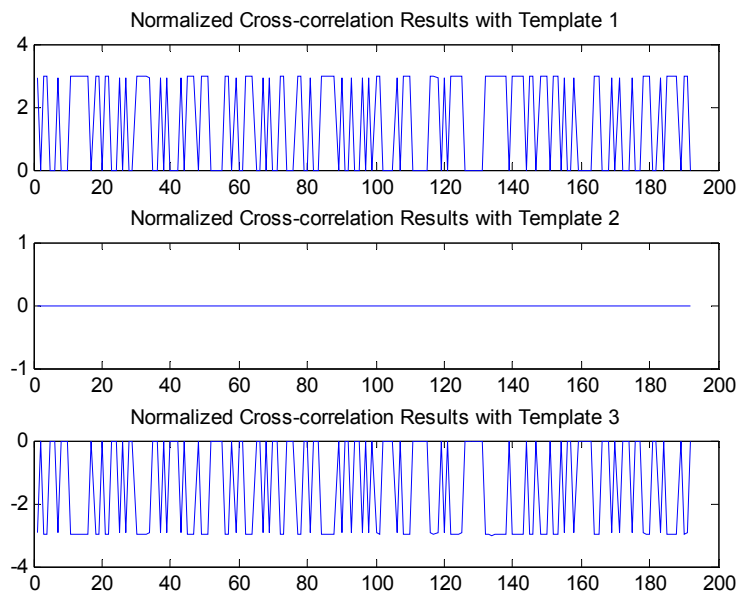
Fig. 6.5. Results of cross-correlation between BFSK test signals and the common features
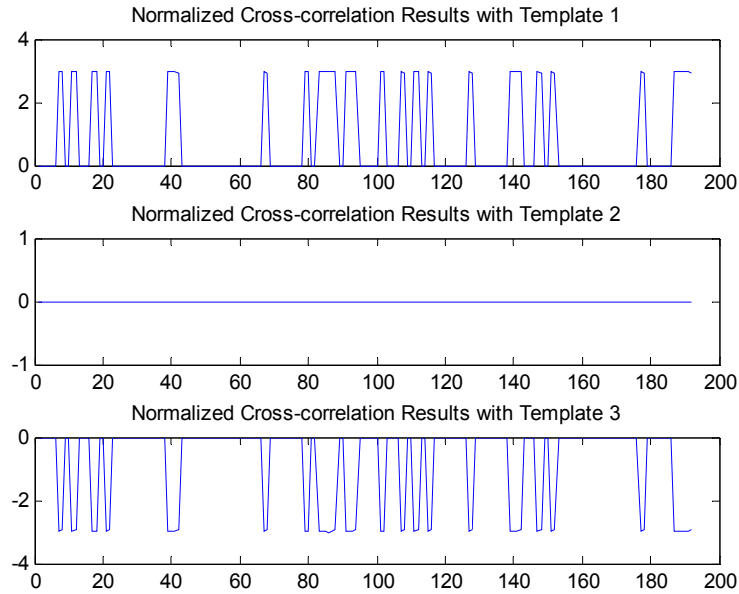
templates.

Fig. 6.6. Results of cross-correlation between 4-FSK test signals and the common

features templates.

In Figs. 6.5 and 6.6, the cross-correlation results for the BFSK and 4-FSK test signals

with all 3 common features templates are shown, respectively. It is seen that plots of the

cross-correlation data obtained using Templates 1 and 3 have constant amplitude

envelopes for both modulation schemes. The results when using Template 2, however,

are zero for both modulation schemes. This is due to the fact that the signal is orthogonal

to the template as noted previously for ASK signals.

Due to the similarity of the correlation results shown for both BFSK and 4-FSK signals,

i.e., the constant envelope for both correlation results with Template 1 and Template 3,

and the zero cross-correlation result with Template 2, it is necessary to introduce

additional templates for use in the WD AMR process.
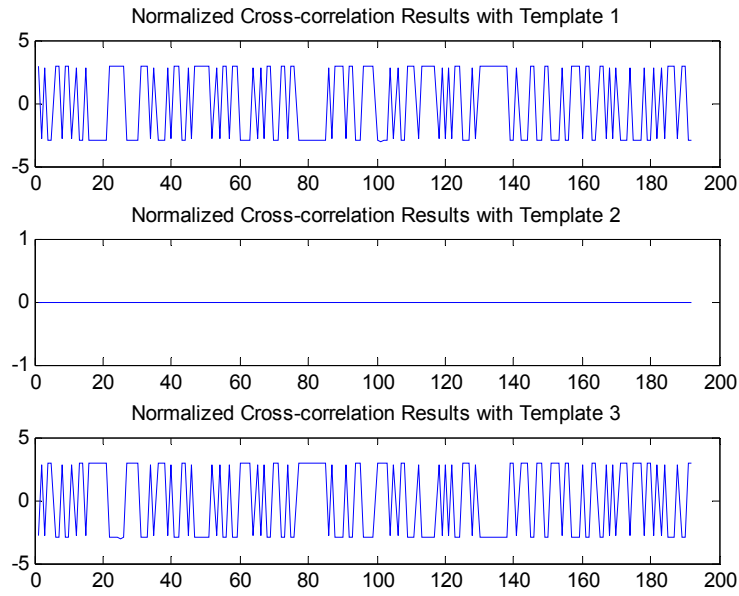
Fig. 6.7. Results of cross-correlation between BPSK test signals and the common features templates.

The WD cross-correlation values for BPSK, QPSK and 8-PSK signals with all 3 common features templates are plotted in Figs. 6.7-6.9, respectively. Among the 3 modulation schemes, only the correlation results for the BPSK test signal with Templates 1 and 3 shows the property of having a constant amplitude envelope, as seen in Fig. 6.7. This constant envelope property has also been exhibited by the WD cross-correlation values for the M-ary ASK and M-ary FSK test signals, as seen in Figs. 6.3-6.6.

The difference between these sets of results is the dynamic range of the cross-correlation values. The dynamic range of the BPSK test signals is that from -3 to 3, while the dynamic range of the M-ary ASK and M-ary FSK test results is strictly positive between 0 and 3.
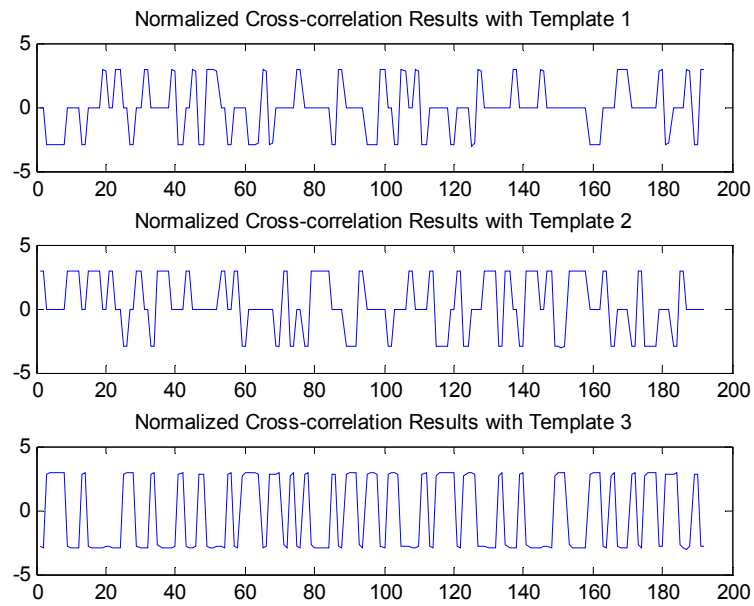
Fig. 6.8. Results of cross-correlation between QPSK test signals and the common

features templates.
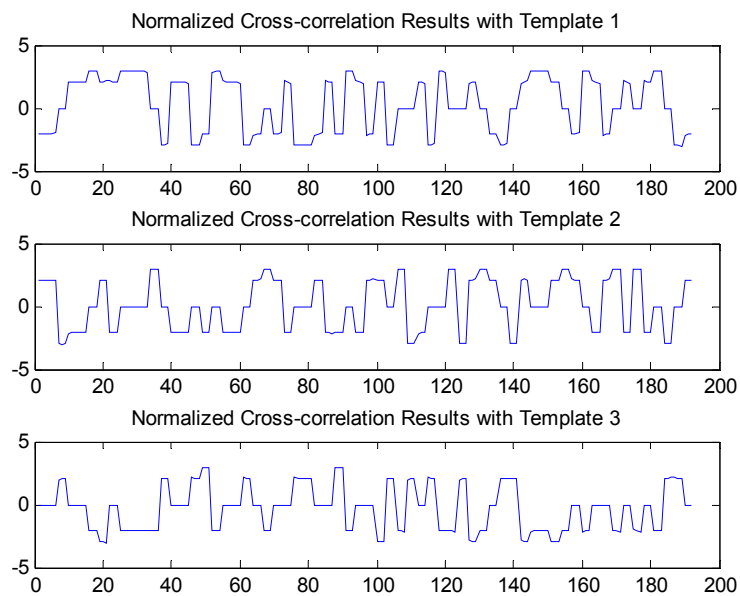
Fig. 6.9. Results of cross-correlation between 8-PSK test signals and the common

features templates.

From Figs. 6.8 and 6.9, it is observed that the WD cross-correlation values of both QPSK and 8-PSK signals with the 2 common features templates have a dynamic range from -3 to 3. However, the data may cluster into multiple levels within this range. In other words, the values do not provide constant amplitude envelopes. It is also seen that the WD cross-correlation results for the 8-PSK test signals when compared with all 3 templates exhibit multi-level characteristics.
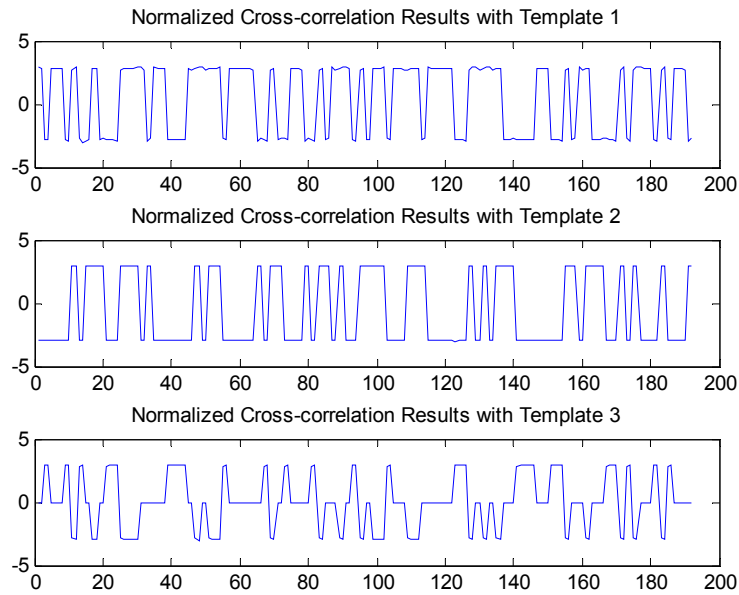
Fig. 6.10. Results of cross-correlation between the 4-QAM ($\pi/4$-QPSK) test signal and the common features templates.

The results of cross-correlating a 4-QAM ($\pi/4$-QPSK) test signal with the common features templates are shown in Fig. 6.10. In this case the values obtained with Templates 1 and 2 have numerical values that again form a constant envelope when plotted versus time. On the other hand, the values obtained when Template 3 is used have 3 different amplitudes.

The results of cross-correlating 16-, 64- and 256-QAM test signals with all 3 common features templates are illustrated graphically in Figs. 6.11-6.13, respectively. It is seen that all the cross-correlation results assume many different numerical values. This observation suggests that additional common features templates must be introduced into the WD AMR process in order to identify and discriminate among the various M-ary QAM schemes.
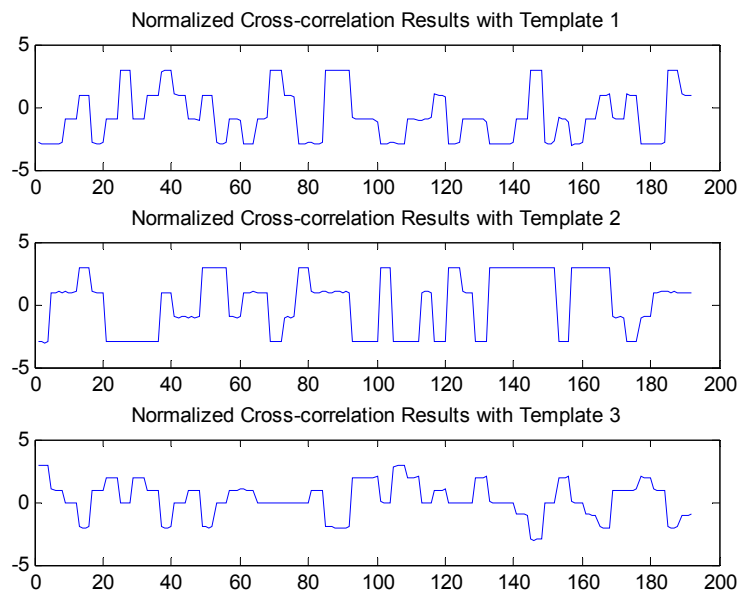
Fig. 6.11. Results of cross-correlation between 16-QAM test signals and the common features templates.
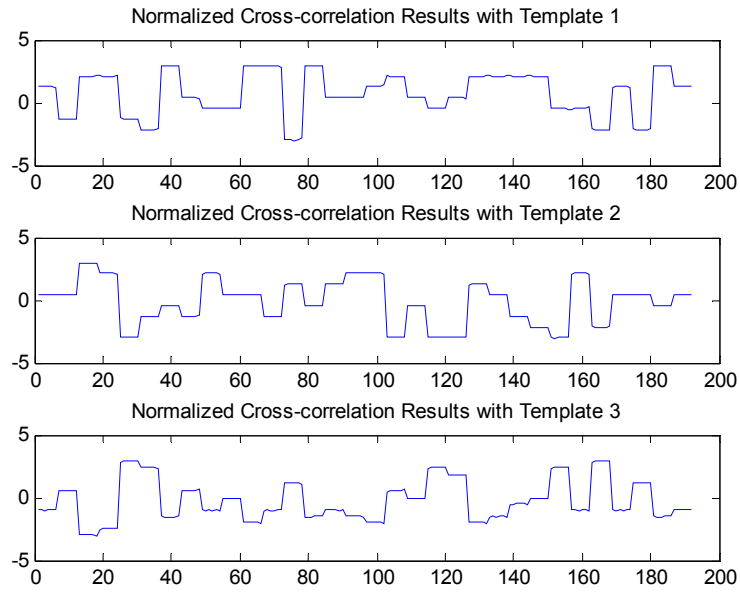
Fig. 6.12. Results of cross-correlation between 64-QAM test signals and the common

features templates.
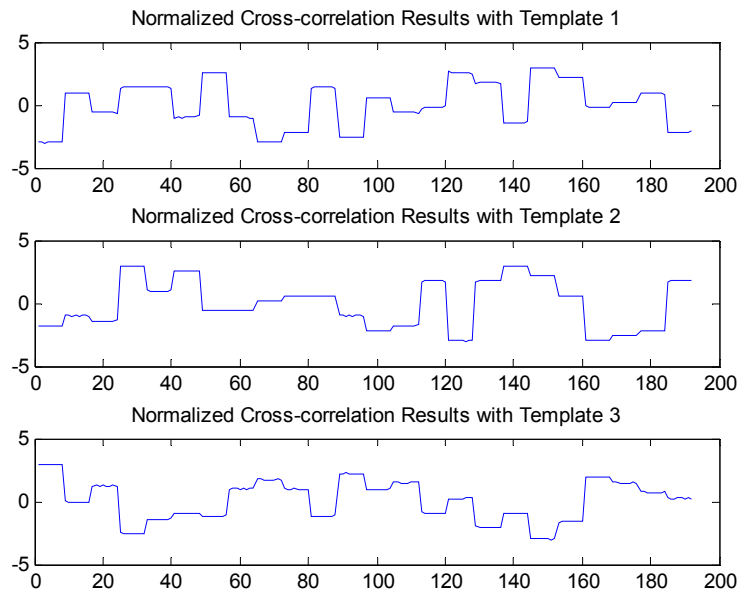
Fig. 6.13. Results of cross-correlation between 256-QAM test signals and the common

features templates.

The cross-correlation values illustrated graphically in Figs. 6.3-6.13 are summarized in tabular form in Tables 6.4-6.6. These tabular summaries focus on two attributes of the results:

1. The dynamic range of the values.

2. Whether the cross-correlation values produce constant envelopes when plotted versus time that consist of two or more distinct levels. This attribute is referred to in an abbreviated manner as being the presence, or absence, of **Multi-Level** values.

Table 6.4 Attributes of WD cross-correlation values from test cases with Template 1

Communications Signal	Dynamic Range	Multi-Level
BASK	0 to 3	No
4-ASK	0 to 3	Yes
BFSK	0 to 3	No
4-FSK	0 to 3	No
BPSK	-3 to 3	No
QPSK	-3 to 3	Yes
8-PSK	-3 to 3	Yes
4-QAM	-3 to 3	No
16-QAM	-3 to 3	Yes
64-QAM	-3 to 3	Yes
256-QAM	-3 to 3	Yes

Table 6.5 Attributes of WD cross-correlation values from test cases with Template 2

Communications Signal	Dynamic Range	Multi-Level
BASK	0 to 3	No
4-ASK	0 to 3	No
BFSK	0 to 3	No
4-FSK	0 to 3	No
BPSK	-3 to 3	No
QPSK	-3 to 3	Yes
8-PSK	-3 to 3	Yes
4-QAM	-3 to 3	Yes
16-QAM	-3 to 3	Yes
64-QAM	-3 to 3	Yes
256-QAM	-3 to 3	Yes

Table 6.6 Attributes of WD cross-correlation values from test cases with Template 3

Communications Signal	Dynamic Range	Multi-Level
BASK	0 to 3	No
4-ASK	0 to 3	Yes
BFSK	0 to 3	No
4-FSK	0 to 3	No
BPSK	-3 to 3	No
QPSK	-3 to 3	Yes
8-PSK	-3 to 3	Yes
4-QAM	-3 to 3	Yes
16-QAM	-3 to 3	Yes
64-QAM	-3 to 3	Yes
256-QAM	-3 to 3	Yes

To summarize the research presented in this section, the concepts used for developing the WD AMR algorithm using the category of common features templates include:

1. Algebraic sign information from the cross-correlation results obtained with Templates 1 and 2 leads to identifying the quadrant locations of the symbol within the signal constellation of a modulation type.

2. Identifying the characteristic combinations of all three template cross-correlation results, e.g., single-level, multi-level or zero-valued datasets.

6.2   Algorithm for the Automatic Modulation Recognition Process

The general WD AMR process using the common features templates is described by the following algorithm:

Step 1:   The received signal with unknown modulation scheme is transformed using the CWT employing a rbio1.3 wavelet.

Step 2:   The transformed signal is cross-correlated with the common features templates defined in the wavelet-domain representing the WD signatures.

Step 3:   The cross-correlation values are examined and modified in the pre-processing blocks so as to have a fixed dynamic range.

Step 4:   The normalized cross-correlation values are processed by three specific decision blocks in order for the unknown modulation scheme to be recognized.

The AMR process using the common features templates is illustrated in Fig. 6.14.

The functionality of the pre-processing block operation described in Step 3 of the algorithm is used to ensure that the cross-correlation data are normalized to have a

dynamic range from -3 to 3. After the data have been processed, AMR decision metrics are developed for each of the decision blocks that are illustrated in Fig. 6.14 in order to discriminate between different modulation schemes.

The decision blocks are developed based on the attributes of all three sets of cross-correlation results, i.e., being zero-valued, having numerical values that are multi-level, or having numerical values that are single-level. Each set of cross-correlation results are examined using either a dynamic range test (to determine if the range is from -3 to 3, or if the range is from 0 to 3), or a multi-level test. A combination of three sets of cross-correlation results is used to classify a particular modulation scheme. The algebraic sign information from the cross-correlation results obtained Template 1 and Template 2 is used particularly to classify modulated signals having phase variations between data symbol transitions.

The development of the various decision block procedures is presented in detail in the remainder of this section. In particular, Sections 6.2.1-6.2.3 describe the procedures for Decision Blocks 1, 2 and 3 using the cross-correlation results obtained with Templates 1, 2 and 3. Due to the change of carrier frequencies in FSK signals, additional templates are introduced for the ASK/FSK Signal Classifier, as described in Section 6.2.4.1. A new concept called the "moving origin" is introduced in order to classify different orders of M-ary QAM signals. The PSK/QAM Signal Classifier is described in Section 6.2.4.2.
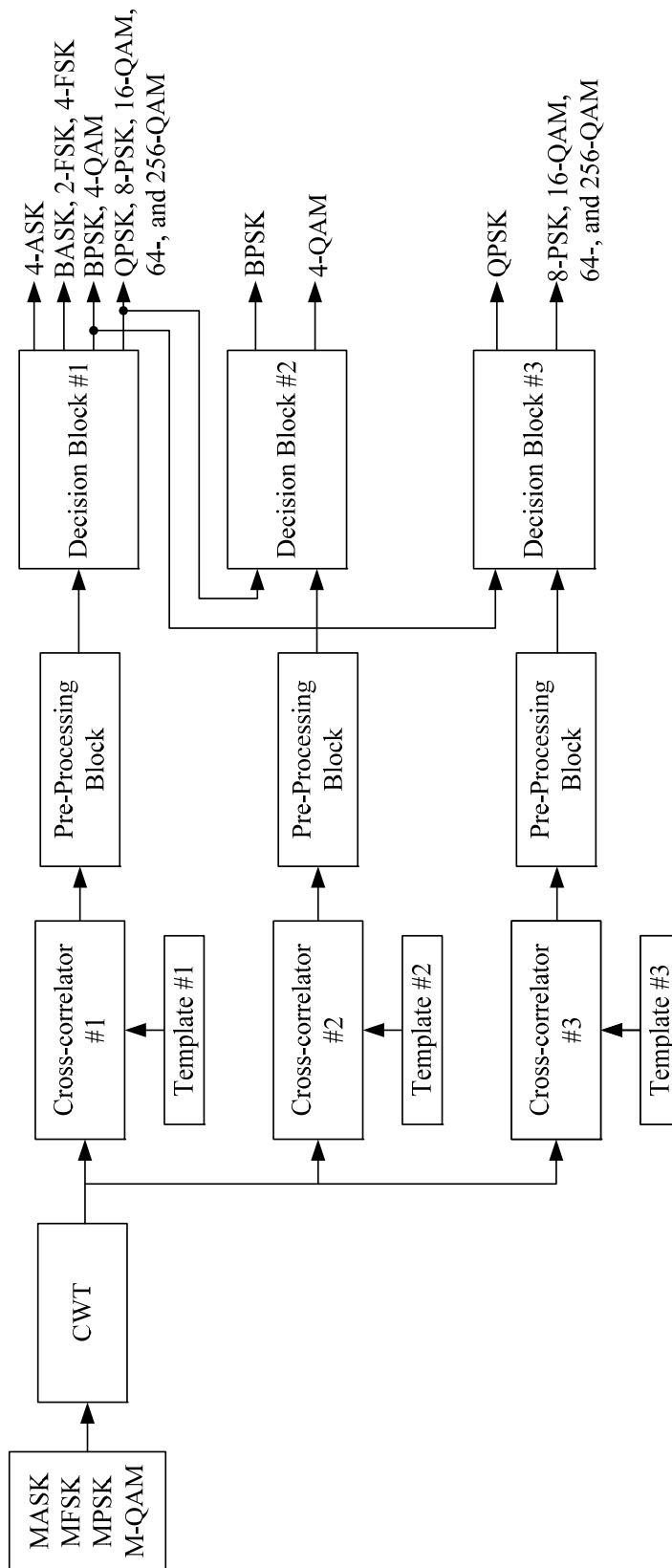
Fig. 6.14. Block diagram of the WD AMR process using common features templates.

6.2.1 Procedure for Decision Block 1

From the cross-correlation results in Table 6.4, the modulated signals can be separated into two groups based on the "dynamic range" attribute of the cross-correlation values and two other additional groups based on the "multi-level" attribute. Note that the values obtained using Template 1 are processed in Decision Block 1.

Based on the dynamic range attribute, one group of modulated signals has a dynamic range that is strictly positive, specifically the range from 0 to 3. The second group of modulated signals has cross-correlation values in the range from -3 to 3. The two groups of modulation schemes are specified in Table 6.7.

Table 6.7 Two groups of data identified from Template 1 using dynamic range

Dynamic Range	Modulation Schemes
0 to 3	BASK,4-ASK, BFSK, 4-FSK
-3 to 3	BPSK, QPSK, 8-PSK, 4-QAM, 16-QAM, 64-QAM, 256-QAM

The second set of groupings is based on whether the cross-correlation values are either single-level, or multi-level. The groupings of modulation schemes based on this attribute are specified in Table 6.8.

Table 6.8 Two groups of data identified from Template 1 using multi-level

Multi-Level	Modulation Schemes
No	BASK, BFSK, 4-FSK, BPSK,4-QAM
Yes	4-ASK, QPSK, 8-PSK,16-QAM, 64-QAM, 256-QAM

Based on the distinct groupings of modulation schemes in Tables 6.7 and 6.8, the procedure for Decision Block 1 can be determined. To this end, four combinations of two

criteria that can be used to help distinguish the various modulation schemes are identified. These are listed in Table 6.9.

Table 6.9 Criteria used in Decision Block 1

Criterion 1: Dynamic Range	Criterion 2: Multi-Level	Modulation Schemes
0 to 3	No	BASK, BFSK, 4-FSK
0 to 3	Yes	4-ASK
-3 to 3	No	BPSK, 4-QAM
-3 to 3	Yes	QPSK, 8-PSK, 16-QAM, 64-QAM, 256-QAM

Based on these criteria, the procedure for Decision Block 1 is described as follows.

Step 1: Apply a **dynamic range test** to the normalized cross-correlation dataset inputted to the decision block and assign an indicator to the dataset. If the data have values in the range from 0 to 3, then assign the indicator 'a' to the dataset. Otherwise, assign an indicator 'b' if the dataset has values in the range from -3 to 3.

Step 2: Perform a **multi-level test** on the normalized cross-correlation dataset inputted to the decision block and assign an indicator to the dataset. Assign a 's' if the data have values that are single-level. Otherwise, assign a 'm' if the values are multi-level.

Step 3: Compare the indicators. If the dynamic range test indicator is 'a' and the multi-level test indicator is also 's,' then assign an output indicator of '1,' which signifies that the modulation scheme employed by the signal is in the group {BASK, BFSK, 4-FSK}.

Step 4:   Repeat Step 3, but if the dynamic range test indicator is 'a' and the multi-level test indicator is 'm,' then the modulation scheme employed by the signal is 4-ASK.

Step 5:   Repeat Step 3, but if the dynamic range test indicator is 'b' and the multi-level test indicator is 's,' then assign an output indicator '2,' which signifies that the modulation scheme employed by the signal is one among the group of {BPSK, 4-QAM}.

Step 6:   Repeat Step 3, but if the dynamic range test indicator is 'b' and the multi-level test indicator is 'm,' then assign an output indicator '3,' which signifies that the modulation scheme employed by the signal is in the group {QPSK, 8-PSK, 16-QAM, 64-QAM, 256-QAM}.

Step 7:   If the output indicator assigned by Decision Block 1, in Steps 3-6, is:

'1,' go to the ASK and FSK Classifier Procedure

'2,' go to Decision Block 2

'3,' go to Decision Block 3

A flowchart that illustrates the procedure for Decision Block 1 is shown in Fig. 6.15.
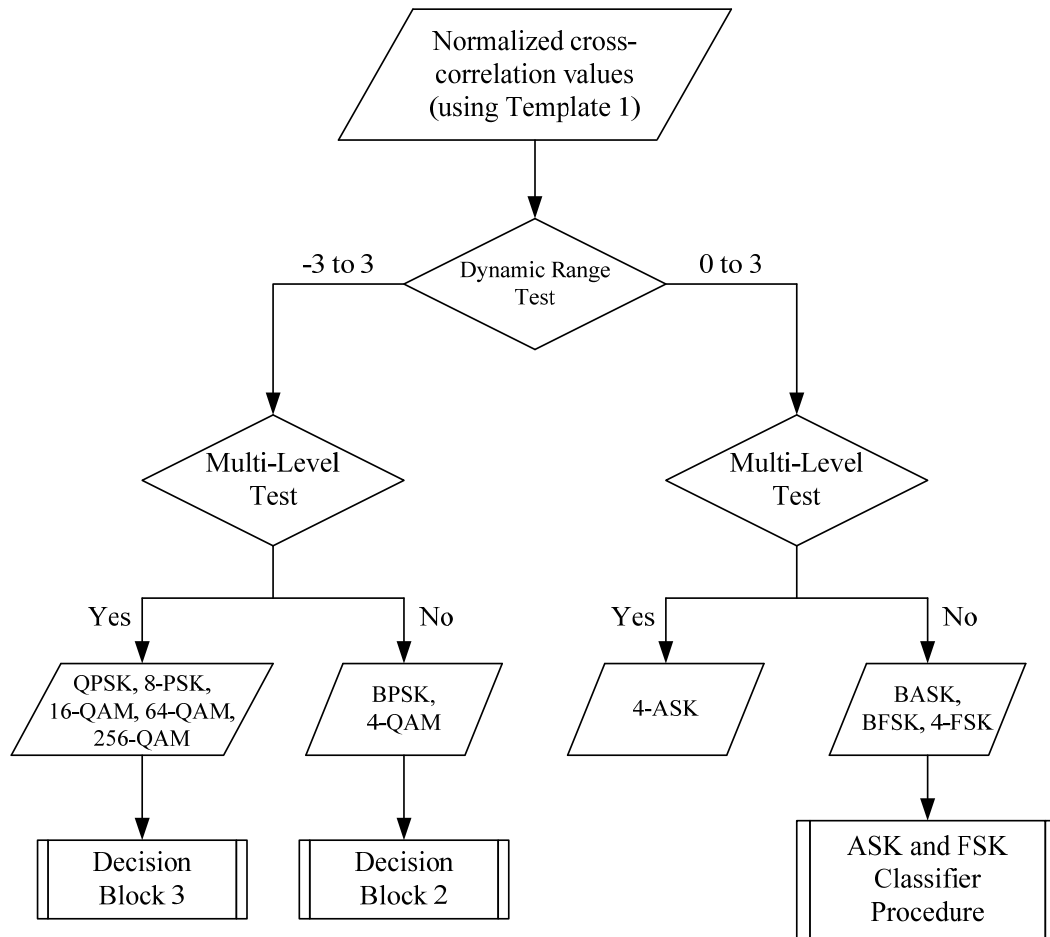
Fig. 6.15. Flowchart of the procedure for Decision Block 1.

6.2.2   Procedure for Decision Block 2

Decision Block 2 is activated if deemed necessary by Decision Block 1, as described in Section 6.2.1. In this case the unknown modulation scheme employed by the signal is either BPSK, or 4-QAM. Decision Block 2 uses the values of the WD cross-correlation between the signal being processed and Template 2. Specifically, the complete set of cross-correlation values is subjected to a dynamic range test and the modulation scheme is recognized based on the results of the test as indicated in Table 6.10.

Table 6.10 Dynamic range of the cross-correlation data using Template 2

Dynamic Range	Modulation Scheme
~0	BPSK
-3 to 3	4-QAM

The procedure for Decision Block 2 is described as follows.

Step 1: The received signal is cross-correlated in the WD with Template 2 and the values are normalized appropriately.

Step 2: A **dynamic range test** is applied to the resulting set of normalized cross-correlation values and output indicators are assigned. If the data lie within the dynamic range of -3 to 3, then the output indicator '0' is assigned. If the values are approximately equal to zero, then the output indicator '1' is assigned.

Step 3: If the output indicator assigned is:

'0,' the modulation scheme is 4-QAM

'1,' the modulation scheme is BPSK.

The flowchart of the procedure is illustrated in Fig. 6.16.
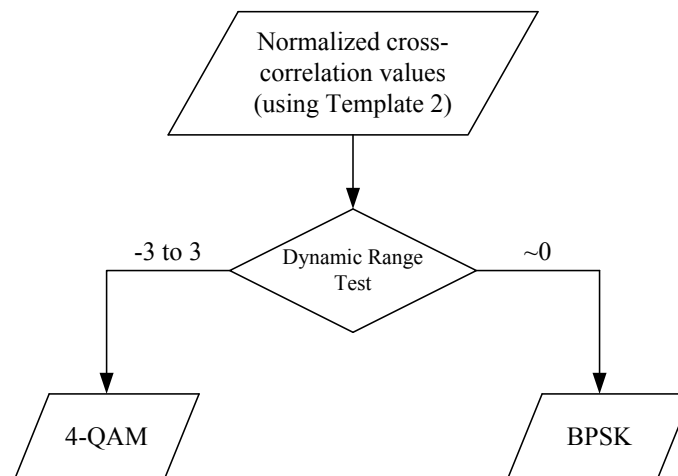
Fig. 6.16. Flowchart of the procedure for Decision Block 2.

6.2.3   Procedure for Decision Block 3

Decision Block 3 is activated when the unknown received signal is identified by Decision Block 1 to be in the set {QPSK, 8-PSK, 16-QAM, 64-QAM, 256-QAM}. The procedure for Decision Block 3 is described as follows.

Step 1:   The received signal is cross-correlated in the WD with Template 3 and the values are normalized appropriately.

Step 2:   A **multi-level test** is applied to the resulting set of normalized cross-correlation values and output indicators are assigned. If the data are composed of single-level values, then the output indicator '0' is assigned. If the values are multi-level, then the output indicator '1' is assigned.

Step 3:   If the output indicator assigned is:

'0,' the modulation scheme is QPSK

'1,' go to the PSK and QAM Classifier Procedure.

The flowchart for the above procedure is provided in Fig. 6.17.
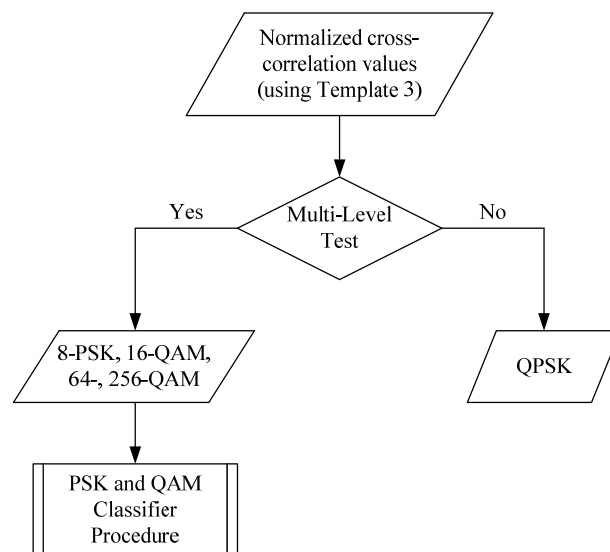
Fig. 6.17. Flowchart of the procedure for Decision Block 3.

6.2.4　Procedures for Other Decision Blocks

Based on the procedures for Decision Blocks 1 and 3, there are two groups of modulation schemes which require additional common features templates for identification. The two groups are:

　　　Group 1: {BASK, BFSK, 4-FSK}

　　　Group 2: {8-PSK, 16-QAM, 64-QAM, 256-QAM}

Therefore, two additional decision making procedures need to be developed for the WD AMR of these modulation schemes. The procedure for classifying the modulation schemes in Group 1 is termed the ASK and FSK Classifier Procedure. While to distinguish between the modulation schemes in Group 2, a detailed PSK and QAM Classifier Procedure has been developed.

6.2.4.1　ASK and FSK Classifier Procedure

As mentioned in Chapter 4, and based on the definition of the FSK modulation scheme, multiple carrier frequencies are required to represent different data symbols using FSK. Therefore, additional common features templates are introduced in order to develop the ASK and FSK Classifier Procedure so as to distinguish among the modulation schemes in Group 1. Specifically, two additional common features templates, Template 4 and Template 5, are introduced. These two new templates are illustrated in Fig. 6.18.

(a) Template 4   (b) Template 5
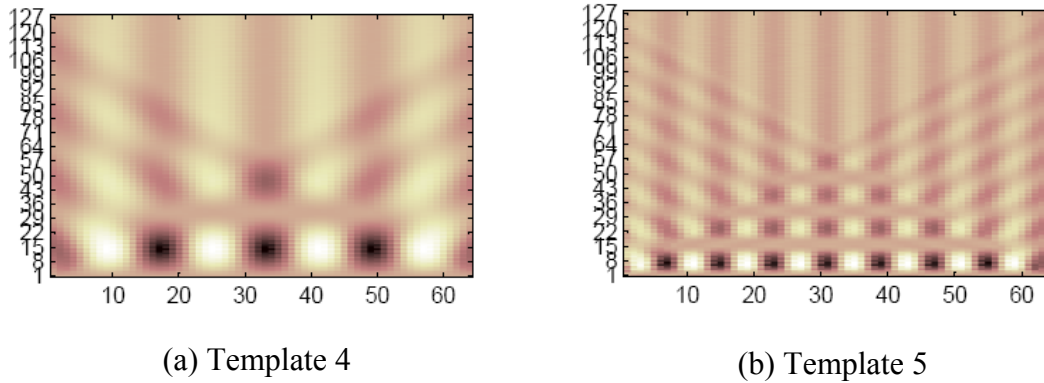
Fig. 6.18. Additional common features templates used in the ASK and FSK Classifier

Procedure.

The templates shown in Fig. 6.18 are extracted from a 4-FSK test signal. The general procedure for extracting templates from test signals that was established in Chapter 4 is used to obtain Templates 4 and 5. Since there are four different carrier frequencies inherent in a 4-FSK signal, ideally there should be a total of four common features templates corresponding to each of these frequencies, all of which can be extracted from a 4-FSK test signal. Templates 1 and 2, however, are two of these four possible templates. Therefore, only two additional templates are needed, namely Templates 4 and 5.

The ASK and FSK Classifier Procedure is described as follows.

Step 1: Cross-correlate the received signal with Template 4 in the WD.

Step 2: Apply the **dynamic range test** to the normalized cross-correlation data and assign an output indicator to the dataset. In particular, assign the output indicator '0' if the values are zero, which signifies that the signal is BASK. Otherwise, assign the indicator '1' if the dataset contains numerical values that are multi-level.

Step 3:   If the output indicator assigned is:

'0,' the modulation scheme is BASK

'1,' go to Step 4.

Step 4:   Cross-correlate the received signal with Template 5 in the WD.

Step 5:   Apply the **dynamic range test** to the normalized cross-correlation data and assign an output indicator to the dataset. Assigning a '0' indicates that the correlation values are zero, and assigning a '1' indicates that the correlation values are in the range from 0 to 3.

Step 6:   If the output indicator assigned is:

'0,' the modulation scheme is BFSK

'1,' the modulation scheme is 4-FSK.
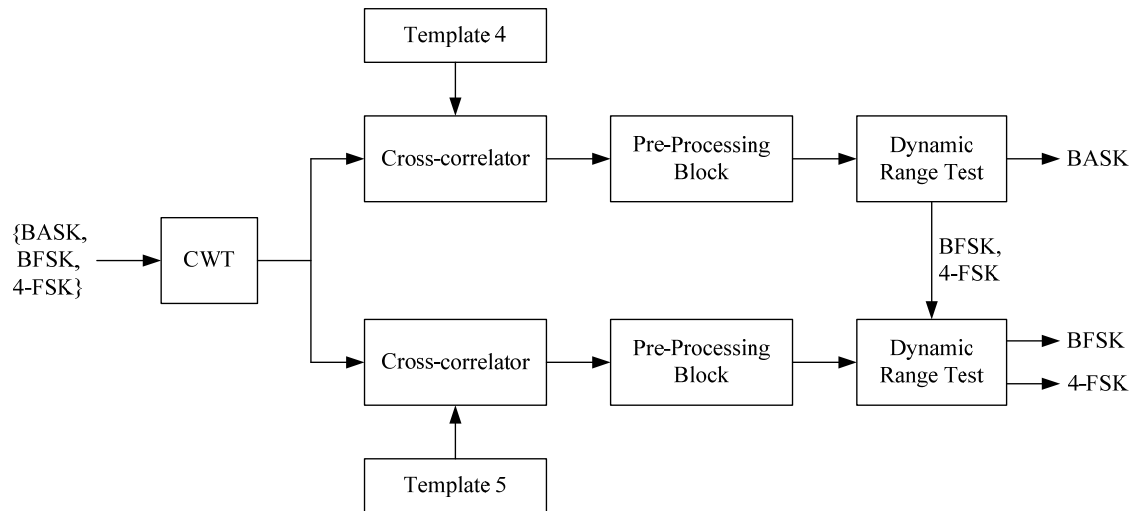
Fig. 6.19. System block diagram implementing the ASK and FSK Classifier Procedure

for Group 1 signals.

6.2.4.2   PSK and QAM Classifier Procedure

The PSK and QAM Classifier Procedure for the classification of signals in Group 2 is activated if needed by Decision Block 3. The modulation schemes included in Group 2 are 8-PSK, 16-QAM, 64-QAM, and 256-QAM.

Unlike all of the algorithms and procedures previously described in this chapter, the PSK and QAM Classifier Procedure is developed based on a new methodology. In order to classify the QAM signal according to its size, additional WD signatures are introduced. The additional templates used to represent the WD signatures are constructed based on the new concept of a "moving origin" applied to the signal constellations in a specific quadrant. The M-ary QAM signals considered in this dissertation all possess square constellation shapes. The QAM signals are illustrated in signal space format in Fig. 6.20.
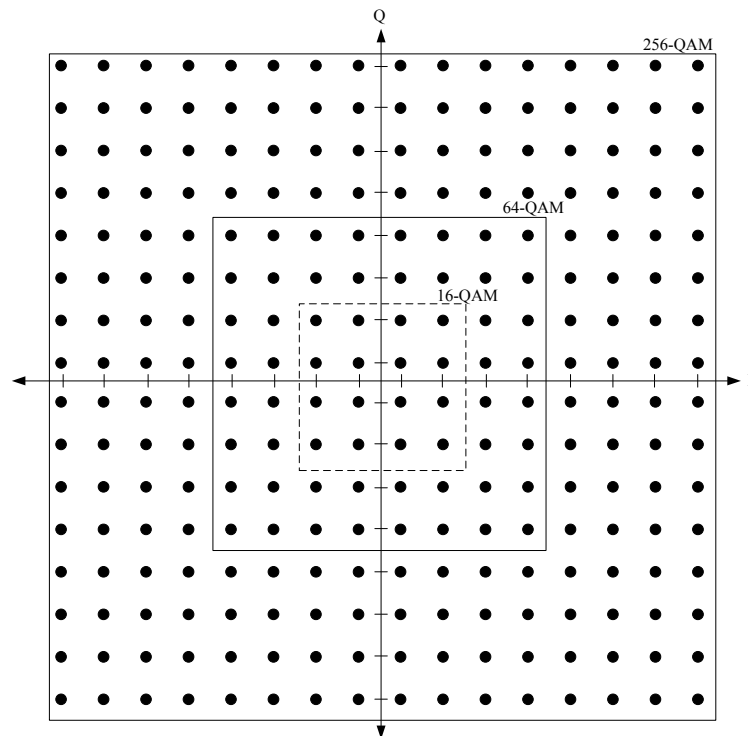
Fig. 6.20. Signal constellations of M-ary QAM signals.

Each dot in Fig.6.20 represents a time-domain data symbol contained in a particular QAM signal. The squares represent all the possible data symbol location for a particular size QAM signal. The cross-correlation results of common features Template 1 and Template 2 compared with the received signals are used for determination of signal constellation quadrant location for each of the data symbols (finite segments) contained in a frame of the received signal. Prior to the development of the PSK and QAM Classifier Procedure, it is necessary to properly define and construct the needed WD signatures.

The additional WD templates are constructed based on the new concept of "moving origin". For simplicity, only the data symbols in Quadrant I for 8-PSK, 16-QAM, 64-QAM and 256-QAM signals are considered and illustrated in Fig. 6.21.
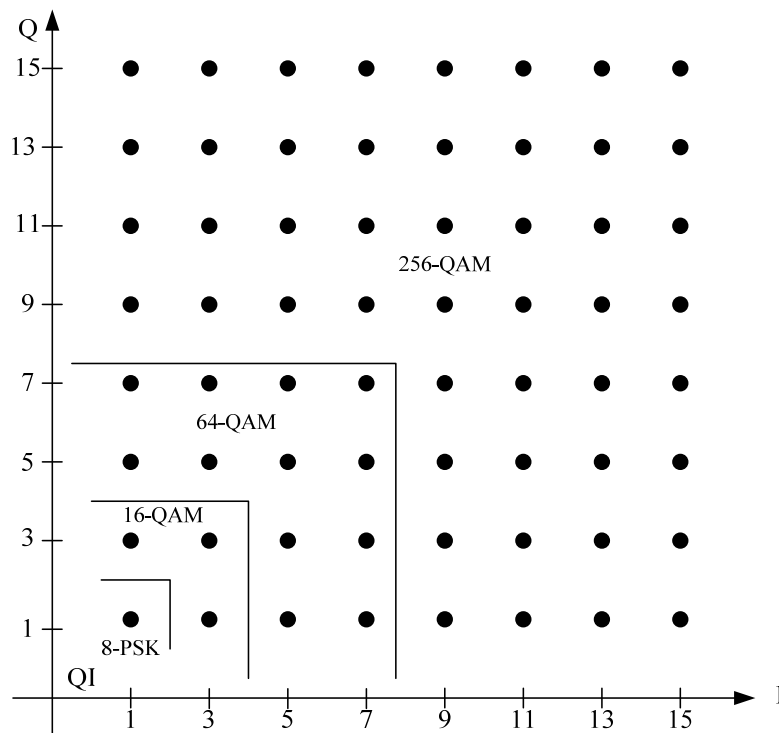
Fig. 6.21. Signal space representation of Group 2 signals in Quadrant I.

As shown in Fig.6.21, the data symbols in Quadrant I can be evenly distributed into four new quadrants.
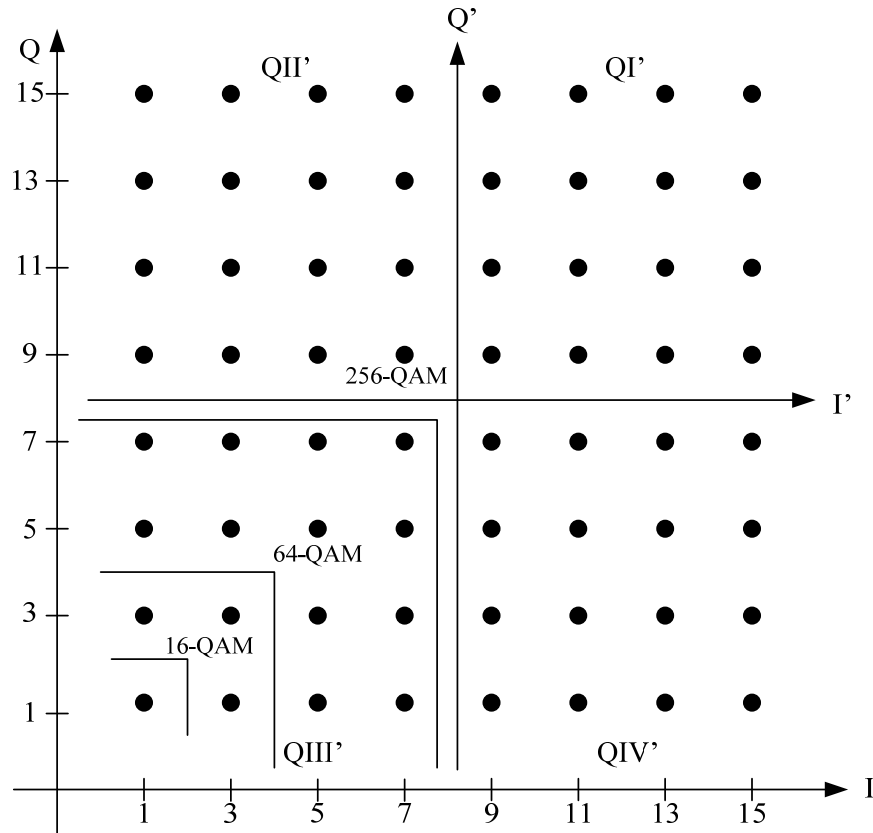
Fig. 6.22. Introduction of new I and Q axes in Quadrant I.

In Fig. 6.22, new axes denoted as I' and Q' are introduced in order to separate the data symbols evenly into four new quadrants denoted as QI', QII', QIII' and QIV'. The templates representing the new WD signatures are constructed heuristically by taking the location of the new origin to be the definition of a new features template for use in the PSK and QAM Classifier Procedure. By examining the cross-correlation values between the signal symbols located in Quadrant I and the newly defined features template, the following observations can be made:

1. For signals representing data symbols located in the upper triangular region of Quadrant I of the signal constellation, the cross-correlation results for the data symbols compared to the new origin are larger than the auto-correlation value of the features template representing the new origin.

2. On the other hand, for the signals located in the lower triangular region of Quadrant I, the cross-correlation results for the data symbols compared to the origin are smaller than the auto-correlation value of the new origin.

3. For the signals that are located on the diagonal co-linear with the new origin, the cross-correlation results obtained are approximately the same as the auto-correlation value of the new origin.

All of the above signal and template locations are illustrated graphically in Fig. 6.23. The dashed line represented the decision boundary for upper and lower triangular region for developing the decision rule for recognizing the different sizes of the various QAM signals.

In Fig. 6.23, the new features template is represented as a square that is coincident with the location of the new origin. Also in the figure, the dashed line serves as the decision boundary reflecting the three observations made above concerning the various comparisons between the cross-correlation and auto-correlation results. With the introduction of this new template, and also the use of its auto-correlation value, it is now possible to identify whether the signal is a 256-QAM signal or not. Therefore, a similar methodology can be applied to the lower triangular region of the signal constellation in order to classify QAM signals of smaller size.
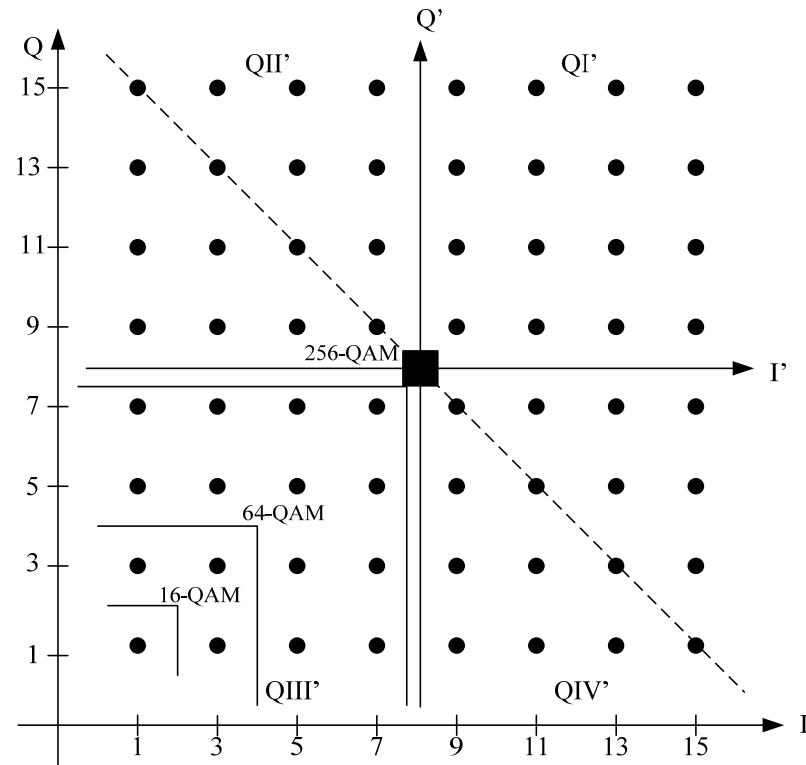
Fig. 6.23. Location of the new features template.

Once again, the "moving origin" concept is utilized within the lower triangular region of the signal constellation. Therefore, additional templates representing WD signatures are constructed as illustrated in Fig. 6.24.
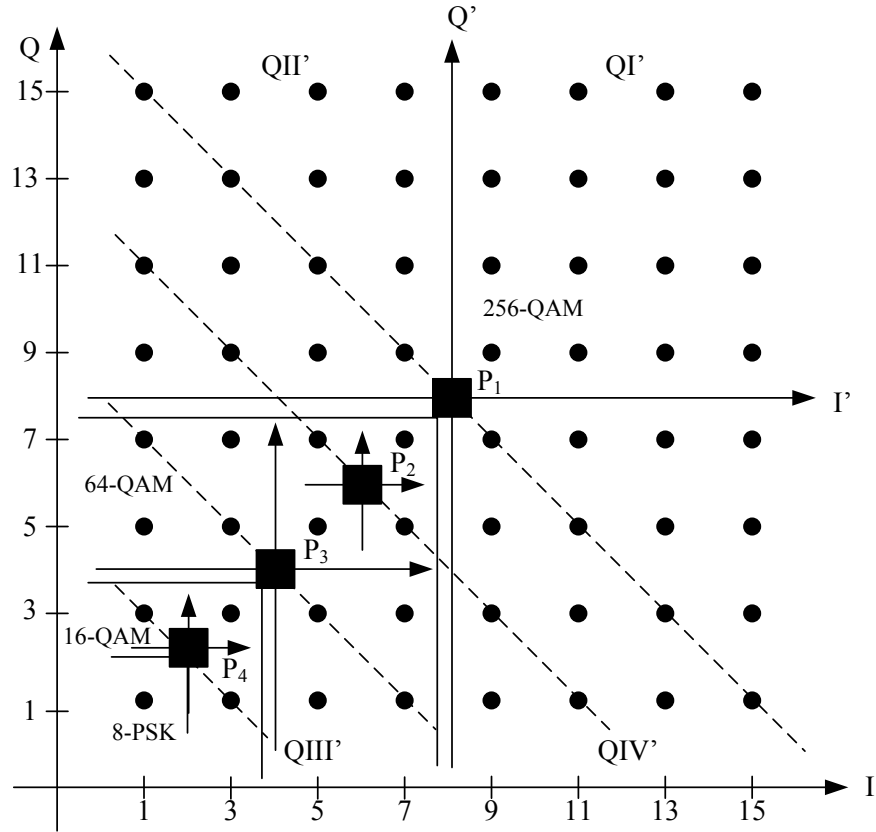
Fig. 6.24. Location of the new features templates used for classifying QAM signals.

In Fig. 6.24, the squares represent the possible templates, denoted as P_1, P_2, P_3, and P_4, for the 256-QAM, 64-QAM, 16-QAM and 8-PSK signal constellations, respectively. The dashed lines once again represent the decision boundaries used to determine the data symbol location within the signal constellation.

In the time-domain, the four new templates shown in Fig. 6.24 are denoted as $P_1(t)$, $P_2(t)$, $P_3(t)$ and $P_4(t)$. The new templates are defined as

$$P_1(t) = A_1 \cos(2\pi f_c t) - A_2 \sin(2\pi f_c t) \qquad T_i < t < T_{i+1} \tag{6.3}$$

$$P_2(t) = B_1 \cos(2\pi f_c t) - B_2 \sin(2\pi f_c t) \qquad T_i < t < T_{i+1} \tag{6.4}$$

$$P_3(t) = C_1 \cos(2\pi f_c t) - C_2 \sin(2\pi f_c t) \qquad T_i < t < T_{i+1} \tag{6.5}$$

$$P_4(t) = D_1 \cos(2\pi f_c t) - D_2 \sin(2\pi f_c t) \qquad T_i < t < T_{i+1} \tag{6.6}$$

where A_1, A_2, B_1, B_2, C_1, C_2, D_1 and D_2 are constants that depend on the location of the templates on the I and Q axes. In (6.3)-(6.6), T_i represents the boundary of the ith data symbol within a frame of the transmitted signal.

In order to distinguish a 64-QAM signal from a 256-QAM signal, not only the templates P_1, P_2 and P_3 are needed, but it is also required to test for special locations as shown in Fig. 6.25. The special locations are denoted by S_1, S_2, S_3, S_4, S_5 and S_6. The cross-correlation results of the received signal with common features Template 1 and Template 2 are used for determining the special locations.

Several assumptions are made for the special locations. When the signal locations coincide with one of the special locations in the figure, the special locations are actually representing the signal symbols that can be present in various M-ary QAM signals. For example, location S_1 can be represented either as one of the symbols in a 256-QAM signal, or as one of the symbols in a 64-QAM signal. Locations S_2 and S_3 can both be represented as symbols in either a 64-QAM signal or a 256-QAM signal. Due to this, if signal symbols are located at the special locations S_1, S_2 or S_3, then they are categorized as belonging to a 64-QAM signal. Symbols located at special locations S_5 and S_6 are categorized as belonging to a 256-QAM signal. The same decision rules are applied to the other three quadrants of the overall constellation.
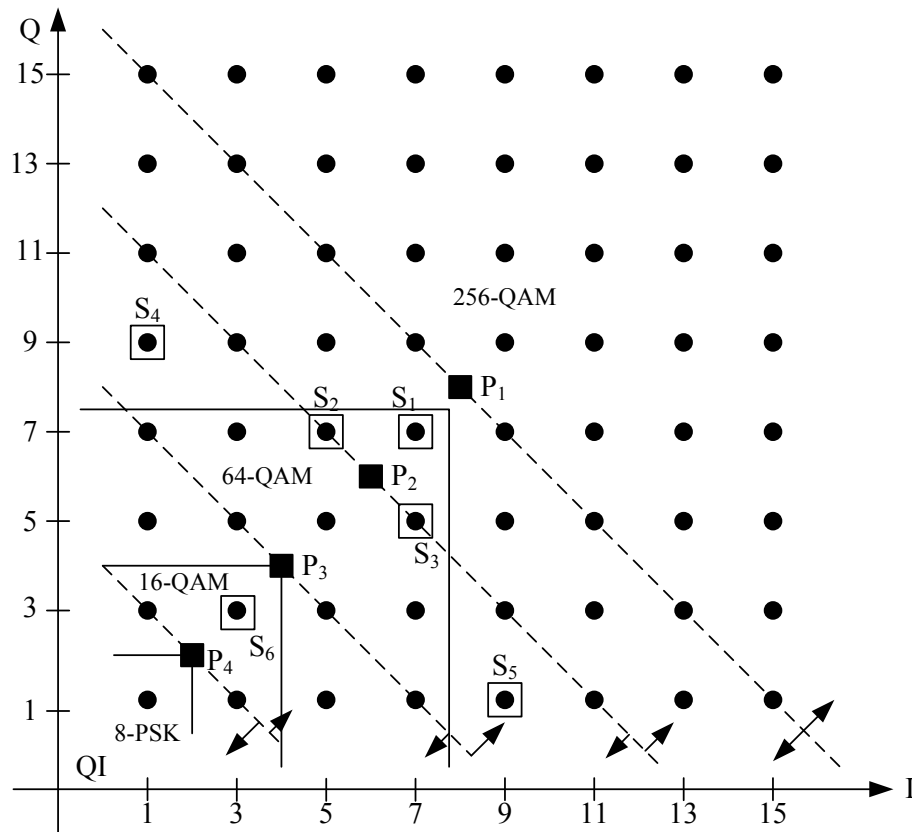
Fig. 6.25. The signal space depicting the new templates with special locations indicated

in Quadrant I.

The procedure to distinguish a 64-QAM signal from a 256-QAM signal is described in the following.

Step 1: Cross-correlate the received signal with Template P_1 and compute the auto-correlation value of P_1.

Step 2: Use the sliding cross-correlation procedure of Fig. 4.18. Compare the resulting cross-correlation values between P_1 and the received signal with the auto-correlation value of P_1. If the cross-correlation values are larger than, or equal

to, the auto-correlation value, then the signal is classified as being that of a 256-QAM signal. Otherwise, cross-correlate the received signal with P_2 and compute the auto-correlation value of P_2.

Step 3: Again use the sliding operation in Fig. 4.18 to obtain cross-correlation results for the received signal compared to Template P_2. Compare the cross-correlation results with the auto-correlation value of P_2. If the cross-correlation values are larger than the auto-correlation value of P_2. Test for special location, S_1. If the cross-correlation values are approximately equal to the auto-correlation value of P_2, test for the other special locations S_2 and S_3. Otherwise, test for the cases of special locations S_4, and S_5.

Step 4: Cross-correlate the received signal with common features Template 1 and Template 2. If the two cross-correlation values are approximately the same, then the signal is classified as that of a 64-QAM signal. Otherwise, the signal is declared to be a 256-QAM signal.

Step 5: If the cross-correlation values between the received, noisy signal and Template P_2, is approximately equal to the auto-correlation value of P_2, test for the special locations of S_2 and S_3. If the cross-correlation values of Template 1 are larger than Template 2, then the signal is classified as being that of a 64-QAM signal. Otherwise, it is declared to be a 256-QAM signal.

Step 6: If the cross-correlation values between the received signal and Template P_2 is smaller than the auto-correlation value of P_2, then test for the special locations

S_4 and S_5. If the cross-correlation values obtained with Template 1 are larger than those obtained with Template 2, then the signal is declared to be a 256-QAM signal. Otherwise, it is declared to be a 64-QAM signal.

Similar procedures are implemented for distinguishing a 16-QAM signal from a 64-QAM signal. However, in this situation, Template P_3 and Template P_4 are used; the auto-correlation values of the templates are used as thresholds; and, the special location S_6 is tested for classifying the actual size of the M-ary QAM signal. All the procedures needed to classify Group 2 signals are summarized using the system block diagram illustrated in Fig. 6.26.

Fig. 6.26. System block diagram implementing the PSK and QAM Classifier Procedure for Group 2 signals in Quadrant I.

The abovementioned procedure has been developed for classifying Group 2 signals in Quadrant I. However, the same procedure is applied for signals representing data symbols that fall into any one of the other three quadrants. The templates and also the special locations are adjusted to the particular quadrant for classify the Group 2 signals.

The overall PSK and QAM Classifier Procedure is described as follows.

Step 1: Cross-correlate the received signal with common features Template 1 and Template 2.

Step 2: Based on the algebraic sign of the cross-correlation result obtained in Step 1, determine the quadrant location of the received signal.

Step 3: Cross-correlate the received signal with the quadrant specific templates.

Step 4: Follow the same procedures as described in Fig. 6.26 in order to classify the particular signal modulation type from among those in Group 2.

6.3   Simulation Experiment and Results

The WD AMR algorithm based on the common features templates developed in Section 6.2 has been implemented in MATLAB. All of the communications test signals used in the simulations have been corrupted by zero-mean AWGN having SNR values in the range from -5 dB to 10 dB. The rates of correct modulation classification have been obtained using 100,000 Monte Carlo trials. The transmitted signal used in each trial consists of 192 symbols per frame transmitted. The signal is oversampled by a factor of sixteen when compared to the Nyquist rate corresponding to the frequency of the

sinusoidal carrier. The system parameters assumed to be known for the AMR process include the carrier frequency and perfect symbol timing with no timing offset.

The results of the experiments for all of the modulation schemes are given in Tables 6.10-6.14, which contain the rates of correct classification for the five different SNR values, i.e., 10 dB, 5 dB, 0 dB, -3 dB, and -5 dB.

Table 6.11 Rates of correct classification for WD AMR process; SNR = 10 dB

	BPSK	QPSK	8-PSK	BASK	4-ASK	BFSK	4-FSK	4-QAM	16-QAM	64-QAM	256-QAM
BPSK	100%										
QPSK		100%									
8-PSK			100%								
BASK				100%							
4-ASK				0.2%	99.8%						
BFSK						100%					
4-FSK							100%				
4-QAM			0.2%					99.8%			
16-QAM									100%		
64-QAM										100%	
256-QAM											100%

Table 6.12 Rates of correct classification for WD AMR process; SNR = 5 dB

	BPSK	QPSK	8-PSK	BASK	4-ASK	BFSK	4-FSK	4-QAM	16-QAM	64-QAM	256-QAM
BPSK	100%										
QPSK	0.2%	99.8%									
8-PSK			100%								
BASK				100%							
4-ASK				0.2%	99.8%						
BFSK						100%					
4-FSK				0.1%			99.9%				
4-QAM			1.1%					98.9%			
16-QAM									100%		
64-QAM										100%	
256-QAM											100%

Table 6.13 Rates of correct classification for WD AMR process; SNR = 0 dB

	BPSK	QPSK	8-PSK	BASK	4-ASK	BFSK	4-FSK	4-QAM	16-QAM	64-QAM	256-QAM
BPSK	100%										
QPSK		97.3%	2.7%								
8-PSK			100%								
BASK				100%							
4-ASK				0.7%	99.3%						
BFSK						99.9%	0.1%				
4-FSK							95.3%				
4-QAM			3.2%					96.8%			
16-QAM									100%		
64-QAM										98.9%	1.1%
256-QAM											100%

Table 6.14 Rates of correct classification for WD AMR process; SNR = -3 dB

	BPSK	QPSK	8-PSK	BASK	4-ASK	BFSK	4-FSK	4-QAM	16-QAM	64-QAM	256-QAM
BPSK	100%										
QPSK		95.4%		4.6%							
8-PSK			100%								
BASK				100%							
4-ASK					98.5%						
BFSK						84.3%	10.5%				
4-FSK							84.1%				
4-QAM			5.3%					94.7%			
16-QAM									100%		
64-QAM										98.1%	1.9%
256-QAM											100%

Table 6.15 Rates of correct classification for WD AMR process; SNR = -5 dB

	BPSK	QPSK	8-PSK	BASK	4-ASK	BFSK	4-FSK	4-QAM	16-QAM	64-QAM	256-QAM
BPSK	100%										
QPSK		94.6%	5.4%								
8-PSK			100%								
BASK				95.8%	4.2%						
4-ASK					95.9%				4.1%		
BFSK						77.3%					
4-FSK							63.2%				
4-QAM			6.2%					93.8%			
16-QAM									100%		
64-QAM										96.1%	3.9%
256-QAM											100%

6.4   Comparison of Results

Several prior works on AMR that are available in the literature, which use both WT-based and non-WT based methodologies, have been surveyed in Chapter 2. In this section the results of simulation experiments reported in these works are compared with the results obtained in Section 6.3. The relevant comparisons are presented in Tables 6.16-6.18.

It must be reiterated that a direct comparison of the different AMR methodologies is impossible due to the fact that the prior works reported in the literature do not necessarily use the same general *a priori* assumptions, such as SNR values, numbers of symbols per transmission, etc.

In this work, it must be highlighted that the actual sizes of M-ary QAM signal constellations are identified based on a new "moving origin" concept. The majority of the work reported in the literature focuses only on classifying signals as being ASK, FSK or PSK. There is no work reported in which the actual sizes of the M-ary QAM signals are classified.

From Table 6.18, the rates of correct classification at SNR = 10 dB and 5 dB, are almost 100% for all the communications signals considered in this work. In the case of SNR = 0 dB, majority of the rates of correct classification achieved are above 97%, except in the cases of 4-FSK and 4-QAM signals for which rates of 95.3% and 96.8% were achieved, respectively. For noisy channels operating at an SNR = -5 dB, the rates of correct classification achieved are near, or above, 94% for most of the modulation schemes. The

exception at SNR = -5 dB is that of the FSK signals. The rates of correct classification at SNR = -5 dB for BFSK and 4-FSK are 77.3% and 63.2%, respectively.

In comparison with the results reported from the literature, the rates of correct classification obtained in this work are either equal to, or better than any other results.

Table 6.16 Non-wavelet transform-based AMR methods

AMR Method Devised by	SNR	Modulation Scheme	Correct Classification Rate
Azzouz, et al. [32]	15 dB	BASK	95.3%
		4-ASK	77.3%
		BPSK	100%
		QPSK	96%
		BFSK	92%
		4-FSK	100%
	20 dB	BASK	96%
		4-ASK	80.2%
		BPSK	100%
		QPSK	100%
		BFSK	92%
		4-FSK	88%
Hsue and Soliman [33]	15 dB (CNR)	BPSK	99%
		QPSK	98%
		8-PSK	100%
		BFSK	100%
		4-FSK	100%
		8-FSK	100%
Dobre, et al. [9]	10 dB	BPSK	100%
		QPSK, 8-PSK,16-QAM, and 64-QAM	100%
	5 dB	BPSK	100%
		QPSK, 8-PSK,16-QAM, and 64-QAM	100%
	0 dB	BPSK	78%
		QPSK, 8-PSK,16-QAM, and 64-QAM	100%

Table 6.17 Wavelet transform-based AMR methods

AMR Method Devised by	SNR	Modulation Scheme	Correct Classification Rate
Ho, et al. [58]	13 dB (CNR)	BPSK	97%
		QPSK	97%
		8-PSK	97%
		2-FSK	100%
		4-FSK	100%
		8-FSK	100%
Hong and Ho [60]	20 dB (CNR)	QPSK	100%
		4-FSK	100%
		16-QAM	99.7%
	15 dB (CNR)	QPSK	99.5%
		4-FSK	100%
		16-QAM	98.7%
	10 dB (CNR)	QPSK	98.8%
		4-FSK	100%
		16-QAM	98.7%
	5 dB (CNR)	QPSK	97.6%
		4-FSK	100%
		16-QAM	100%
Jin, et al. [54]	13 dB	BPSK	100%
		QPSK	100%
		8-PSK	100%
		BFSK	100%
		4-FSK	100%
	10 dB	BPSK	100%
		QPSK	99.9%
		8-PSK	100%
		BFSK	98.1%
		4-FSK	100%
	8 dB	BPSK	100%
		QPSK	97.5%
		8-PSK	100%
		BFSK	95.3%
		4-FSK	100%

Table 6.18 AMR classification rates obtained in this research work

Modulation Scheme	SNR = 10 dB	SNR = 5 dB	SNR = 0 dB	SNR = -5 dB
BPSK	100%	100%	100%	100%
QPSK	100%	99.8%	97.3%	94.6%
8-PSK	100%	100%	100%	100%
BASK	100%	100%	100%	95.8%
4-ASK	99.8%	99.8%	99.3%	95.9%
BFSK	100%	100%	99.9%	77.3%
4-FSK	100%	99.9%	95.3%	63.2%
4-QAM	100%	98.9%	96.8%	93.8%
16-QAM	100%	100%	100%	100%
64-QAM	100%	100%	98.1%	96.1%
256-QAM	100%	100%	100%	100%

6.5   Conclusions

In this chapter, an effective WD AMR process has been developed and its efficacy has been demonstrated with the use of the pattern recognition technique of cross-correlation along with templates defined in the wavelet-domain. The system parameters that are assumed to be known for the AMR process include the carrier frequency and perfect symbol timing with no timing offset. It has been demonstrated that the AMR process can correctly classify signals with very high reliability even at low values of SNR. It is shown in Tables 6.16-6.18, that the rates of correct classification obtained in this work are equal to, or better than, those reported in the literature. Furthermore, the WD AMR algorithm developed in this work can classify the actual sizes of M-ary QAM signal constellations while a classification algorithm for inter-class QAM signals is absent in the literature.

Given the reliability of the AMR process developed in this chapter, it can be used to advance the state of the art in communications receiver design so as to permit interoperability between various communications standards. In other words, the AMR process can be used to enable the development of agile radio receivers and transceivers. Such agile radios can be used in military signal analysis applications, such as threat analysis, spectrum management, electronic warfare, and electronics surveillance systems. Finally, the AMR process devised can be extended to enable classification of more modulation schemes by using similar methodologies and multiple wavelet families.

Chapter 7

Techniques for Demodulation Using Wavelet-Domain Templates

Having hypothesized, described, and validated two WT-based AMR algorithms, it is now necessary to develop the techniques for demodulation in order to complete the baseband processing system based on the Wavelet Platform concept. After correctly classifying the previously unknown modulation scheme employed by a received communications signal, an appropriate demodulation process must be activated in order to recover the information-bearing baseband data.

As described in Chapter 4, the details for constructing templates corresponding to WD signatures for the WD AMR algorithms have been described. These two types of templates, i.e., the unique features templates and the common features templates, are also used to develop a WD Demodulation process. Specifically, the WD cross-correlation results are used to obtain the decision metrics needed for the recovery of the baseband data contained within a communications signal.

In Section 7.1, WD Demodulation techniques using the unique features templates are developed. As with the AMR process, techniques developed using such symbol transition templates are only suitable for binary modulated signals. WD Demodulation techniques using the common features templates are developed in Section 7.2. The communications signals considered in this case are BASK, 4-ASK, BFSK, 4-FSK, BPSK, QPSK, 8-PSK, 4-QAM (also denoted as $\pi/4$-QPSK), 16-QAM, 64-QAM and 256-QAM. In addition, a

new methodology is developed in this chapter for the demodulation of M-ary QAM signals. The performance of the demodulation techniques is evaluated and BER curves are plotted for cases of signals corrupted with AWGN resulting in SNR values in the range from -5 dB to 10 dB.

7.1   Demodulation Using Unique Features Templates

The WD Demodulation techniques for digitally modulated communications signals are developed based on the cross-correlation of the received communications signals with the unique features templates in the WD. The cross-correlation data are then compared with the auto-correlation values for each of the unique features templates. The result of the comparison is assigned an indicator. Based on the indicator the data bit sequence can then be recovered. Fig. 7.1 illustrates the system block diagram for the demodulation procedures for BASK, BFSK or BPSK signals using the unique features templates. The functionality of the pre-processing block is to normalize the cross-correlation values to have a dynamic range from -3 to 3.
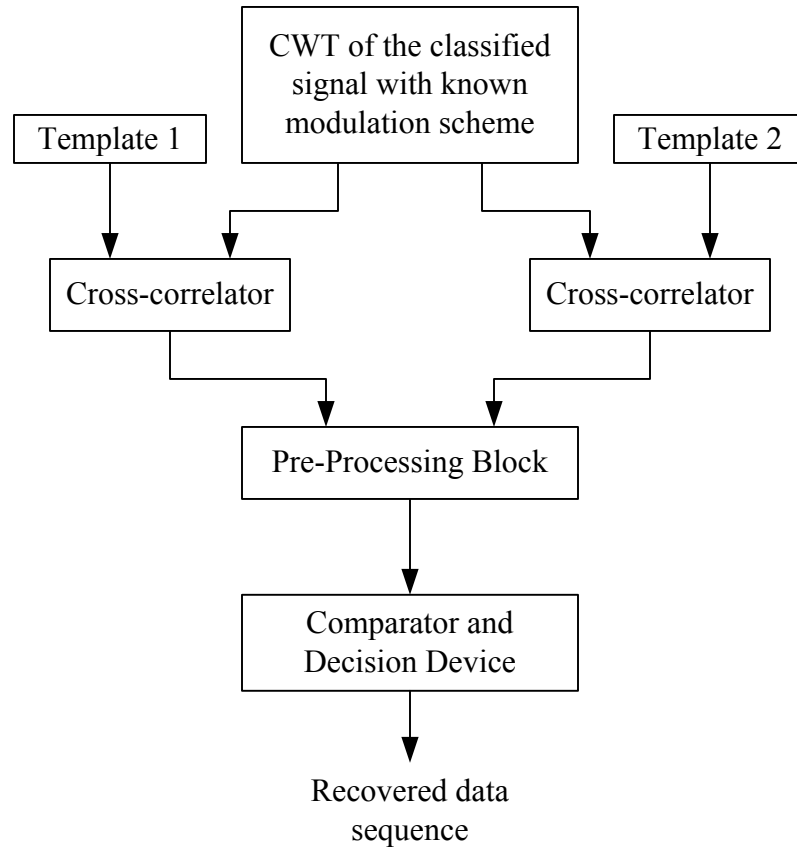
Fig. 7.1. System-level block diagram for the WD Demodulation process.

The algorithm for the WD Demodulation technique is described as follows.

Step 1:   Obtain the classified received signal having the known modulation scheme declared by the WD AMR process.

Step 2:   Cross-correlate the WD coefficients of the signal with the two unique features templates corresponding to the known modulation type, Templates 1 and 2, in the WD.

Step 3:   Compare the cross-correlation data with both the auto-correlation values of each of the unique features templates and the cross-correlation values between the two unique features templates. Assign indicators for each cross-correlation

value obtained at each signal segment corresponding to a data symbol period.

Step 4:   Based on the results from Step 3, output the data bit sequence.

Known Modulation Signal	1	1	0	1	1	0	0	1
Cross-correlation with Template 1	M	H	L	M	H	M	L	
Cross-correlation with Template 2	M	L	H	M	L	M	H	
Recovered digital data sequence	1	1	0	1	1	0	0	1

Fig. 7.2. Example of WD Demodulation process using Templates 1 and 2.

An example of the demodulation process using the unique features templates for a signal with a known modulation scheme is illustrated in Fig. 7.2. The demodulation process is based on the cross-correlation between the WD scalogram of the known signal having a modulation signal and the WD scalogram of the appropriate features templates. For clarity, the unknown transmitted data are illustrated in the top row of the figure. First, the transformed signal with known modulation type is cross-correlated at each symbol transition with the two unique features templates in the WD corresponding to the modulation type. Two sets of cross-correlation results are obtained. Each resulting data element in the cross-correlation dataset represents the cross-correlation value between specific transition location of the communications signal at a specific transition location and the unique features template. In Fig. 7.2, the following notations are used:

H   High cross-correlation value

L   Low cross-correlation value

M   Intermediate cross-correlation value within the cross-correlation dataset

Next, each of cross-correlation values is compared with two threshold values. One threshold value corresponds to the cross-correlation between two distinct unique features templates, P_y. The other threshold value corresponds to the auto-correlation of one of the unique features templates, P_x. The auto-correlation values are the same for both templates because the templates are mirror images of each other. Therefore, only one of the auto-correlation values is used as the threshold value. With the use of the two threshold values applied to the cross-correlation dataset, the decision rule is defined as followings

$$\text{output} = \begin{cases} 'H' & x \geq P_x \\ 'M' & P_y < x < P_x \\ 'L' & x \leq P_y \end{cases} \tag{7.1}$$

where x is a cross-correlation value obtained when comparing the communications signal with a unique features template at each symbol transition location, as shown in Fig. 7.2. Here again, P_x is the auto-correlation value of the template, and P_y is the value of cross-correlation between Template 1 and Template 2. The notation H indicates that the cross-correlation value is larger than P_x, while M denotes that the value of the cross-correlation is in between P_x and P_y, and L indicates that the value is less than P_y.

The cross-correlation operation is computed for every symbol transition in a binary modulation communications signal. Based on (7.1), a decision algorithm can be developed to recover the digital data sent by the transmitter.

This algorithm has been implemented in MATLAB. Using Monte Carlo simulations the BER performances have been obtained for the binary digitally modulated test signals, i.e., BASK, BFSK, and BPSK. Typically, the BER is very low, with only a few errors occurring at SNR = -5 dB. The results at different SNR values are presented in Table 7.1.

Table 7.1 BER results for WD Demodulation process using unique features templates

Modulation Scheme	SNR	BER
BPSK	-5 dB	0.001
	0 dB	0
	5 dB	0
BASK	-5 dB	0.023
	0 dB	0.001
	5 dB	0
BFSK	-5 dB	0.049
	0 dB	0.037
	5 dB	0.001
	10 dB	0

As seen from the results, the WD Demodulation process is very successful. There is, however, a drawback to this demodulation process when used for binary modulated signals. The digital data cannot be recovered if the data bit sequence is made up entirely of either all data "1"s or all data "0"s. This is due to the use of unique features templates. The unique features templates are defined based on symbol transitions within a communications signals as described in Section 4.1. When there are no symbol transitions within a communications signals, the decision algorithm will not be able to detect symbol transitions since they are not present. The resulting BER would, therefore, either be 100% or 0% as the system would pick the symbols to be either '1' or '0' by

default. In order to overcome this deficiency, a Return-to-Zero (RZ) data symbol format is required instead of the Non-Return-to-Zero (NRZ) data symbol format that was used in this work. In the next section, a WD Demodulation process based on the use of the common features templates is explored.

7.2   Demodulation Using Common Features Templates

A WD demodulation process that utilizes the common features templates instead of the unique features templates is now developed in this section. Again, the templates are cross-correlated with the communications signal in the WD. The normalized cross-correlation values are used to develop a new decision metric that is needed to recover the baseband data sequence. The common features templates defined in Section 4.1 are utilized for the demodulation of M-ary PSK signals. The demodulation of PSK signals is described in Section 7.2.1. Additional common features templates are, however, required to demodulate M-ary FSK, M-ary ASK and M-ary QAM signals. These additional templates will be described Sections 7.2.2-7.2.4.

7.2.1   Demodulation Techniques for Phase Shift Keyed Signals

In order to demodulate M-ary PSK signals, the common features templates defined in Section 6.1 are used. The first step of the demodulation process is to cross-correlate the received communications signal with the appropriate common features templates in the WD. Based on the cross-correlation results, several decision metrics are developed in order to recover the baseband data. The common features templates used here are denoted as Template 1, Template 2 and Template 3, all of which are illustrated in Fig. 6.2.

The desired demodulation decision metrics can be developed using the data in Tables 6.1-6.3. The PSK signal constellations considered in this dissertation are provided in Fig. 7.3. In order to distinguish between these signal constellations a decision metric is developed based on the cross-correlation results and also specific threshold values. Again, the cross-correlation values are computed on a block-by-block basis, as had been illustrated in Fig. 7.2. In this case, however, the templates are aligned with the data symbols in the WD, and not the transitions between symbols. Three different procedures have been developed for demodulating M-ary PSK signals.
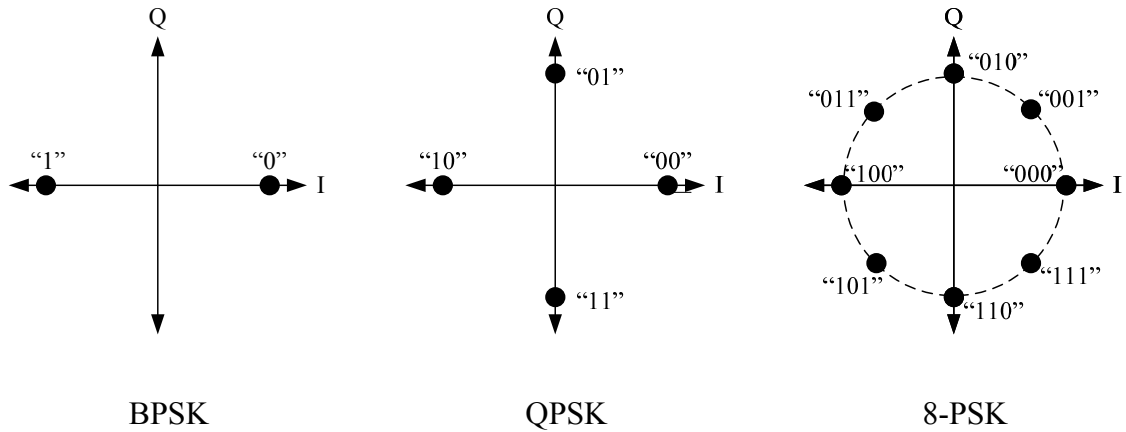
Fig. 7.3. Signal constellations for M-ary PSK signals.

For BPSK signals, only common feature Template 1 is required for the demodulation process in the WD. Therefore, the following decision rule for demodulation is used:

$$\text{output} = \begin{cases} \text{"0"} & \text{if } X_{W1} > 0 \\ \text{"1"} & \text{if } X_{W1} < 0 \end{cases} \tag{7.2}$$

where X_{W1} denotes the cross-correlation value of the received signal and Template 1 in the WD. The threshold value used for the decision metric is zero. This is due to the signal definition.

The algorithm for the demodulation of BPSK signals in the WD using the decision metric in (7.2) is described as follows.

Step 1: Cross-correlate the received BPSK signal with Template 1 in the WD.

Step 2: Compare each of the cross-correlation values with the fixed threshold, and assign an indicator for each cross-correlation value.

Step 3: Based on the indicator, output the baseband data.

The algorithm described above is illustrated in Fig. 7.4.
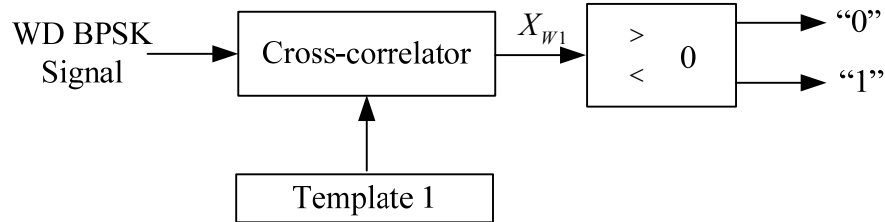
Fig. 7.4. System block diagram for the BPSK demodulator in the WD.

Based on the signal constellation for the QPSK modulation scheme, it is necessary to use both common features Template 1 and Template 2. The decision rule is described as

$$
\text{output} = \begin{cases}
"00" & \text{if } X_{W1} > 0 \text{ and } X_{W2} \sim= 0 \\
"01" & \text{if } X_{W1} \sim= 0 \text{ and } X_{W2} > 0 \\
"10" & \text{if } X_{W1} < 0 \text{ and } X_{W2} \sim= 0 \\
"11" & \text{if } X_{W1} \sim= 0 \text{ and } X_{W2} < 0
\end{cases}
\tag{7.3}
$$

where X_{W1} is the value resulting from the cross-correlation of the signal with Template 1, and X_{W2} is the value resulting from the cross-correlation of the signal with Template 2 in the WD.

Based on (7.3), the algorithm for demodulating QPSK signals in the WD is described as follows.

Step 1: Cross-correlate the received QPSK signal with Templates 1 and 2 in the WD.

Step 2: Examine each segment of the cross-correlation data for both Template 1 and Template 2 and assign indicators for each segment. Apply the decision rule in Eqn. (7.3) to the correlation values and assign an indicator for each cross-correlation value.

Step 3: Based on the indicator, output the baseband data.

The QPSK demodulation algorithm described above is illustrated in Fig. 7.5.
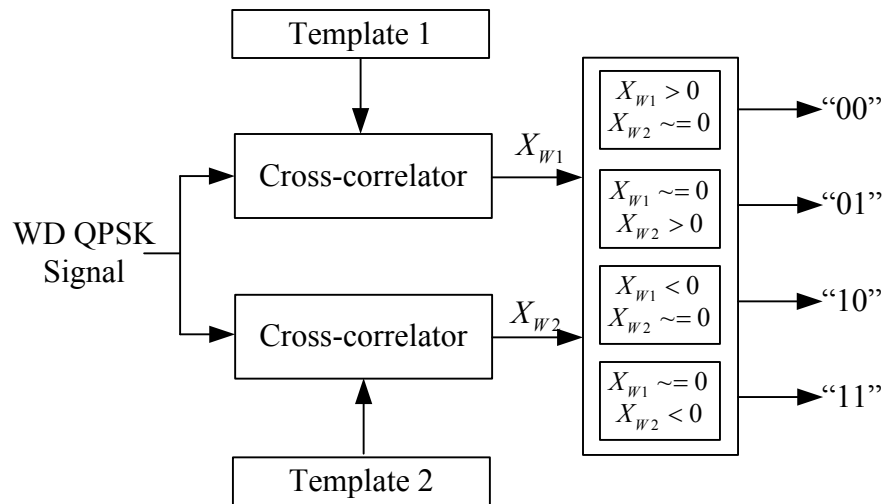
Fig. 7.5. System block diagram for the QPSK demodulator in the WD.

Having defined the demodulation techniques for BPSK and QPSK, a demodulation technique for 8-PSK is now described. In this case all three common features templates and the observations from Tables 6.1-6.3 are used for development of the decision rule. The decision rule is described according to

$$
\text{output} = \begin{cases}
\text{"000"} & \text{if } X_{W1} > 0, \quad X_{W2} \sim= 0 \text{ and } X_{W3} < 0 \\
\text{"001"} & \text{if } X_{W1} > 0, \quad X_{W2} > 0 \quad \text{and } X_{W3} < 0 \\
\text{"010"} & \text{if } X_{W1} \sim= 0, X_{W2} > 0 \quad \text{and } X_{W3} < 0 \\
\text{"011"} & \text{if } X_{W1} < 0, \quad X_{W2} > 0 \quad \text{and } X_{W3} \sim= 0 \\
\text{"100"} & \text{if } X_{W1} < 0, \quad X_{W2} \sim= 0 \text{ and } X_{W3} > 0 \\
\text{"101"} & \text{if } X_{W1} < 0, \quad X_{W2} < 0 \quad \text{and } X_{W3} > 0 \\
\text{"110"} & \text{if } X_{W1} \sim= 0, X_{W2} < 0 \quad \text{and } X_{W3} > 0 \\
\text{"111"} & \text{if } X_{W1} > 0, \quad X_{W2} < 0 \quad \text{and } X_{W3} \sim= 0
\end{cases}
\tag{7.4}
$$

where X_{W1}, X_{W2} and X_{W3} are the cross-correlation values that result from comparing

the received signal with Template 1, Template 2 and Template 3, respectively.

Based on (7.4), the algorithm for demodulating an 8-PSK signal is described as follows.

Step 1: Cross-correlate the received 8-PSK signal with Templates 1, 2 and 3 in the WD.

Step 2: Compare the resulting cross-correlation data with the threshold value of zero as described in Eqn. (7.4).

Step 3: Based on the result from Step 2, assign an appropriate indicator corresponding to one of the threshold combinations shown in Eqn. (7.4).

Step 4: Based on the indicator, output the baseband data.

The 8-PSK demodulation algorithm is described above is shown in Fig. 7.6.
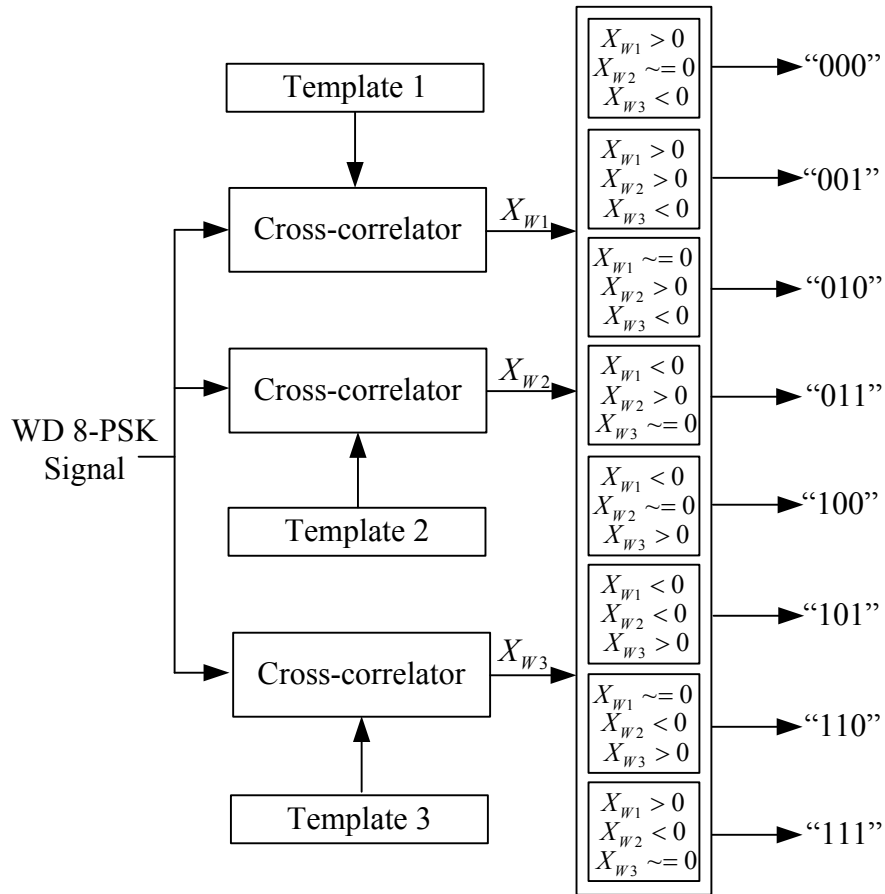
Fig. 7.6. System block diagram for the 8-PSK demodulator in the WD.

7.2.2 Demodulation Techniques for Frequency Shift Keyed Signals

Recall from Chapter 6 that in order to perform a WD AMR process for M-ary FSK signals, it was required to introduce additional common features templates along with Template 1 and Template 2. Similarly, in the WD Demodulation process, additional templates are required. The same templates described in Section 6.2.3.1 are used here. Therefore, the common features templates used are Templates 1, 4 and 5.

In order to demodulate BFSK signals, only Template 1 is used. The demodulation decision rule is described as follows

$$\text{output} = \begin{cases} \text{"0"} & \text{if } X_{W1} \approx 0 \\ \text{"1"} & \text{if } X_{W1} > 0 \end{cases} \tag{7.5}$$

where X_{W1} denotes the cross-correlation result of the signal with Template 1 in the WD.

The demodulation algorithm for BFSK signals is described as follows.

Step 1: Cross-correlate the received BFSK signal with Template 1 in the WD.

Step 2: Compare the cross-correlation data with the threshold value of zero as described in Eqn. (7.5).

Step 3: Based on the results from Step 2, assign the appropriate indicators according to Eqn. (7.5)

Step 4: From the results from Step 3, recover the baseband data.

The system block diagram for the BFSK demodulator is depicted in Fig. 7.7.
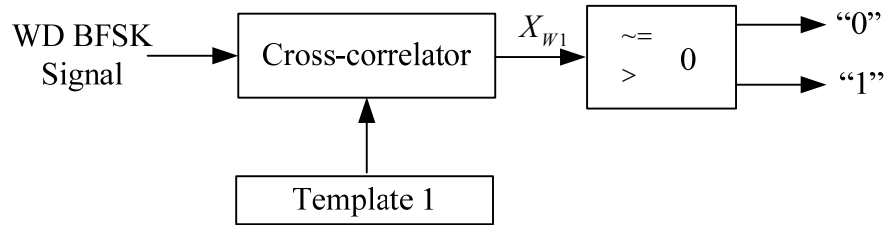
Fig. 7.7. System block diagram for the BFSK demodulator in the WD.

For 4-FSK signals, the two additional common features templates denoted as Templates 4 and 5 are needed. The demodulation process for 4-FSK signals is described according to the following decision rule

$$\text{output} = \begin{cases} \text{"00"} & \text{if } X_{W1} > 0, \ X_{W4} \approx 0 \text{ and } X_{W5} \approx 0 \\ \text{"01"} & \text{if } X_{W1} \approx 0, \ X_{W4} > 0 \text{ and } X_{W5} \approx 0 \\ \text{"10"} & \text{if } X_{W1} \approx 0, \ X_{W4} \approx 0 \text{ and } X_{W5} > 0 \\ \text{"11"} & \text{if } X_{W1} \approx 0, \ X_{W4} \approx 0 \text{ and } X_{W5} \approx 0 \end{cases} \tag{7.6}$$

where X_{W1}, X_{W4} and X_{W5} are the cross-correlation values obtained when comparing the received, noisy signal to Templates 1, 4 and 5, respectively.

Based on (7.6), the algorithm for demodulating 4-FSK signals in the WD is described as follows.

Step 1: Cross-correlate the received 4-FSK signal with Templates 1, 4 and 5 in the WD.

Step 2: Compare the cross-correlation data with the threshold value of zero as described in Eqn. (7.6).

Step 3: Based on the results from Step 2, assign appropriate indicators corresponding to one of the threshold combinations.

Step 4: From the results of Step 3, recover the baseband data.

The corresponding block diagram for the demodulation of 4-FSK is illustrated in Fig. 7.8.
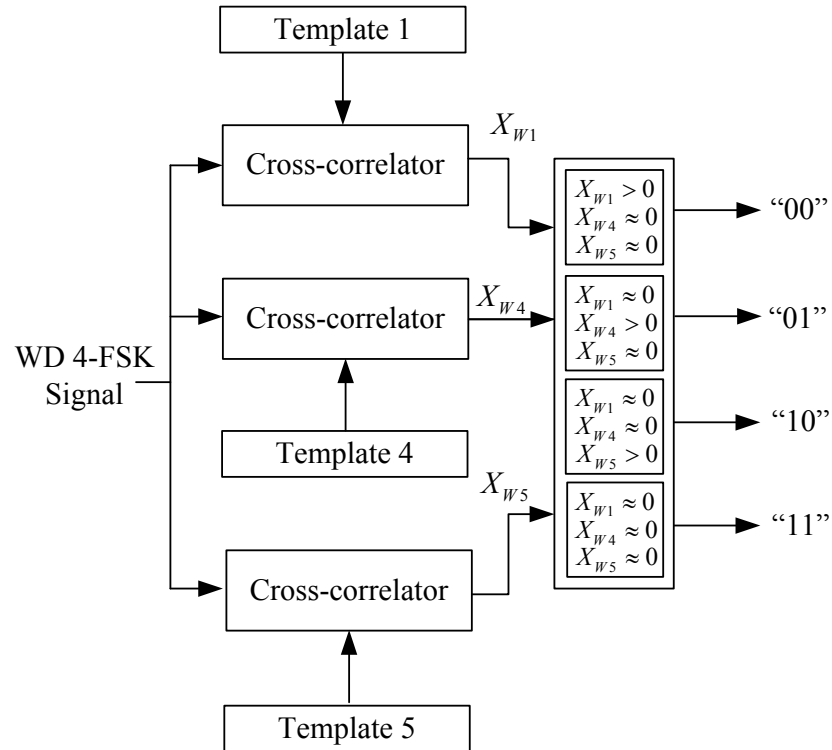
Fig. 7.8. System block diagram for the 4-FSK demodulator in the WD.

7.2.3   Demodulation Techniques for Amplitude Shift Keyed Signals

It had been observed from Figs. 6.3 and 6.4, that the cross-correlation results of the signal when compared with Template 1 are used as the distinguishing characteristics for recognizing BASK and 4-ASK signals. Recall that the WD cross-correlation values obtained for BASK signals compared with Template 1 had formed a constant envelope in time, and were termed single-level values. In the case of 4-ASK signals the cross-correlation results produce multi-level values.

These characteristics are now exploited for use in the WD Demodulation of BASK and 4-ASK signals.

For BASK signals, the decision rule is described by

$$\text{output} = \begin{cases} "0" & \text{if } X_{W1} \approx 0 \\ "1" & \text{if } X_{W1} > 0 \end{cases}. \tag{7.7}$$

Based on (7.7), the demodulation algorithm for BASK signals is described as follows.

Step 1: Cross-correlate the received BASK signal with Template 1 in the WD.

Step 2: Compare the cross-correlation data with the threshold value of zero as described in Eqn. (7.7).

Step 3: Assign indicators for the results obtained from Step 2.

Step 4: Based on the indicators, recover the baseband data.

A system block diagram of the demodulation of BASK signals is illustrated in Fig. 7.9.
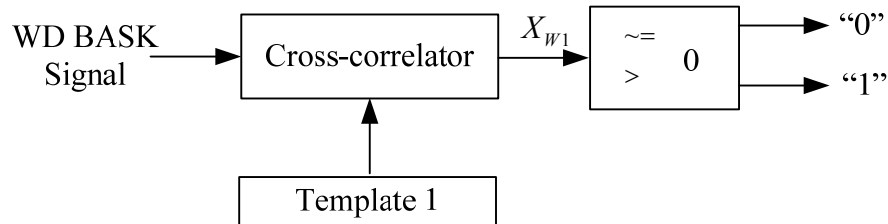
Fig. 7.9. System block diagram for the BASK demodulator in the WD.

In a manner similar to BASK, decision rules the WD demodulation of 4-ASK signals are developed based on the cross-correlation results of comparing the received signal with Template 1 in the WD. The cross-correlation values are normalized to have a dynamic range from 0 to 3. In Fig. 7.10 an example of a plot of the cross-correlation results of a 4-ASK signal when compared to Template 1 is shown. In the figure, the quantities T_1, T_2 and T_3 represent the three threshold values used in developing the decision rule for the demodulation algorithm for 4-ASK signals.
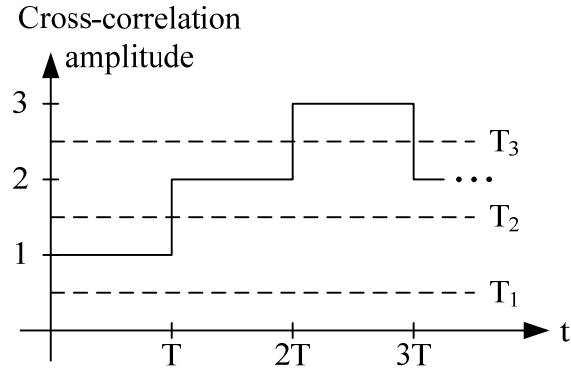
Fig. 7.10. Example plot of the WD cross-correlation of a 4-ASK signal with Template 1.

For the example shown in Fig. 7.10, the threshold values are

$$\text{Threshold values} = \begin{cases} T_1 = 0.5 \\ T_2 = 1.5 \\ T_3 = 2.5 \end{cases}$$

Since the cross-correlation values between the signal and the templates are normalized to have a dynamic range from 0 to 3, and noting the observations based on Fig. 6.4, there are four distinct levels in the cross-correlation plot corresponding to Template 1. Therefore, the threshold values are identified to be 0.5, 1.5 and 2.5, for T_1, T_2 and T_3, respectively. The thresholds are chosen to be the mid-point of each interval between the four distinct levels.

The decision rule for the demodulation of 4-ASK signals is

$$\text{output} = \begin{cases} \text{"00"} & \text{if} \quad X_{W1} \approx 0 \\ \text{"01"} & \text{if } T_1 < X_{W1} < T_2 \\ \text{"10"} & \text{if } T_2 < X_{W1} < T_3 \\ \text{"11"} & \text{if} \quad X_{W1} > T_3 \end{cases} \tag{7.8}$$

where X_{W1} is the result of cross-correlation between the received 4-ASK signal and Template 1.

The demodulation algorithm for 4-ASK is described as follows.

Step 1: Cross-correlate the received 4-ASK signal with Template 1 in the WD.

Step 2: Compare the cross-correlation data with the threshold values T_1, T_2, and T_3, according to Eqn. (7.8).

Step 3: Based on the results from Step 2, assign indicators for each cross-correlation data element.

Step 4: Recover the baseband data based on the indicators assigned in Step 3.

A system block diagram describing the demodulation algorithm for 4-ASK signals is depicted in Fig. 7.11.
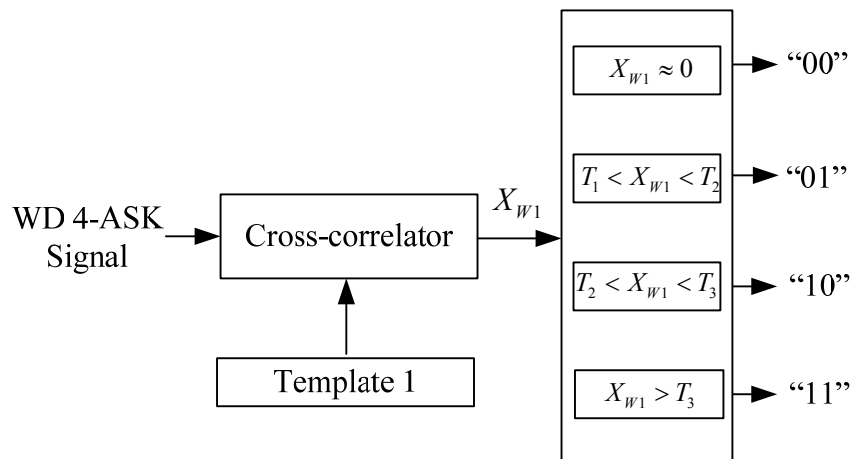
Fig.7.11. System block diagram for the 4-ASK demodulator in the WD.

7.2.4   Demodulation Techniques for Quadrature Amplitude Modulated Signals

QAM signals consist of amplitude and phase changes made to a carrier wave in order to represent different baseband data symbols. The demodulation methodologies developed here are again based on the cross-correlation values obtained when comparing M-ary

QAM signals with common features templates in the WD. The threshold values are defined as the auto-correlation values of the templates as described in Section 6.2.3.2. Also, additional templates are required for demodulation of the M-ary QAM signals. This is due to the requirement that the different sizes of signal constellations be identified for various M-ary QAM signals. The methods of extracting these templates are similar to the methods used in the WD AMR process for M-ary QAM signals. The concept of a "moving origin" is also used in constructing the templates representing the WD signatures for the M-ary QAM signals. Figs. 7.12-14 illustrate the locations of the additional common features templates for different size M-ary QAM signal constellations. With the use of common features Template 1, Template 2 and the additional templates, the baseband data represented by M-ary QAM symbols can be recovered throughout an entire frame.
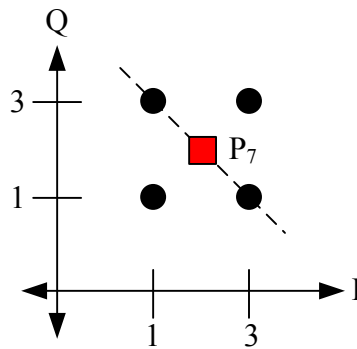
Fig. 7.12. Quadrant I of the 16-QAM signal constellation.
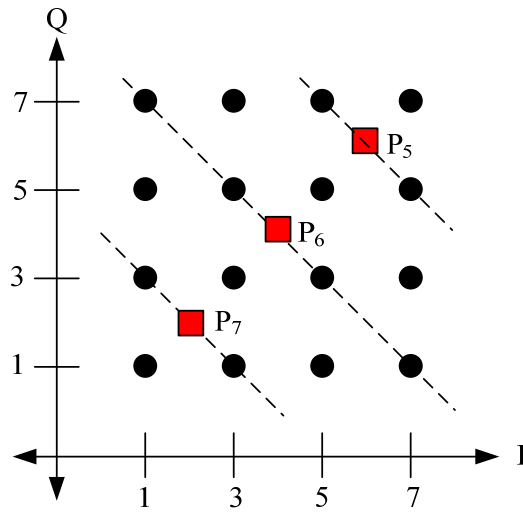
Fig. 7.13. Quadrant I of the 64-QAM signal constellation.
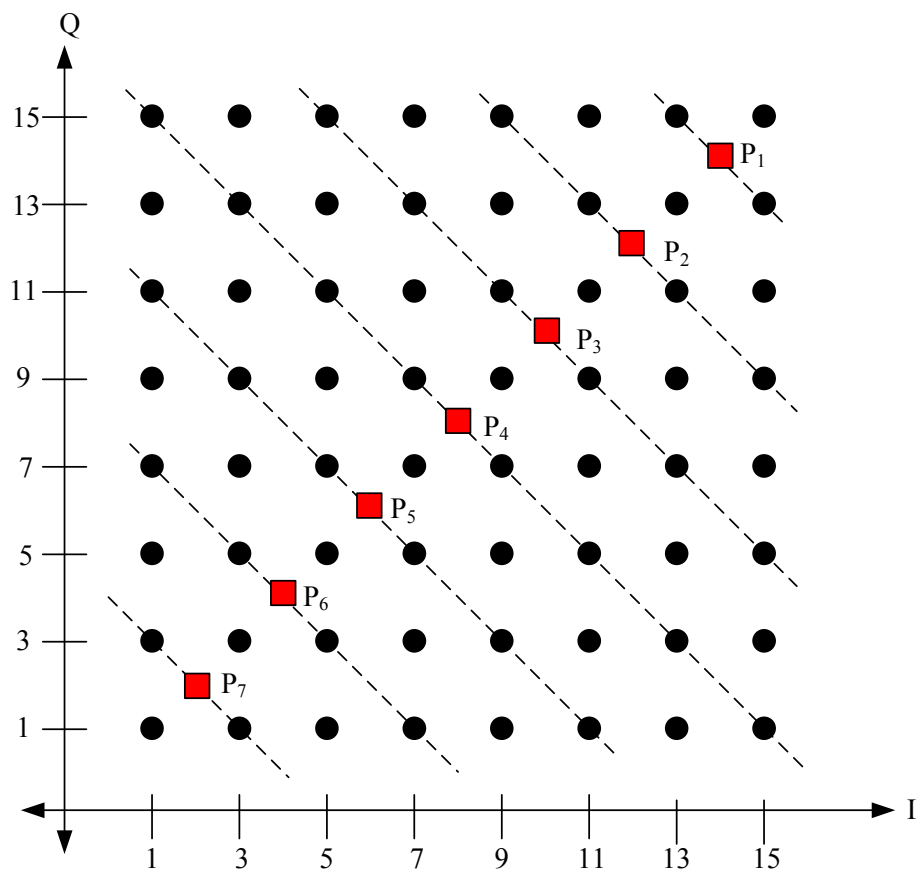
Fig. 7.14. Quadrant I of the 256-QAM signal constellation.

Again, only the first quadrant of the signal constellations for the 16-, 64- and 256-QAM

schemes are shown in Figs. 7.12-7.14, along with locations of the additional templates

required, namely P_1, P_2, ..., P_7. The same concepts, however, can readily be applied to

the other 3 quadrants. The additional common features represented by the template in

Figs. 7.12-7.14 are defined in the time-domain as

$$P_1(t) = A_1 \cos(2\pi f_c t) + A_2 \sin(2\pi f_c t) \qquad T_i < t < T_{i+1} \qquad (7.9)$$

$$P_2(t) = B_1 \cos(2\pi f_c t) + B_2 \sin(2\pi f_c t) \qquad T_i < t < T_{i+1} \qquad (7.10)$$

$$P_3(t) = C_1 \cos(2\pi f_c t) + C_2 \sin(2\pi f_c t) \qquad T_i < t < T_{i+1} \qquad (7.11)$$

$$P_4(t) = D_1 \cos(2\pi f_c t) + D_2 \sin(2\pi f_c t) \qquad T_i < t < T_{i+1} \qquad (7.12)$$

$$P_5(t) = E_1 \cos(2\pi f_c t) + E_2 \sin(2\pi f_c t) \qquad T_i < t < T_{i+1} \qquad (7.13)$$

$$P_6(t) = F_1 \cos(2\pi f_c t) + F_2 \sin(2\pi f_c t) \qquad T_i < t < T_{i+1} \qquad (7.14)$$

$$P_7(t) = G_1 \cos(2\pi f_c t) + G_2 \sin(2\pi f_c t) \qquad T_i < t < T_{i+1}. \qquad (7.15)$$

where A_j, B_j, C_j, D_j, E_j, F_j and G_j, for $j = 1, 2$, are constants. The appropriate values for the

constants are assigned depending on the particular size of the signal constellation.

Appendix C lists the values of the constants used for the common features templates for

M-ary QAM signals.

The methodology for demodulating 4-QAM signals is similar to the demodulation of

QPSK signals. However, for 4-QAM signals the cross-correlation results are obtained

with Templates 1 and 3 instead of Templates 1 and 2 as was done in the case of QPSK

signals. Again, using observations based on Table 6.3 and Fig. 6.10, the decision rule for

the 4-QAM modulation scheme is

$$\text{output} = \begin{cases} \text{"00"} & \text{if } X_{W1} > 0 \text{ and } X_{W3} < 0 \\ \text{"01"} & \text{if } X_{W1} < 0 \text{ and } X_{W3} \approx 0 \\ \text{"10"} & \text{if } X_{W1} < 0 \text{ and } X_{W3} > 0 \\ \text{"11"} & \text{if } X_{W1} > 0 \text{ and } X_{W3} \approx 0 \end{cases} \tag{7.16}$$

where X_{W1} denotes the cross-correlation values obtained by comparing the received 4-QAM signal with Template 1, and X_{W3} represents the cross-correlation values obtained with Template 3.

The algorithm for demodulation of 4-QAM signals is described as follows.

Step 1: Cross-correlate the received 4-QAM signal with Template 1 and Template 3 in the WD.

Step 2: Compare the cross-correlation data with the threshold value of zero.

Step 3: Based on the results from Step 2, assign an indicator to each individual comparison using Eqn. (7.16).

Step 4: Recover the baseband data sequence based the indicators assigned in Step 3.

A system block diagram for the demodulation of 4-QAM signals is illustrated in Fig. 7.15.
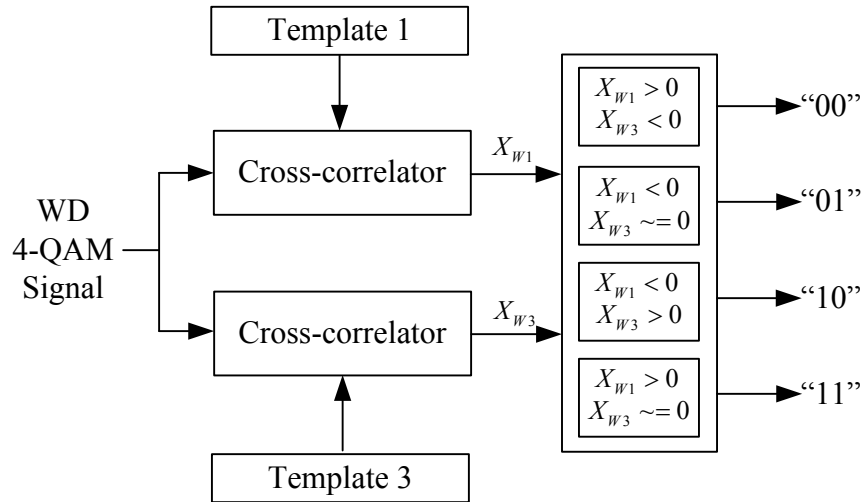
Fig. 7.15. System block diagram for the 4-QAM demodulator in the WD.

In order to develop the algorithm for the WD Demodulation of 16-QAM signals common features templates, namely Template 1 and Template 2, are used along with the additional templates defined in (7.9)-(7.15). As illustrated in Fig. 7.12, each dot represents a data symbol within a 16-QAM signal in quadrant I. First, the signal quadrant location is determined based on the algebraic signs of the cross-correlation results using Template 1 and Template 2, as described in Table 6.3. Then, the auto-correlation value of the template is used as the threshold value for determining the size of the signal constellation. The decision rule is described as

$$
\text{output} = \begin{cases}
\text{"1"} & \text{if } X_{P7} < T_{7\_x} \\
\text{"2"} & \text{if } X_{P7} \approx T_{7\_x} \text{ and } X_{W1} > X_{W2} \\
\text{"3"} & \text{if } X_{P7} > T_{7\_x} \\
\text{"4"} & \text{if } X_{P7} \approx T_{7\_x} \text{ and } X_{W1} < X_{W2}.
\end{cases}
\tag{7.17}
$$

where X_{P7} represents the cross-correlation value obtained when comparing the received signal with the specific features Template P_7, the quantity T_{7_x} denotes the auto-correlation value of Template P_7, and the quantities X_{W1} and X_{W2} denote the cross-

correlation value obtained with common features Template 1 and Template 2, respectively.

Based on (7.17) and Table 6.3, the algorithm for the demodulation of 16-QAM signals in the WD is described as follows.

Step 1:   Cross-correlate the received 16-QAM signal with Templates 1 and 2 in the WD.

Step 2:   Determine the quadrant location of each data symbol and cross-correlate Template P_7 with the signal.

Step 3:   Compute the auto-correlation of P_7.

Step 4:   Compare the cross-correlation results from Step 1 with the thresholds as described in Eqn. (7.17), and assign the appropriate indicator for each signal segment.

Step 5:   Recover the baseband data sequence based on the results obtained in Step 4.

A similar methodology is applied to both 64- and 256-QAM with additional templates introduced. The detailed algorithms and decision rules are described in Appendices A and B.

7.3   Simulation Experiments and Results

The algorithms developed in this chapter are all realized using the MATLAB computer simulation environment. All of the signals used in this study have been corrupted by zero-mean AGWN resulting in SNR values in the range of -5 dB to 10 dB. The WD Demodulator performance has been evaluated based on 10^5 Monte Carlos trials wherein each simulation experiment consists of 192 bits per frame for ASK, FSK and PSK

signals, and 1024 bits per frame for M-ary QAM signals. The signal is oversampled by a factor of 16 over the Nyquist rate corresponding to the carrier frequency in order to maintain a high degree of resolution in the WD scalograms. The key parameter assumed to be known for the demodulation process is that of perfect symbol timing with no timing offset.

Each received, noisy signal has been demodulated using the appropriate WD demodulator. Each set of demodulator performance results presented in Figs. 7.16-7.26 contains two BER curves. The curves which have data points marked with square symbols correspond to the traditional matched filter demodulation performance results. The curves having data points marked with asterisks are the simulation results for the WD Demodulators developed in this dissertation.
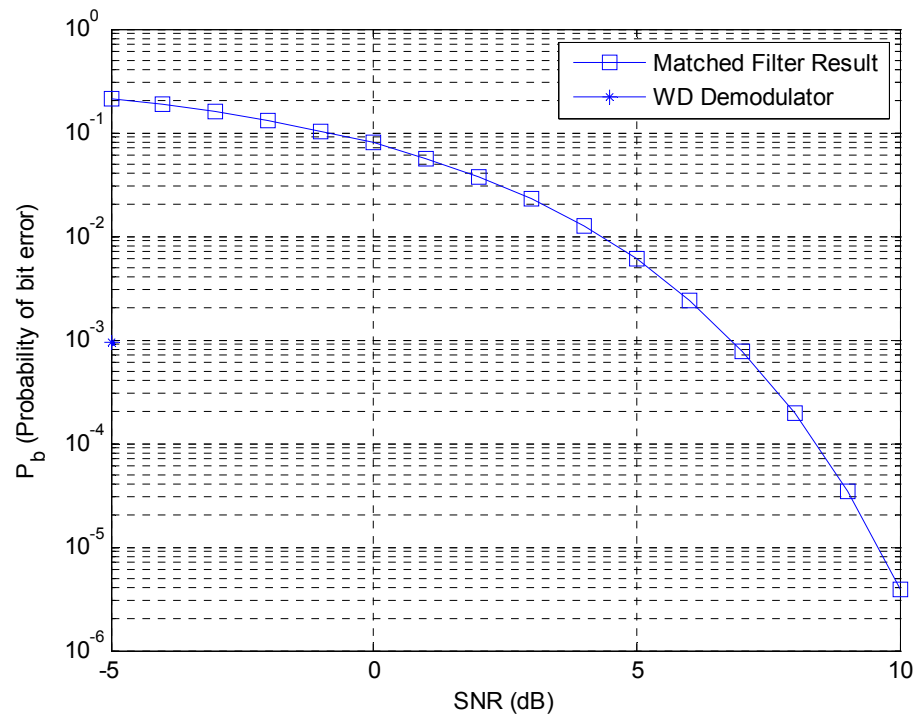
Fig. 7.16. WD demodulation performance for BPSK.
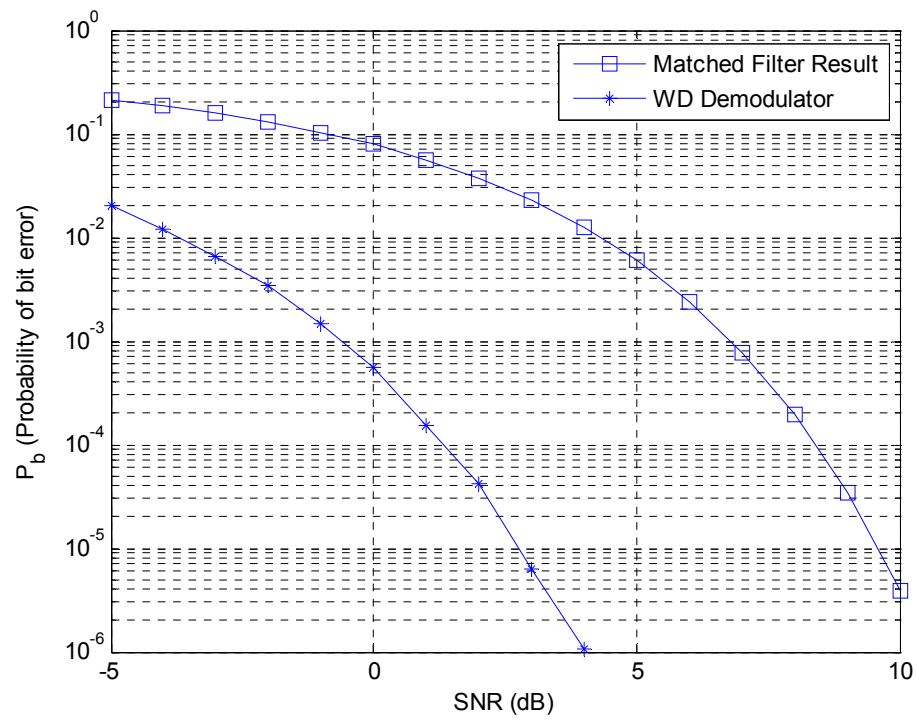
Fig. 7.17. WD demodulation performance for QPSK.
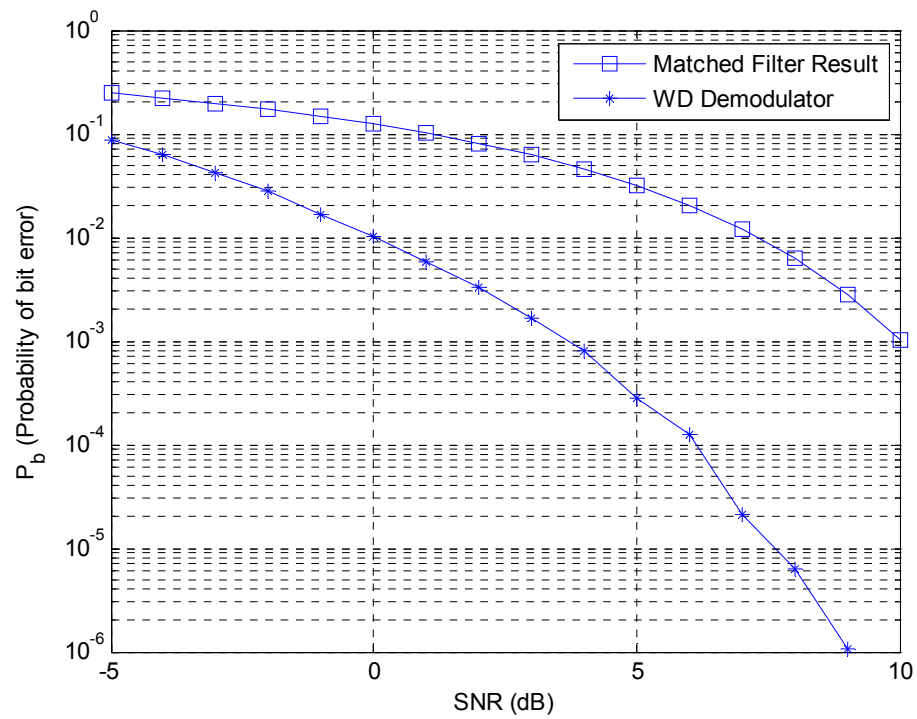
Fig. 7.18. WD demodulation performance for 8-PSK.
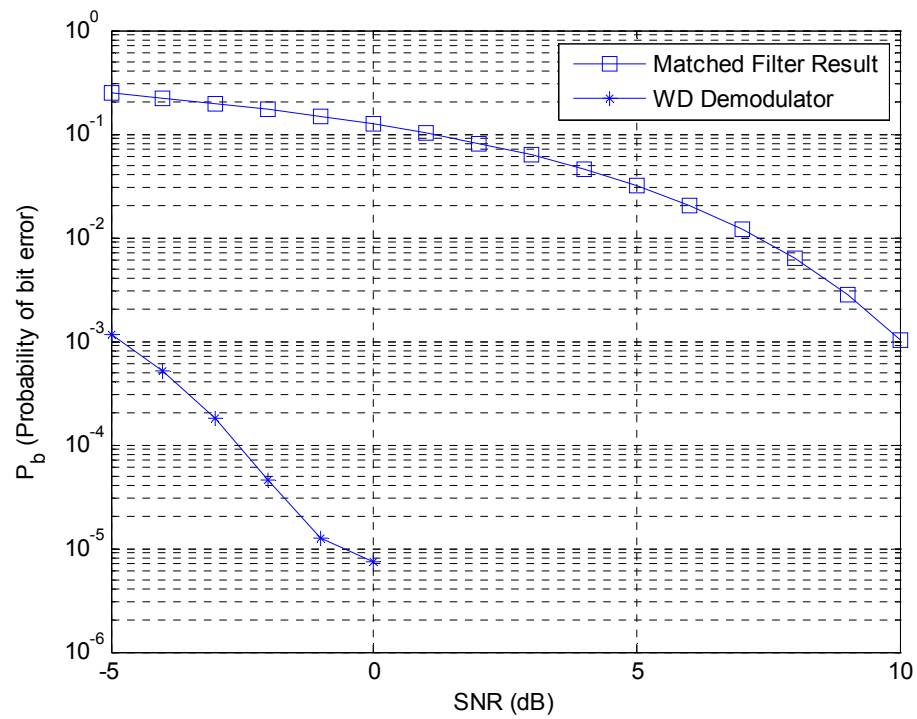
Fig. 7.19. WD demodulation performance for BASK.
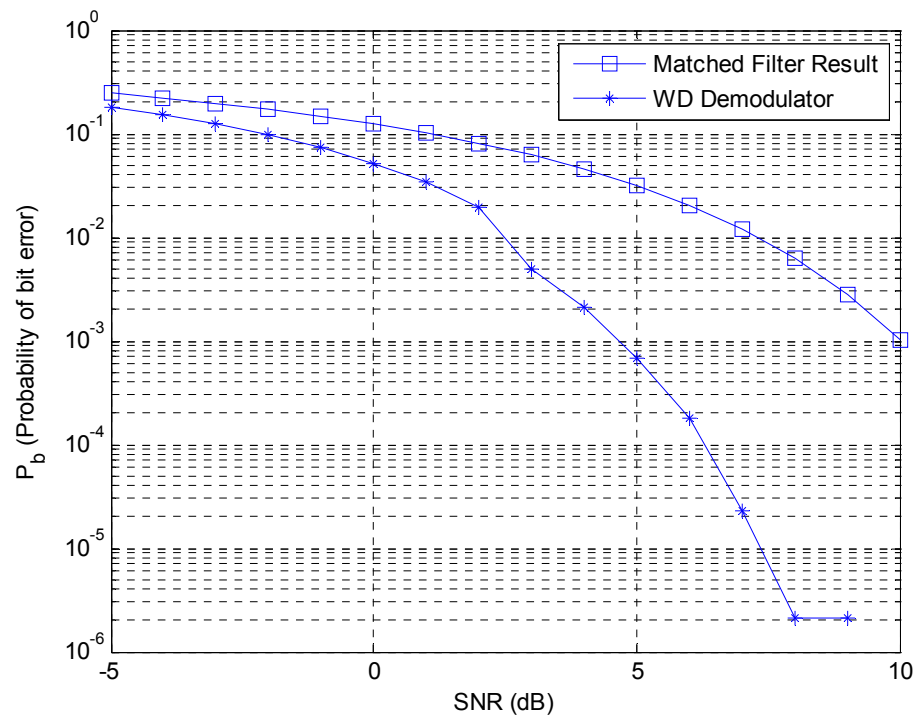
Fig. 7.20. WD demodulation performance for 4-ASK.
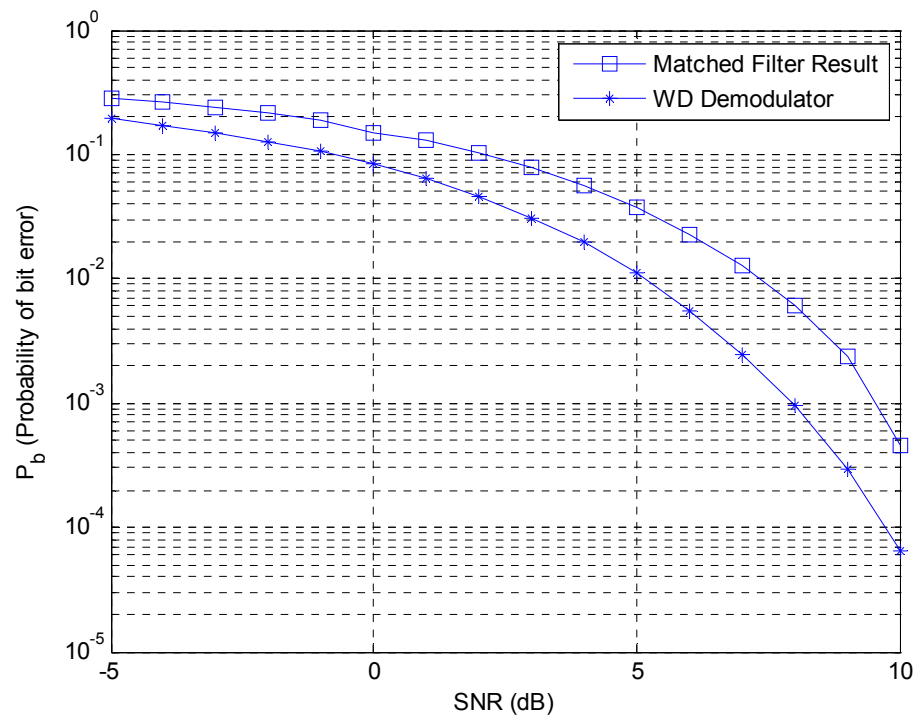
Fig. 7.21. WD demodulation performance for BFSK.
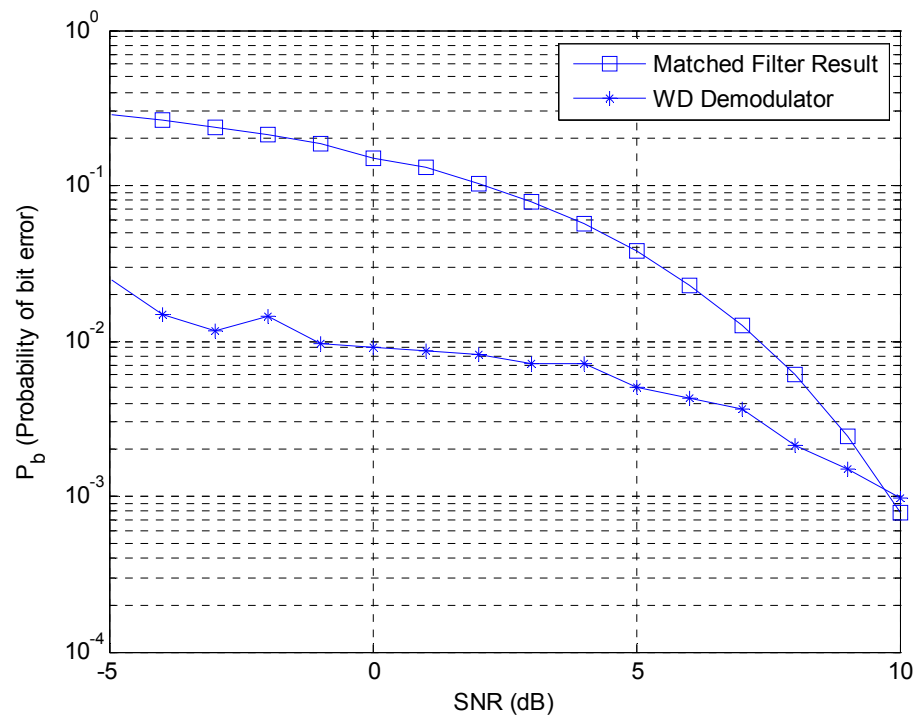
Fig. 7.22. WD demodulation performance for 4-FSK.
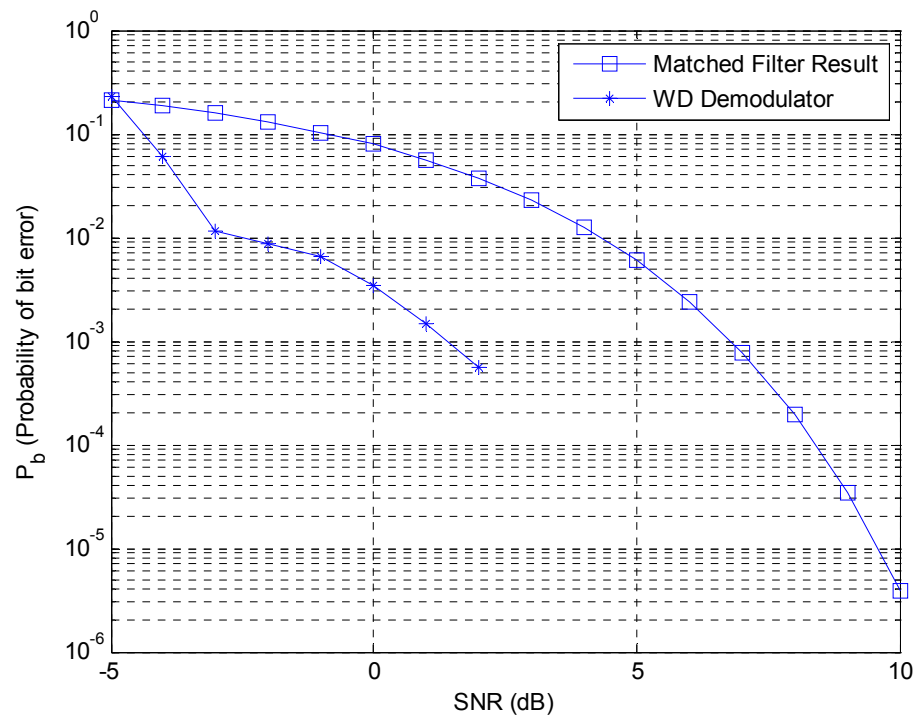
Fig. 7.23. WD demodulation performance for 4-QAM ($\pi/4$-QPSK).
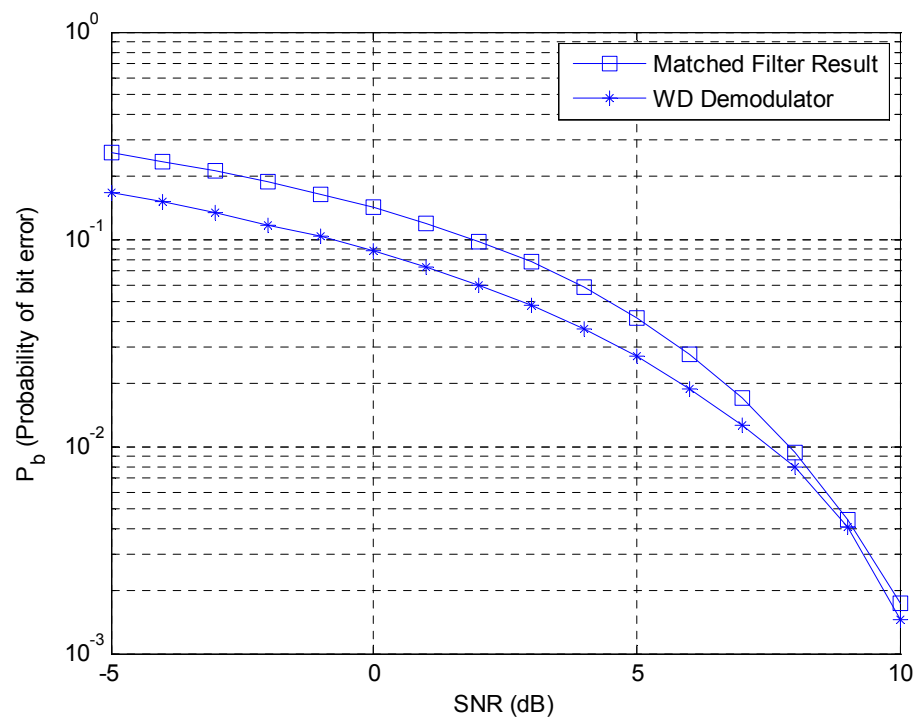
Fig. 7.24. WD demodulation performance for 16-QAM.
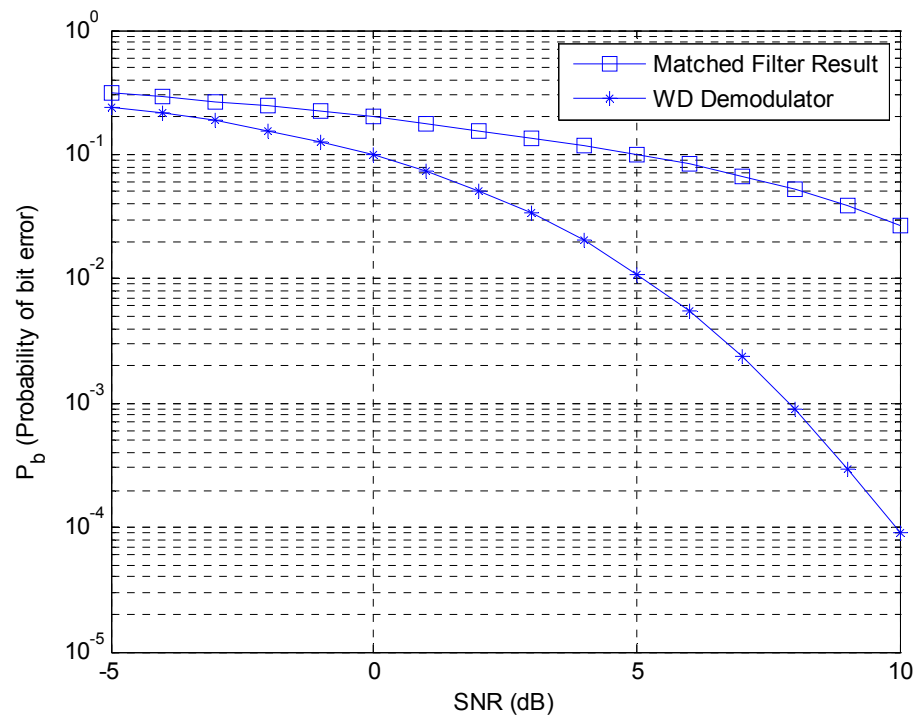
Fig. 7.25. WD demodulation performance for 64-QAM.
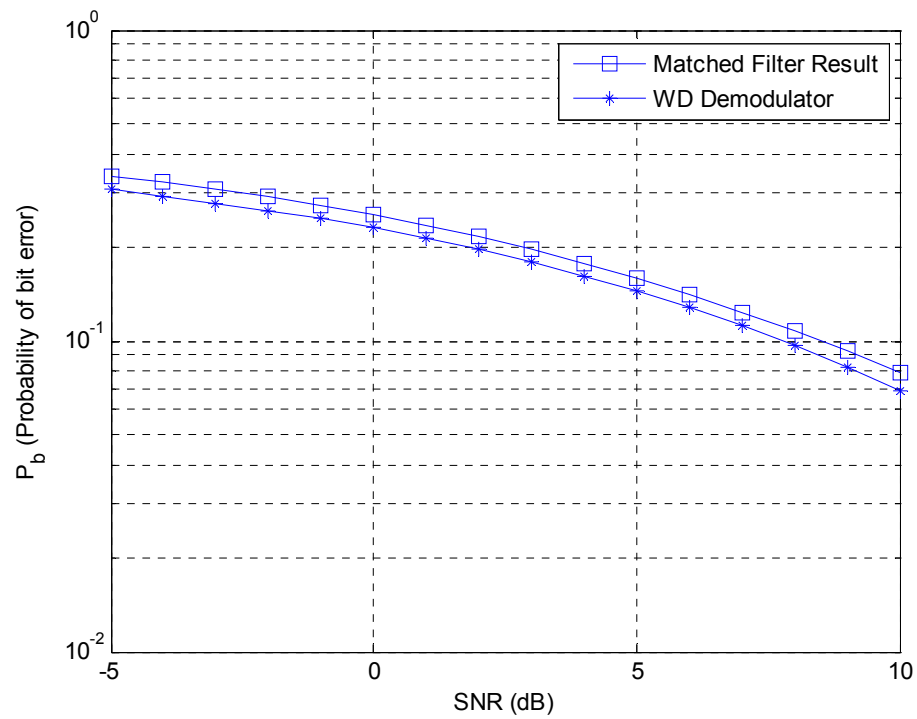
Fig. 7.26. WD demodulation performance for 256-QAM.

The BER curves obtained using the WD Demodulation techniques developed in this dissertation are compared with BER curves corresponding to standard matched filter-based demodulation in Figs. 7.16-7.26. It has been observed that the probability of error is almost zero for BPSK signals for WD Demodulation using the common features templates. The exception is when SNR= -5 dB where the BER is found to be P_b = 9.3×10^{-4}. For the cases of QPSK and 8-PSK, the experimental BER curves based on WD Demodulation are one or two orders of magnitude better than the matched filter-based demodulation BER curves.

In the case of a BFSK signal, however, there is only slight improvement in performance when WD Demodulation employing the common features templates is used as compared to the matched filter-based BER curve. The BER curve corresponding to the WD Demodulation of 4-FSK is, however, an order of magnitude better than the matched filter-based BER curve for low SNR values, while the performances are comparable at higher SNR values.

For 4-QAM signals, the BER curve obtained using WD Demodulation shows better performance when compared with the matched filter-based BER curve at high SNR values. However, there is only slight improvement in the experimental BER results compared to the matched filter-based results for 16-QAM signals. For 64 QAM signals the BERs are at least one order of magnitude smaller at high SNR values when WD Demodulation is used as compared with traditional matched filtering. In the case of 256-QAM signals both methods produce similar performance. This might be due to the number of symbols employed in the demodulation simulations. The number of symbols used per frame transmitted is 128 symbols in the demodulation of QAM signals. There

are 256 different symbols defined in a 256-QAM signal, therefore, increasing the number of symbols per trial might yield improved BER performance for the WD Demodulator.

7.4 Discussion of Results

In this chapter two WD Demodulation methodologies have been described in detail. Both the unique features templates and the common features templates have been used for WD Demodulation of digitally modulated communications signals. The WD Demodulation methodologies have also been devised in a manner such that automatic demodulation of a communications signal is possible after the modulation scheme has been recognized by the WD AMR processor. This feature, which ensures that a signal-specific demodulator can be selected automatically, is advantageous for the development of agile radio receivers.

The WD Demodulation methodology described in Section 7.1 based on unique features templates is only useful for demodulating binary modulation schemes. The BER performance of this methodology for the cases of BASK, BFSK and BPSK signals show that only a few errors occur for SNR less than 0 dB. There is, however a drawback to this method. If all data symbols transmitted are the same, then the probability of error could either be unity, or zero. This is because the unique features templates are based on symbol transitions, and no data changes were present to create symbol transitions in such transmitted signals. In order to overcome this deficiency, an RZ data symbol format is required to be implemented instead of an NRZ format used in this work.

The second WD Demodulation methodology described in Section 7.2 utilizes common features templates, which are described based on the sinusoidal carrier within a symbol period in a digitally modulated signal. The operation of cross-correlation in the wavelet-domain between known templates and a received, noisy signal is again central to this methodology. Based on the application of specific decision rules the baseband data are recovered. Due to the variations of both amplitude and phase that occur in M-ary QAM signals, additional templates are introduced in order to recognize the size of a particular QAM signal. The additional templates are used for development of the decision rule for the demodulation of M-ary signals. It is seen from Figs. 7.24-7.26 that the WD Demodulator produces improved BER performance as compared to the traditional match filter-based methods via Monte Carlo simulations.

For every modulation scheme considered in this dissertation, the WD Demodulation methodologies performed better than traditional matched filter-based method. This observation is based on comparing the BER performances obtained using both types of demodulators. This trend is seen in the cases of WD Demodulation based on unique features templates, as well as in the cases where common features templates are used. The BER performance results of WD Demodulation for PSK signals are at least two to three orders of magnitude better as compared to the traditional matched filter-based methods at lower values of SNR. On the other hand, the WD Demodulator produced no errors at SNR > -4 dB for BPSK signals; at SNR > 4 dB for QPSK signals; and at SNR > 9 dB for 8-PSK signals. For more complex modulation schemes, such as 16-, 64- and 256-QAM signals, the WD Demodulator BER performance for the 16-QAM signal shows slight improvement over the matched filter-based method. In the case of a 64-

QAM signal, the BER performance of the WD Demodulator shows at least an order of magnitude improvement over the BER performance for the matched filtered-based method at SNR > 5 dB. The BER performances for both methods in the case of a 256-QAM signal are almost the same.

The first reason for the superior performance of WD Demodulation could be due to the number of templates that are used. In the case of common features templates, the sinusoidal carrier within a symbol is used to define the various common features templates. Additional templates are also introduced for higher-order modulation schemes, such as 4-FSK and M-ary QAM. By doing so, WD Demodulation makes use of at least 1 template for lower-order modulation schemes, and up to 9 templates for higher-order modulation schemes. In contrast, traditional matched filtering-based demodulation uses at most two templates representing the *I* and - bases of a signal constellation (which are orthogonal basis functions) for all signals considered in this dissertation. It can, therefore, be hypothesized that the increased number of templates in the case of WD Demodulation contributes to more robust detection of the data-bearing symbols.

A second reason for the superior BER performance realized by WD Demodulation is the increase in dimensionality of both the templates and the communications signals when considered in the WD. Fundamentally, the CWT is the time-domain cross-correlation between a signal and a wavelet. Specifically, the signal is cross-correlated with several copies of a wavelet, each copy having been dilated in functional shape and translated across the signal along the time axis. A one-dimensional time-domain signal is expressed in a two-dimensional form in the WD by using a joint time-scale representation. Due to this property of WTs, each time-domain modulation characteristic of a communications

signal is expressed in many different ways, depending of the specific dilation of the wavelet used. A transformation of this nature is perhaps most appreciated visually when plotted in the form of a scalogram (as shown in Figs. 4.4-4.6, for example), in which the modulation characteristics that comprise the overall communications signal in the time-domain are expressed in a variety of ways due to the dilation and translation of the wavelet. It is this observation that is used advantageously in the WD Demodulation methodology described in this chapter. Every template representing a WD signature, whether a unique features template, or a common features template, explicitly contains multiple WD representation corresponding to a single feature of a time-domain signal. In other words, the features of a time-domain signal are manifested in a much richer form of representations in the WD. Therefore, it is possible that better robustness in demodulation and resiliency to noise are obtained by expressing communications signals and their templates in the WD.

In Fig. 7.27, a BFSK test signal, corrupted with AWGN at SNR = 10 dB, is shown in both the time- and wavelet-domains. It is observed from the WD scalogram that the effect of noise at higher levels of resolution (from level 128 to level 4096 along the ordinate) has been reduced compared to the lower levels of resolution (from level 2 to level 64). In the figures, the darker area represents the smaller wavelet coefficient values, while the lighter area represents larger wavelet coefficient values.
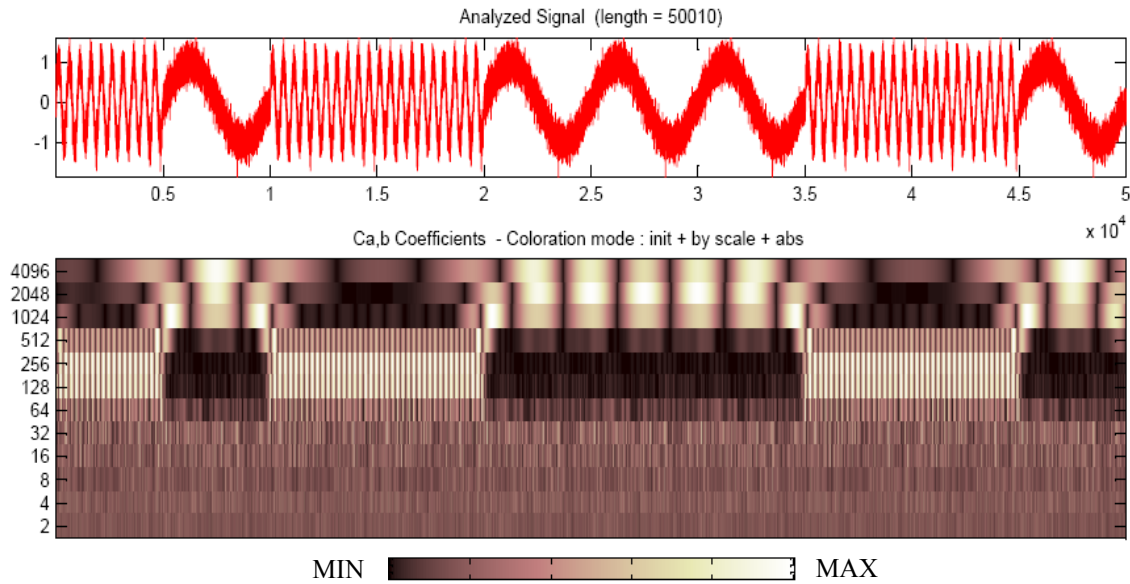
Fig. 7.27. (Top) BFSK signal at 10 dB SNR, (bottom) 12-level wavelet-domain

decomposition using the Reverse Biorthogonal 1.3 wavelet.

By comparing the scalogram for a noisy BFSK signal shown in Fig. 7.27 and the

scalogram for a noise-free BFSK signal shown in Fig. 7.28, the scalogram from level

128 to level 4096 remained either unchanged, or has been less affected by the additive

noise. Therefore, one conclusion that can be drawn from this observation is that the

cross-correlation between the transformed signal and the WD noise-free template at

higher levels of resolution become dominant due to the nature of the wavelet coefficients

of the signal being large in amplitude and also the noise-free template has large amplitude

values.
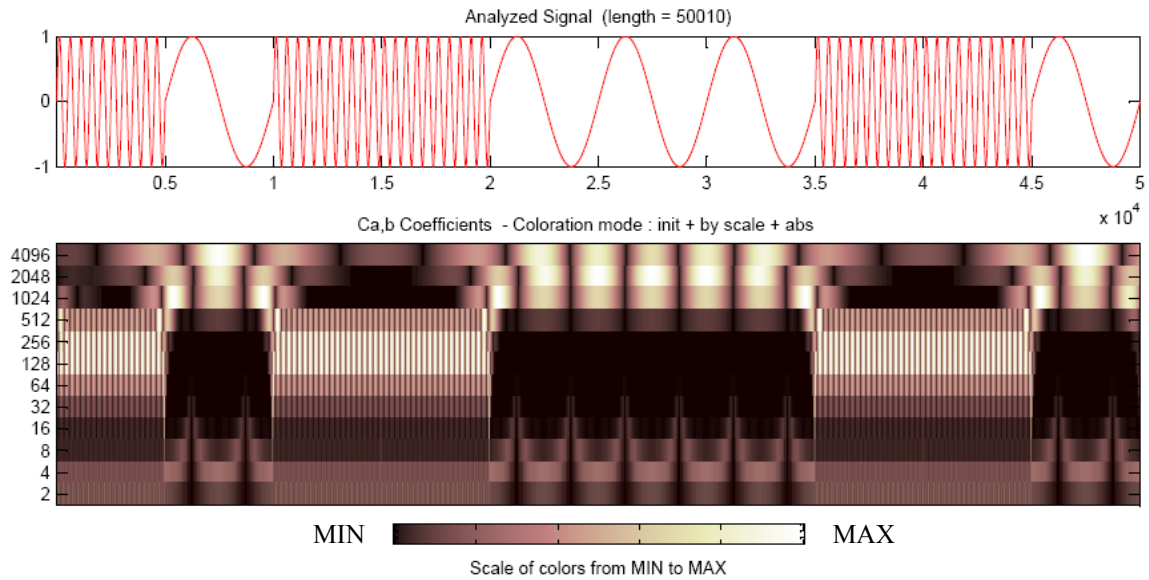
Fig. 7.28 (Top) BFSK signal without noise, (bottom) 12-level wavelet-domain

decomposition using the Reverse Biorthogonal 1.3 wavelet.

The third reason for better BER performance results obtained using the WD Demodulator is due to the larger values of cross-correlation that exist between the best-matched wavelet and the known modulation type signal at higher levels of resolution. The WD Demodulation algorithm developed in this work is based on cross-correlation values being compared with a fixed threshold value. Therefore, due to this observation, the effect of noise on the cross-correlation values has been reduced which provides an improvement in the BER performance as compared to the traditional matched filter-based demodulation method.

Chapter 8

Summary and Conclusions

8.1   Summary

The WD AMR algorithms invented in this dissertation are based on the cross-correlation of received, noisy digitally modulated communications signals with WD signatures corresponding to a known set of modulation schemes. The WD signatures are represented as templates obtained from noise-free digitally modulated signals. Two categories of WD signatures are defined, namely the unique features templates and the common features templates. The unique features contain the symbol transition characteristics of a communications signal. Each feature is unique to a particular digital modulation scheme. Therefore, for higher-order modulation schemes, more unique features templates are needed. Due to that fact, the computational effort increased.

 The common features templates represent the sinusoidal carrier characteristics present within a symbol period of a communications signal. Therefore, fewer numbers of templates are needed for the WD AMR process. For example, only 28 common features templates are needed to recognize 256-QAM signals as compared to the need for a total of 65536 unique features templates otherwise.

The rates of correct classification reported in Chapter 4 show that all results are better than those reported in the literature. The only drawback when using the unique features templates is that because the templates are extracted so as to capture the symbol transition characteristics, the WD AMR process might not able to recognize the particular

modulation scheme when the communications signal data sequences contain either all data "1" or data "0" symbols.

The WD Demodulation method developed in this work is also based on the cross-correlation of the WD signatures with received, noisy communications signals. It was shown in Chapter 7 that the BER performance of the WD Demodulation process offers an improvement over the traditional matched filtering method. The WD Demodulation process is the first such methodology devised in the context of WTs.

Both the WD AMR and Demodulation processes devised in this dissertation are based on the cross-correlation operations and feature extractions of signatures templates. Both processes developed in this dissertation are based on a blind recognition technique. Other methods, i.e., SVMs and ANNs, reported in the literature are use to enhance the classification performance. However, they required a training sequence in order for the sub-system to adapt to specific modulation scheme. Use of a training sequence further increases the complexity and the computational effort of an AMR system. On the other hand, the WD AMR and WD Demodulation processes developed in this work use signatures templates and do not require the use of a training sequences.

8.2   Contributions of the Dissertation

Several key contributions of this work include:

1. Identification of WD signatures for the sets of modulation schemes considered in this work. Development and construction of two WD signatures categories, namely the unique features templates and the common features templates.

2. Development of techniques for choosing the best-suited wavelet(s) for use in both the WD AMR and the WD Demodulation processes.

3. Development of two WD AMR algorithms using WD signatures of digitally modulated communications signals.

4. Development of WD Demodulation algorithms using WD signatures of digitally modulated communications signals.

5. Introduction of a new concept to be used for constructing templates for the recognition of M-ary QAM signals.

6. Development of new techniques for recognizing different sizes of signal constellations for M-ary QAM signals. The techniques are used in both the WD AMR and the WD Demodulation processes.

7. Development and demonstration of the first WD Demodulation algorithm in the context of WTs.

8.3   Applications

With the observations and results obtained for both the WD AMR and the WD Demodulation algorithms, the ultimate goal of this dissertation work is to enable the development of a Wavelet Platform as illustrated in Fig. 1.4 of Section 1.1. Such a signal processing platform can be used to advance the state-of-the-art for communications receiver design so as to permit interoperability between a variety of communications standards. This type of receiver can be used in military signal analysis applications, such as threat analysis, spectrum management, electronic warfare, and electronics surveillance system.

Some of the potential application scenarios are presented below:

Application Scenario #1: Reconfigurable Radios in Hostile Environments

Communications systems that are ideally suited to hostile environments, such as those encountered in battlefield conditions, can be developed with the use of the Wavelet Platform. Such systems would feature rugged signal identification and demodulation capabilities, the ability to de-noise received passband signals after characterization of the noise process, and the ability to continuously compensate for channel fading characteristics using adaptive channel equalization in the WD.

Application Scenario #2: Underwater Acoustic Communications

A key feature of the Wavelet Platform is that a wide variety of signals, noise, or channel fading characteristics can be analyzed. Such analysis is very useful in communications systems that transport data via acoustic signals, as is the case in underwater acoustic communications. Time and spatially varying channel conditions can be identified, tracked, and exploited to recover data in digitally modulated signals employed in underwater communications systems.

8.4   Suggestions for Future Work

The research work in this dissertation involved the development of WD AMR and WD Demodulation algorithms. The methodologies used for both processes represent a relatively new area as compared to the work reported in the literature. Therefore, the research activities pursued in connection with this dissertation have opened many new directions that can be further explored.

Both the WD AMR and WD Demodulation processes require that a preliminary setup procedure be performed. The initial tasks involve the construction of WD signatures in the form of scalogram templates and selection of a suitable wavelet to be used for both the construction of the WD signatures and the transformation of the received communications signals via the CWT.

A natural extension of the work described in this dissertation is to improve upon the correct classification rates for the WD AMR process by using different wavelets. It has been observed that certain wavelets easily highlight the unique features of particular communications signals that employ variations in carrier amplitude, frequency, or phase. Based on the results obtained in Figs. 4.30 and 4.32, it seems reasonable that by using a different wavelet for each distinguishing feature contained in a particular type of modulation scheme, especially in the case of FSK signals, the rate of correct classification, and also the quality of the demodulation accuracy, may be improved. The use of different and/or multiple wavelets for extraction of key features of digital signals corresponding to particular modulation schemes can enable the development of a Hybrid WD AMR method.

The WD AMR and WD Demodulation processes can also be expanded to include other communications signals such as Gaussian Minimum Shift Keying (GMSK), and non-square M-ary QAM signal constellations.

Also, this research work has limited attention to communications signals that have been corrupted with zero-mean AWGN. System performance assessment could be exteneded

to other noise scenarios such as impulsive noise (of different bandwidth), band-limited noise, etc.

The communications signals were oversampled by a factor of sixteen over the Nyquist rate in relation to the carrier frequency in this work. Further investigation aimed at reducing the number of samples within a symbol is warranted. Additional reduction in computational effort may be possible. However, it is important to assess the affect on the overall modulation classification rate and also the BER performance of the demodulator.

Having demonstrated the efficacy of the developed WD AMR process and the WD Demodulation process, these processes can be implemented in hardware. The algorithms developed for WD AMR and WD Demodulation can both be realized using Field Programmable Gate Array (FPGA) technology for use in a radio receiver system. Therefore, a WD-based radio receiver can be demonstrated using an FPGA prototype.

Based on the definitions of the decision rules and the algorithms for the WD Demodulation process, a theory can be developed so as to predict the demodulation performance. The procedural steps in development of such a theory should be parallel to the steps taken in the development of the matched filter theory describing the matched filter performance.

8.5   Conclusions

In this work, it has been demonstrated that with the use of the pattern recognition methodology of template matching, along with appropriately defined WD templates, both the AMR and demodulation processes can be implemented in the WD. It has been

demonstrated that the WD AMR process can correctly classify modulation schemes with very high reliability even for low values of SNR. At SNR = -5 dB, the correct classification rates are 100% for both BPSK and 8-PSK signals, 94.7% for QPSK signals, and above 95% for BASK as well as 4-ASK signals. The rates of correct classification are 100% for both 16-QAM and 256-QAM signals, and 96.1% for 64-QAM signals. These results meet, or exceed, those reported in the literature for other AMR schemes.

Furthermore, it has also been demonstrated that the WD Demodulator provides improvement in BER performance over the traditional matched filter-based methods. In particular, a few orders of magnitude of improvement is seen for PSK signals, while approximately equal performances are obtained for M-ary QAM signals.

Given the reliability of both the WD AMR and WD Demodulation processes devised in this work, they can be used to advance the state-of-the-art of communications receiver design, more specifically, by enabling the development of a Wavelet Platform. The Wavelet Platform provides the agility to permit interoperability between different communications standards to subsequent automatic demodulation with a single demodulator.

References

1. Vaz, C. and Ho, K. M., "Development of Adaptive Radio Transceivers," Technical Report 06/09, Dept. Elect. Comput. Eng., Rutgers, The State University of New Jersey, Piscataway, NJ, June 2009.

2. Vaz, C. and Ho, K. M., "Illustrative Conceptualization of the Wavelet Platform," Technical Report 07/09, Dept. Elect. Comput. Eng., Rutgers, The State University of New Jersey, Piscataway, NJ, July 2009.

3. IEEE 802.11a-1999 Standard. (2007, October). [Online]. Available: http://standards.ieee.org/getieee802/802.11.html

4. ZigBee Specification Document 053474r13. (2007, October). [Online]. Available: http://www.zigbee.org/en/

5. IEEE 802.11b-1999 Standard. (2007, October). [Online]. Available: http://standards.ieee.org/getieee802/802.11.html

6. Bluetooth Specification Version 2.1 + EDR [vol 0]. (2007, October). [Online]. Available: http://www.bluetooth.com/Bluetooth/Learn/Technology/Specifications/

7. ETSI EN 300 744 V1.5.1 (2004-11). Digital Video Broadcasting (DVB); Framing Structure, Channel Coding and Modulation for Digital Terrestrial Television. (2007, October). [Online]. Available: http://www.etsi.org/WebSite/Standards/Standard.aspx

8. American National Standard ANSI/SCTE 07 2006. Digital Transmission Standard for Cable Television. (2007, October). [Online]. Available: http://www.scte.org/content/index.cfm?pID=102

9. Dobre, O. A., Abdi, A., Bar-Ness, Y. and Su, W., "A Survey of Automatic Modulation Classification Techniques: Classical Approaches and New Trends," *IET Comm.*, Vol. 1, Issue 2, pp. 137-157, Apr. 2007.

10. Abrahamzadeh, A., Seyedin, S. A. and Dehghan, M., "Digital-Signal-Type Identification Using an Efficient Identifier," *EURASIP Journal on Advances in Signal Processing*, Vol. 2007, 2007.

11. Ebrahimzadeh, A. and Seyedin, S. A., "Digital Signal Types Identification Using a Hierarchical SVM-Based Classifier and Efficient Features," *Proc. 2007 Int. Conf. Computing: Theory and Applications*, pp. 521-525, Mar. 2007.

12. Wu, Z. Wang, X., Gao, Z. and Ren, G., "Automatic Digital Modulation Recognition Based on Support Vector Machines," *Proc. 2005 Int. Conf. on Neural Networks and Brain*, Vol. 2, pp. 1025- 1028, Oct. 2005.

13. Han, G., Li, J. and Lu, D., "Study of Modulation Recognition Based on HOCs and SVM," *Proc. 59th Vehicular Tech. Conf.*, Vol. 2, pp. 898- 902, May 2004.

14. Richterova, M., "Signal Modulation Recognizer Based on Method of Artificial Neural Networks," *Proc. 2005 Progress in Electromagnetics Research Symp.*, pp. 575-578, Aug. 2005.

15. Yang, C.-Q., Zhong, Z.-F. and Yang, J.-A., "Recognition of Digital Modulation Using Radial Basis Function Neural Networks," *Proc. 2003 Int. Conf. Machine Learning and Cybernetics*, Vol. 5, pp. 3012- 3015, Nov. 2003.

16. Zhao, Y., et al., "Automatic Digital Modulation Recognition Using Artificial Neural Networks," *Proc. 2003 Int. Conf. on Neural Networks and Signal Processing*, Vol. 1, pp. 257-260, Dec. 2003.

17. Wong, M. L. D. and Nandi, A. K., "Automatic Digital Modulation Recognition Using Spectral Andstatistical Features With Multi-Layer Perceptrons," *Proc. Sixth International Symp. Signal Processing and its Applications*, Vol. 2, pp. 390-393, Aug. 2001.

18. Chen, J., et al., "Digital Modulation Identification Based on Software Radio Platform," *Proc. Sixth Int. Conf. Parallel and Distributed Computing, Applications and Technologies*, pp. 945- 949, Dec. 2005.

19. Dobre, O. A., Abdi, A., Bar-Ness, Y. and Su, W., "Blind Modulation Classification: A Concept Whose Time Has Come," *Proc. 2005 IEEE/Sarnoff Symp. on Advances in Wired and Wireless Comm.*, pp. 223-228, Apr. 2005.

20. Li, J., He, C. and Chen, J., "Automatic Digital Modulation Identification Basing on Decision Method and Cumulants," *Proc. 2005 IEEE Int. Workshop VLSI Design and Video Tech.*, pp. 264- 267, May 2005.

21. Pedzisz, M. and Mansour, A., "Automatic Modulation Recognition of MPSK Signals Using Constellation Rotation and its 4th Order Cumulant," *Digital Signal Processing*, Vol. 15, Issue 3, pp. 295-304, May 2005.

22. Wang, B. and Ge, L., "Blind Identification of OFDM Signal in Rayleigh Channels," *Proc. Fifth Int. Conf. on Information, Comm. and Signal Processing*, pp. 950- 954, Dec. 2005.

23. Wu, Y.-X., Ge, L.-D. and Liu, F.-F., "Comprehensive Features Based Digital Modulation Identification Using a Neural Tree Network," *Proc. 2005 Int. Conf. on Communications, Circuits and Systems*, Vol. 2, pp. 748-752, May 2005.

24. Cai, Q., Wei, P. and Xiao, X., "A Digital Modulation Recognition Method," *Proc. Int. Conf. Communications, Circuits and Systems*, Vol. 2, pp. 863- 866, Jun. 2004.

25. Hong, L. and Ho, K. C., "Classification of BPSK and QPSK Signals with Unknown

Signal Level Using the Bayes Technique," *Proc. 2003 International Symposium on Circuits and Systems*, Vol. 4, pp. 1- 4, May 2003.

26. Le Guen, D. and Mansour, A., "Automatic Recognition Algorithm for Digitally Modulated Signals," *Proc. IASTED Int. Conf. on Signal Processing, Pattern Recognition and Applications*, pp. 32-37, Jun. 2002.

27. Hong, L. and Ho, K. C., "Modulation Classification of BPSK and QPSK Signals Using a Two Element Antenna Array Receiver," *Proc. 2001 Mil. Comm. Conf.*, Vol. 1, pp. 118- 122, 2001.

28. Boudreau, D., et al., "A Fast Automatic Modulation Recognition Algorithm and Its Implementation in a Spectrum Monitoring Application," *Proc. 21st Century Mil. Comm. Conf.*, Vol. 2, pp. 732-736, Oct. 2000.

29. Taira, S., "Automatic Classification of QAM Signals in Fading Channel," *Proc. 51st Vehicular Tech. Conf.*, Vol. 3, pp. 1717-1721, May 2000.

30. Chan, Y., Gadbois, L. and Yansouni, P., "Identification of the Modulation Type of a Signal," *Proc. 1985 IEEE Int. Conf. on Acoustics, Speech, and Signal Processing*, Vol. 10, pp. 838- 841, Apr. 1985.

31. Nagy, P. A. J., "A Modulation Classifier for Multi-Channel Systems and Multi-Transmitter Situations," *Conf. IEEE Mil. Comm. Conf.,* Vol. 3, pp. 816 - 820, Oct. 1994.

32. Azzouz, E. E. and Nandi, A. K., "Automatic Identification of Digital Modulation Types," *Signal Processing*, Vol. 47, No. 1, pp. 55-69, 1995.

33. Soliman, S. S. and Hsue, S.-Z., "Signal Classification Using Statistical Moments," *IEEE Trans. Comm.*, Vol. 40, No. 5, pp. 908-916, May 1992.

34. Nandi, A. K. and Azzouz, E. E., "Algorithms for Automatic Modulation Recognition of Communication Signals," *IEEE Trans. Commum.*, Vol. 46, No. 4, pp. 431-436, April 1998.

35. Azzouz, E. E. and Nandi, A. K., "Procedure for Automatic Recognition of Analogue and Digital Modulations," *IEE Proc.-Communications*, Vol. 143, Issue 5, pp. 259-266, Oct. 1996.

36. Park, C.-S., Jang, W., Nah, S.-P. and Kim, D. Y., "Automatic Modulation Recognition using Support Vector Machine in Software Radio Applications," *Proc. 9th Int. Conf. Advanced Communication Tech.*, Vol. 1, pp. 9-12, Feb. 2007.

37. Feng, X. Z., Yang, J., Luo, F. L., Chen, J. Y. and Zhong, X. P., "Automatic Modulation Recognition by Support Vector Machines Using Wavelet Kernel," *J. Phys.: Conf. Ser.*, Vol. 48, pp. 1264-1267, 2006.

38. Hossen, A., Al-Wadahi, F. and Jervase, J. A., "Classification of Modulation Signals Using Statistical Signal Characterization and Artificial Neural Networks," *Engineering Applications of Artificial Intelligence*, Vol. 20, Issue 4, pp. 463-472, Jun. 2007.

39. Kamarthi. S. V., Zeid, I. and Subramaniam, L., "Multiresolution Approach to Identification of Recurring Signal Patterns," *Proc. SPIE, Wavelet Applications in Industrial Processing IV*, Vol. 6383, Oct. 2006.

40. Rashid, I., Maqbool, H., Mehmood-ur-Rehman and Nadir, F., "Digital Modulation Identification by Basic Modulation Parameters," *Proc. 9th Int. Multioptic Conference*, pp. 1-6, Dec. 2005.

41. Shahmohammadi, M. and Nikoofar, H. R., "Modulation Classification for QAM/PSK Using a Soft Clustering Algorithm," *Proc. 2002 IEEE Int. Symp. Info. Theory*, p. 19, 2002.

42. Lopatka, J. and Pedzisz, M., "Automatic Modulation Classification Using Statistical Moments and a Fuzzy Classifier," *Proc. 5th Int. Conf. on Signal Processing*, Vol. 3, pp. 1500-1506, Aug. 2000.

43. Al-Jalili, Y. O., "Identification Algorithm of Upper Sideband and Lower Sideband SSB Signals," *Signal Processing*, Vol. 42, No. 2, pp. 207-213, 1995.

44. Martin, A., "A Signal Analysis and Classification Strategy for Implementation in an EW Communications Receiver," *Proc. Fifth International Conference on Radio Receivers and Associated Systems*, pp. 222-226, Jul. 1990.

45. Liedtke, F. F., "Computer Simulation of an Automatic Classification Procedure for Digitally Modulated Communication Signals with Unknown Parameters," *Signal Processing*, Vol. 6, Issue 4, pp. 311-323, August 1984.

46. Jondral, F., "Automatic Classification of High Frequency Signals," *Signal Processing*, Vol. 9, Issue 3, pp. 177 - 190, Oct. 1985.

47. Park, C., Choi, J., Nah, S., Jang, W. and Kim, D.Y., "Automatic Modulation Recognition of Digital Signals using Wavelet Features and SVM," *10th Int. Conf. Advanced Comm. Tech.,* Vol. 1, pp. 387-390, February 2008.

48. Prakasam, P. and Madheswaran, M., "Automatic Modulation Identification of QPSK and GMSK Using Wavelet Transform for Adaptive Demodulator in SDR," *IEEE Int. Conf. Signal Process., Comm. and Networking,* pp. 507-511, Feb. 2007.

49. Feng, X. Z., Yang, J., Luo, F. L., Chen, J. Y. and Zhong, X. P., "Automatic Modulation Recognition by Support Vector Machines Using Wavelet Kernel," *J. Phy. Conf. Series,* Vol. 48, Issue 1, pp. 1264-126, 2006.

50. Wei, X. and Cao, Z., "Fast Identification of Amplitude Modulated Signals at Low

SNR," *IEEE Int. Symp. Microwave, Antenna, Propagation and EMC Tech. Wireless Comm.,* Vol. 2, pp. 1119-1112, Aug. 2005.

51. Chen, J., Kuo, Y., Li, J., Fu, F. and Ma, Y., "Digital Modulation Identification by Wavelet Analysis," *Proc. 6th Int. Conf. Computational Intelligence and Multimedia Application*, pp. 29-34, Aug. 2005.

52. Pavlik, R., "Binary PSK/CPFSK and MSK Bandpass Modulation Identifier Based on the Complex Shannon Wavelet Transform," *J. Elect. Eng.*, Vol. 56, No. 3-4, pp. 71-77, 2005.

53. Ou, X., Huang, X., Yuan, X. and Yang, W., "Qusai-Haar Wavelet and Modulation Identification of Digital Signals," IEEE *Int. Conf. Comm. Circuits and Systems*, Vol. 2, pp. 733-737, Jun. 2004.

54. Jin, J-D., Kwak, Y., Lee, K-W., Lee, K. H. and Ko, S-J., "Modulation Type Classification Method using Wavelet Transform for Adaptive Modulator," *IEEE Proc. Int. Symp. Intelligent Signal Processing and Communication Systems*, pp. 282-292, Nov. 2004.

55. Hippenstel, R., El-Kishky, H., Frick, C. and Datasprasad, S., "Modulation Identification using Neural Network and Wavelet Domain Based Approaches," *IEEE 38th Asilomar Conf. Signals, Systems and Computers*, Vol. 2, pp. 2116-2120, Nov. 2004.

56. Zeng, X., Tan, X. and Liu, J., "PN Code Acquisition Detection for CDMA Networks Based on Wavelet Transform and Artificial Neural Network," *IEEE Proc. Int. Conf. Wavelet Anal. and Its Applicat.,* Vol. 2, pp. 1524-1527, Apr. 2003.

57. Wilson, S. S., "Using a Pseudo-random Binary Sequence as a Mother Wavelet in the Wavelet-correlation System Identification Method," *IEEE Proc. SoutheastCon*, pp. 58-61, Apr. 2002.

58. Ho, K. C., Prokopiw, W. and Chan, Y.T., "Modulation Identification of Digital Signals by the Wavelet Transform," *Proc. IEE – Radar, Sonar, and Navigation*, Vol. 147, pp. 169-176, Aug. 2000.

59. Liu, H., and Ho, K. C., "Identification of CDMA Signal and GSM Signal Using the Wavelet Transform", *IEEE 42nd Midwest Symp. on Circuits and Systems*, Vol. 2, pp. 678-681, Aug. 1999.

60. Hong, L. and Ho, K. C., "Identification of Digital Modulation Types using the Wavelet Transform," *Mil. Comm. Conf. Proc.*, Vol. 1, pp. 427-431, Nov. 1999.

61. Ho, K. C., Liu, H., and Hong, L., "On Improving the Accuracy of a Wavelet Based Identifier to Classify CDMA Signal and GSM Signal", *Proc. IEEE International Symp. on Circuits and Systems VLSI*, Vol. 4, pp. 564-567, 1999.

62. Ho, K. C., Prokopiw, W. and Chan, Y. T., "Modulation Identification by the Wavelet Transform," *Mil. Comm. Conf. Proc.*, Vol. 2, pp. 886-890, Nov. 1995.

63. Zhang, D. and Wang, X., "MPSK Modulation Recognition Based on Wavelet Transformation," *Int. Conf. on Networking and Dig. Society*, Vol. 1, pp. 202-205, May 2009.

64. Chen, G., Ren, Z. and Li, Y., "Study of Signal Feature Recognition Method Based on Morlet Combined Wavelets," *Int. Conf. Measuring Tech. Mech. Automation,* pp. 313-317, April, 2009.

65. Mallat, S., *A Wavelet Tour of Signal Processing*, Second Edition, Academic Press, San Diego, CA, 1999.

66. Turin, G. L., "An Introduction to Matched Filters", *IRE Trans. Info. Theory*, Vol. 6, pp. 311-329, Jun. 1960.

67. Turin, G. L., "An Introduction to Matched Filters", *Proc. of IEEE*, Vol. 64, pp. 1092-1112, Jul. 1976.

68. Bruce, A. G., Gao, H., Mulligan, J. J. and Satrius, E. H., "Application of Wavelet De-Noising to Signal Demodulation," *IEEE 29th Asilomar Conf. Signals, Systems and Computer*, Vol. 2, pp. 1142-1146, Nov. 1995.

69. Ho, K. M., Vaz, C. and Daut, D. G., "Improved Demodulation of Phase Shift Keyed Signals Using Wavelet Thresholding," *2008 IEEE Sarnoff Symposium,* Princeton, NJ, USA, pp. 1-6, April 2008.

70. Daubechies, I., *Ten Lectures on Wavelets*, Eighth Printing, Society for Industrial and Applied Mathematics, Philadelphia, PA, 2004.

71. Beylkin, G., Coifman, R. and Rokhlin, V., "Fast Wavelet Transforms and Numerical Algorithms," *Comm. Pure Applied Math.*, Vol. 44, Issue 2, pp. 141-183, 1991.

72. Grossmann, A. and Morlet, J., "Decomposition of Hardy Functions into Square Integrable Wavelets of Constant Shape," *SIAM J. Math. Analysis*, Vol. 15, Issue 4, pp. 723-736, July 1984.

73. Mallat, S., "Multiresolution Approximation and Wavelet Orthogonal Bases of L2," *Trans. AMS*, Vol. 315, No. 1, pp. 69-87, September 1989.

74. Bracewell, R. N., *The Fourier Transform and Its Applications*, McGraw-Hill, New York, NY, 1986.

75. Daubechies, I., "The Wavelet Transform, Time-Frequency Localization and Signal Analysis," *IEEE Trans. Inf. Theory*, Vol. 36, No. 5, pp. 961-1005, September 1990.

76. Sarkar, T. K., el. al, "A Tutorial on Wavelets from an Electrical Engineering Perspective, Part 1: Discrete Wavelet Techniques," *IEEE Trans. Antennas Propag. Mag.*, Vol. 40, No. 5, pp. 49-68, October 1998.

77. Poularikas, A. D., Ed., *The Transforms and Applications Handbook*, CRC Press, Boca Raton, FL, 1996.

78. Benedetto, J. J. and Frazier, M. W., *Wavelets: Mathematics and Applications*, CRC Press, Inc., Boca Raton, FL, 1994.

79. Rao, R. M. and Bopadrikar, A. S., *Wavelet Transforms*, Addison-Wesley, Reading, MA, 1998.

80. Wickerhauser, M. V., *Adapted Wavelet Analysis from Theory to Software*, A. K. Peters, Ltd., Wellesley, MA, 1994.

81. Jansen, M., *Noise Reduction by Wavelet Thresholding*, Springer-Verlag, New York, NY, 2001.

82. Oppenheim, A. V., Schafer, R. W. and Buck, J. R., *Discrete-Time Signal Processing*, Second Edition, Prentice Hall, Upper Saddle River, NJ, 1999.

83. Mallat, S., *A Wavelet Tour of Signal Processing*, Second Edition, Academic Press, San Diego, CA, 1999.

84. Proakis, J. G., *Digital Communications*, Fourth Edition, McGraw-Hill, NY, NY, 2001.

85. Ho, K. M., Vaz, C. and Daut, D. G., "A Wavelet-Based Method for Classification of Binary Digitally Modulated Signals," *2009 IEEE Sarnoff Symposium*, pp. 1-5, March 2009.

86. Azzouz, E. E. and Nandi, A. K., *Automatic Modulation Recognition of Communication Signals*, First Edition, Kluwer Academic Publishers, Dordrecht, The Netherlands,1996.

Appendix A:

Algorithm for Demodulating a 64-QAM Signal

In order to develop the algorithm for the WD Demodulation of 64-QAM signals, common features Templates 1, 2 and the additional templates defined in Eq. (7.14) are required. As illustrated in Fig. A1, each dot represents a data symbol within a 64-QAM signal in Quadrant I. First, the signal quadrant location is determined based on the algebraic sign of the cross-correlation value obtained by using Template 1 and Template 2, as described in Table 6.3. Then, the auto-correlation values of the new features templates are used as the threshold values for determining the signal constellation location. The threshold values used are

$$\text{Threshold values} = \begin{cases} T_1 = A_1 \\ T_2 = A_2 \\ T_3 = A_3 \end{cases}$$

where A_1, A_2 and A_3 are constants that correspond to the distinct levels within the cross-correlation dataset with Template 1.
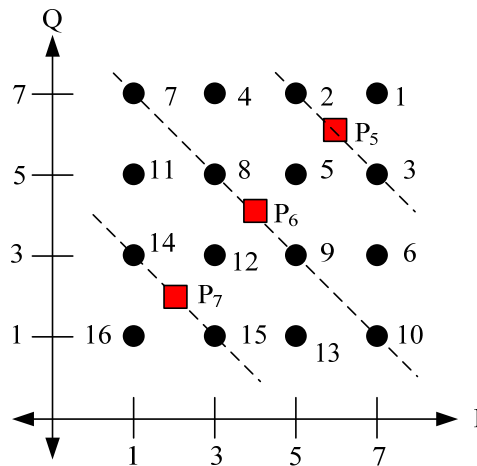

Fig. A1. Quadrant I of the 64-QAM signal constellation.

The decision rule is described as

$$
\text{output} = \begin{cases}
\text{"1"} & X_{P5} > X_{5\_x} \\
\text{"2"} & X_{P5} \sim= X_{5\_x} \text{ and } X_{W1} < X_{W2} \\
\text{"3"} & X_{P5} \sim= X_{5\_x} \text{ and } X_{W1} > X_{W2} \\
\text{"4"} & X_{P5} < X_{5\_x}, X_{P6} > X_{6\_x} \text{ and } X_{W1} < X_{W2} \\
\text{"5"} & X_{P5} < X_{5\_x}, X_{P6} > X_{6\_x} \text{ and } X_{W1} \sim= X_{W2} \\
\text{"6"} & X_{P5} < X_{5\_x}, X_{P6} > X_{6\_x} \text{ and } X_{W1} > X_{W2} \\
\text{"7"} & X_{P5} < X_{5\_x}, X_{P6} > X_{6\_x} \text{ and } X_{W1} < X_{T1} \\
\text{"8"} & X_{P5} < X_{5\_x}, X_{P6} > X_{6\_x} \text{ and } X_{T1} \leq X_{W1} < X_{T2} \\
\text{"9"} & X_{P5} < X_{5\_x}, X_{P6} > X_{6\_x} \text{ and } X_{T2} \leq X_{W1} < X_{T3} \\
\text{"10"} & X_{P5} < X_{5\_x}, X_{P6} > X_{6\_x} \text{ and } X_{W1} \geq X_{T3} \\
\text{"11"} & X_{P5} < X_{5\_x}, X_{P6} > X_{6\_x}, X_{P7} > X_{7\_x} \text{ and } X_{W1} < X_{W2} \\
\text{"12"} & X_{P5} < X_{5\_x}, X_{P6} > X_{6\_x}, X_{P7} > X_{7\_x} \text{ and } X_{W1} \sim= X_{W2} \\
\text{"13"} & X_{P5} < X_{5\_x}, X_{P6} > X_{6\_x}, X_{P7} > X_{7\_x} \text{ and } X_{W1} > X_{W2} \\
\text{"14"} & X_{P5} < X_{5\_x}, X_{P6} > X_{6\_x}, X_{P7} \sim= X_{7\_x} \text{ and } X_{W1} < X_{W2} \\
\text{"15"} & X_{P5} > X_{5\_x}, X_{P6} > X_{6\_x}, X_{P7} \sim= X_{6\_x} \text{ and } X_{W1} > X_{W2} \\
\text{"16"} & X_{P5} > X_{5\_x}, X_{P6} > X_{6\_x} \text{ and } X_{P7} > X_{7\_x}
\end{cases}
\tag{A.1}
$$

where $X_{P\#}$ represents the cross-correlation value obtained when comparing the specific features templates with the received signal, $X_{\#\_x}$ denotes the auto-correlation value of the specific location templates, X_{W1} and X_{W2} denote as the cross-correlation results obtained using common features Template 1 and Template 2. Based on the observations of the cross-correlation dataset for both Template 1 and Template 2, there are four distinct levels found to be characteristic of the dataset. Therefore, X_{T1}, X_{T2} and X_{T3} are identified as the threshold values corresponding to the different levels of the cross-correlation values obtained with Template 1.

Based on Eqn. (A.1) and Table 6.3, the algorithm for the WD Demodulation of 16-QAM signals is described as follows.

Step 1: Cross-correlate the received 64-QAM signal with Templates 1 and 2 in the WD.

Step 2: Determine the quadrant location of each signal symbol and cross-correlate the quadrant specific Templates P_5, P_6 and P_7 with the received signal.

Step 3: Compute the auto-correlation of each of the templates P_5, P_6 and P_7.

Step 4: Compare the cross-correlation results from Step 1 with the different combination of thresholds as described in (A.1), and assign the appropriate indicator for each signal segment.

Step 5: Recover the baseband data sequence based on the results obtained in Step 4.

Appendix B:

Algorithm for Demodulating a 256-QAM Signal

A similar algorithm to that presented in Appendix A is developed for the demodulation of a 256-QAM signal. However, a different decision rule and threshold values are applied. The threshold values are as follows:

$$\text{Threshold values} = \begin{cases} T_1 = B_1 \\ T_2 = B_2 \\ T_3 = B_3 \\ T_4 = B_4 \\ T_5 = B_5 \\ T_6 = B_6 \\ T_7 = B_7 \end{cases}$$

where B_1, B_2, B_3, B_4, B_5, B_6 and B_7 are constants that correspond to the distinct levels of cross-correlation values obtained with the common features Template 1.

The decision rule is divided into four distinct sets. Set 1 corresponds to symbol "1" through to symbol "16"; Set 2 corresponds to symbol "17" through to symbol "32"; Set 3 corresponds to symbol "33" through to symbol "48"; and, Set 4 corresponds to symbol "47" through to symbol "64".

Decision rule for Set 1 is given by

$$
\text{output} = \begin{cases}
\text{"1"} & X_{P1} > X_{1\_x} \\
\text{"2"} & X_{P1} \sim= X_{1\_x} \text{ and } X_{W1} < X_{W2} \\
\text{"3"} & X_{P1} \sim= X_{1\_x} \text{ and } X_{W1} > X_{W2} \\
\text{"4"} & X_{P1} < X_{1\_x}, X_{P2} > X_{2\_x}, \text{ and } X_{W1} < X_{W2} \\
\text{"5"} & X_{P1} < X_{1\_x}, X_{P2} > X_{2\_x}, \text{ and } X_{W1} \sim= X_{W2} \\
\text{"6"} & X_{P1} < X_{1\_x}, X_{P2} > X_{2\_x}, \text{ and } X_{W1} > X_{W2} \\
\text{"7"} & X_{P1} < X_{1\_x}, X_{P2} \sim= X_{2\_x}, \text{ and } X_{W1} < X_{T5} \\
\text{"8"} & X_{P1} < X_{1\_x}, X_{P2} \sim= X_{2\_x}, \text{ and } X_{T5} \leq X_{W1} < X_{T6} \\
\text{"9"} & X_{P1} < X_{1\_x}, X_{P2} \sim= X_{2\_x}, \text{ and } X_{T6} \leq X_{W1} < X_{T7} \\
\text{"10"} & X_{P1} < X_{1\_x}, X_{P2} \sim= X_{2\_x}, \text{ and } X_{W1} \geq X_{T7} \\
\text{"11"} & X_{P1} < X_{1\_x}, X_{P2} < X_{2\_x}, X_{P3} > X_{3\_x} \text{ and } X_{W1} < X_{T4} \\
\text{"12"} & X_{P1} < X_{1\_x}, X_{P2} < X_{2\_x}, X_{P3} > X_{3\_x} \text{ and } X_{T4} \leq X_{W1} < X_{T5} \\
\text{"13"} & X_{P1} < X_{1\_x}, X_{P2} < X_{2\_x}, X_{P3} > X_{3\_x} \text{ and } X_{W1} \sim= X_{W2} \\
\text{"14"} & X_{P1} < X_{1\_x}, X_{P2} < X_{2\_x}, X_{P3} > X_{3\_x} \text{ and } X_{T6} \leq X_{W1} < X_{T7} \\
\text{"15"} & X_{P1} < X_{1\_x}, X_{P2} < X_{2\_x}, X_{P3} > X_{3\_x} \text{ and } X_{W1} \geq X_{T7} \\
\text{"16"} & X_{P1} < X_{1\_x}, X_{P2} < X_{2\_x}, X_{P3} \sim= X_{3\_x} \text{ and } X_{W1} < X_{T3}
\end{cases}
$$

Decision rule for Set 2 is given by

$$
\text{output} = \begin{cases}
\text{"17"} & X_{P1} < X_{1\_x},\ X_{P2} < X_{2\_x},\ X_{P3} \sim= X_{3\_x} \text{ and } X_{T3} \le X_{W1} < X_{T4} \\
\text{"18"} & X_{P1} < X_{1\_x},\ X_{P2} < X_{2\_x},\ X_{P3} \sim= X_{3\_x} \text{ and } X_{T4} \le X_{W1} < X_{T5} \\
\text{"19"} & X_{P1} < X_{1\_x},\ X_{P2} < X_{2\_x},\ X_{P3} \sim= X_{3\_x} \text{ and } X_{T5} \le X_{W1} < X_{T6} \\
\text{"20"} & X_{P1} < X_{1\_x},\ X_{P2} < X_{2\_x},\ X_{P3} \sim= X_{3\_x} \text{ and } X_{T6} \le X_{W1} < X_{T7} \\
\text{"21"} & X_{P1} < X_{1\_x},\ X_{P2} < X_{2\_x},\ X_{P3} \sim= X_{3\_x} \text{ and } X_{W1} \ge X_{T7} \\
\text{"22"} & X_{P1} < X_{1\_x},\ X_{P2} < X_{2\_x},\ X_{P3} < X_{3\_x}, X_{P4} > X_{4\_x} \text{ and } X_{W1} < X_{T2} \\
\text{"23"} & X_{P1} < X_{1\_x},\ X_{P2} < X_{2\_x},\ X_{P3} < X_{3\_x}, X_{P4} > X_{4\_x} \text{ and } X_{T2} \le X_{W1} < X_{T3} \\
\text{"24"} & X_{P1} < X_{1\_x},\ X_{P2} < X_{2\_x},\ X_{P3} < X_{3\_x}, X_{P4} > X_{4\_x} \text{ and } X_{T3} \le X_{W1} < X_{T4} \\
\text{"25"} & X_{P1} < X_{1\_x},\ X_{P2} < X_{2\_x},\ X_{P3} < X_{3\_x}, X_{P4} > X_{4\_x} \text{ and } X_{W1} \sim= X_{W2} \\
\text{"26"} & X_{P1} < X_{1\_x},\ X_{P2} < X_{2\_x},\ X_{P3} < X_{3\_x}, X_{P4} > X_{4\_x} \text{ and } X_{T5} \le X_{W1} < X_{T6} \\
\text{"27"} & X_{P1} < X_{1\_x},\ X_{P2} < X_{2\_x},\ X_{P3} < X_{3\_x}, X_{P4} > X_{4\_x} \text{ and } X_{T6} \le X_{W1} < X_{T7} \\
\text{"28"} & X_{P1} < X_{1\_x},\ X_{P2} < X_{2\_x},\ X_{P3} < X_{3\_x}, X_{P4} > X_{4\_x} \text{ and } X_{W1} \ge X_{T7} \\
\text{"29"} & X_{P1} < X_{1\_x},\ X_{P2} < X_{2\_x},\ X_{P3} < X_{3\_x}, X_{P4} \sim= X_{4\_x} \text{ and } X_{W1} < X_{T1} \\
\text{"30"} & X_{P1} < X_{1\_x},\ X_{P2} < X_{2\_x},\ X_{P3} < X_{3\_x}, X_{P4} \sim= X_{4\_x} \text{ and } X_{T1} \le X_{W1} < X_{T2} \\
\text{"31"} & X_{P1} < X_{1\_x},\ X_{P2} < X_{2\_x},\ X_{P3} < X_{3\_x}, X_{P4} \sim= X_{4\_x} \text{ and } X_{T2} \le X_{W1} < X_{T3} \\
\text{"32"} & X_{P1} < X_{1\_x},\ X_{P2} < X_{2\_x},\ X_{P3} < X_{3\_x}, X_{P4} \sim= X_{4\_x} \text{ and } X_{T3} \le X_{W1} < X_{T4}
\end{cases}
$$

Both of the decision rules for Set 3 and Set 4 must meet the conditions in (B.1) before proceeding to other combination of thresholds in order to recover the data symbol.

$$
\text{conditions} = \begin{cases}
X_{P1} < X_{1\_x} \\
X_{P2} < X_{2\_x} \\
X_{P3} < X_{3\_x}
\end{cases}
\tag{B.1}
$$

Decision rule for Set 3 is given by

$$\text{output} = \begin{cases} \text{"33"} \ X_{P4} \sim= X_{4\_x} \ \text{and} \ X_{T4} \leq X_{W1} < X_{T5} \\ \text{"34"} \ X_{P4} \sim= X_{4\_x} \ \text{and} \ X_{T5} \leq X_{W1} < X_{T6} \\ \text{"35"} \ X_{P4} \sim= X_{4\_x} \ \text{and} \ X_{T6} \leq X_{W1} < X_{T7} \\ \text{"36"} X_{P4} \sim= X_{4\_x}, \ \text{and} \ X_{W1} \geq X_{T7} \\ \text{"37"} X_{P4} < X_{4\_x}, X_{P5} > X_{5\_x} \ \text{and} \ X_{W1} < X_{T1} \\ \text{"38"} X_{P4} < X_{4\_x}, X_{P5} > X_{5\_x} \ \text{and} \ X_{T1} \leq X_{W1} < X_{T2} \\ \text{"39"} \ X_{P4} < X_{4\_x}, X_{P5} > X_{5\_x} \ \text{and} \ X_{T2} \leq X_{W1} < X_{T3} \\ \text{"40"} X_{P4} < X_{4\_x}, X_{P5} > X_{5\_x} \ \text{and} \ X_{W1} \sim= X_{W2} \\ \text{"41"} X_{P4} < X_{4\_x}, X_{P5} > X_{5\_x} \ \text{and} \ X_{T4} \leq X_{W1} < X_{T5} \\ \text{"42"} X_{P4} < X_{4\_x}, X_{P5} > X_{5\_x} \ \text{and} \ X_{T5} \leq X_{W1} < X_{T6} \\ \text{"43"} X_{P4} < X_{4\_x}, X_{P5} > X_{5\_x} \ \text{and} \ X_{W1} \geq X_{T6} \\ \text{"44"} X_{P4} < X_{4\_x}, X_{P5} \sim= X_{5\_x}, \ \text{and} \ X_{W1} < X_{T1} \\ \text{"45"} X_{P4} < X_{4\_x}, X_{P5} \sim= X_{5\_x}, \ \text{and} \ X_{T1} \leq X_{W1} < X_{T2} \\ \text{"46"} \ X_{P4} < X_{4\_x}, X_{P5} \sim= X_{5\_x}, \ \text{and} \ X_{T2} \leq X_{W1} < X_{T3} \\ \text{"47"} \ X_{P4} < X_{4\_x}, X_{P5} \sim= X_{5\_x}, \ \text{and} \ X_{T3} \leq X_{W1} < X_{T4} \\ \text{"48"} \ X_{P4} < X_{4\_x}, X_{P5} \sim= X_{5\_x}, \ \text{and} \ X_{T4} \leq X_{W1} < X_{T5} \end{cases}$$

Decision rule for Set 4 is given by

$$
\text{output} = \begin{cases}
\text{"49"} \ X_{P4} < X_{4\_x}, X_{P5} \sim= X_{5\_x}, \text{ and } X_{W1} \ge X_{T5} \\
\text{"50"} \ X_{P4} < X_{4\_x}, X_{P5} < X_{5\_x}, \ X_{P6} > X_{6\_x}, \text{ and } X_{W1} < X_{T1} \\
\text{"51"} \ X_{P4} < X_{4\_x}, X_{P5} < X_{5\_x}, \ X_{P6} > X_{6\_x}, \text{ and } X_{T1} \le X_{W1} < X_{T2} \\
\text{"52"} \ X_{P4} < X_{4\_x}, X_{P5} < X_{5\_x}, \ X_{P6} > X_{6\_x}, \text{ and } X_{W1} \sim= X_{W2} \\
\text{"53"} \ X_{P4} < X_{4\_x}, X_{P5} < X_{5\_x}, \ X_{P6} > X_{6\_x}, \text{ and } X_{T3} \le X_{W1} < X_{T4} \\
\text{"54"} \ X_{P4} < X_{4\_x}, X_{P5} < X_{5\_x}, \ X_{P6} > X_{6\_x}, \text{ and } X_{W1} \ge X_{T4} \\
\text{"55"} \ X_{P4} < X_{4\_x}, X_{P5} < X_{5\_x}, \ X_{P6} \sim= X_{6\_x}, X_{P7} > X_{7\_x}, \text{ and } X_{W1} < X_{T1} \\
\text{"56"} \ X_{P4} < X_{4\_x}, X_{P5} < X_{5\_x}, \ X_{P6} \sim= X_{6\_x}, X_{P7} > X_{7\_x}, \text{ and } X_{T1} \le X_{W1} < X_{T2} \\
\text{"57"} \ X_{P4} < X_{4\_x}, X_{P5} < X_{5\_x}, \ X_{P6} \sim= X_{6\_x}, X_{P7} > X_{7\_x}, \text{ and } X_{T2} \le X_{W1} < X_{T3} \\
\text{"58"} \ X_{P4} < X_{4\_x}, X_{P5} < X_{5\_x}, \ X_{P6} \sim= X_{6\_x}, X_{P7} > X_{7\_x}, \text{ and } X_{W1} \ge X_{T3} \\
\text{"59"} \ X_{P4} < X_{4\_x}, X_{P5} < X_{5\_x}, \ X_{P6} < X_{6\_x}, X_{P7} > X_{7\_x}, \text{ and } X_{W1} < X_{W2} \\
\text{"60"} \ X_{P4} < X_{4\_x}, X_{P5} < X_{5\_x}, \ X_{P6} < X_{6\_x}, X_{P7} > X_{7\_x}, \text{ and } X_{W1} \sim= X_{W2} \\
\text{"61"} \ X_{P4} < X_{4\_x}, X_{P5} < X_{5\_x}, \ X_{P6} < X_{6\_x}, X_{P7} > X_{7\_x}, \text{ and } X_{W1} > X_{W2} \\
\text{"62"} \ X_{P5} < X_{5\_x}, \ X_{P6} < X_{6\_x}, X_{P7} \sim= X_{7\_x}, \text{ and } X_{W1} < X_{W2} \\
\text{"63"} \ X_{P4} < X_{4\_x}, X_{P5} < X_{5\_x}, \ X_{P6} < X_{6\_x}, X_{P7} \sim= X_{7\_x}, \text{ and } X_{W1} > X_{W2} \\
\text{"64"} \ X_{P4} < X_{4\_x}, X_{P5} < X_{5\_x}, \ X_{P6} < X_{6\_x}, X_{P7} < X_{7\_x}
\end{cases}
$$

where $X_{P\#}$ denotes the cross-correlation values obtained with specific features templates, $X_{\#\_x}$ corresponds to the auto-correlation values for specific location templates, X_{W1} and X_{W2} represent the cross-correlation obtained with common features Template 1 and Template 2, and $X_{T\#}$ corresponds to the distinct levels within the dataset of cross-correlation values obtained with Template 1.

The algorithm for demodulating a 256-QAM signal is described as follows.

Step 1: Cross-correlate the received 256-QAM signal with Templates 1 and 2 in the WD.

Step 2:   Determine the quadrant location of each signal symbol and cross-correlate the templates P_1, P_2, P_3, P_4, P_5, P_6 and P_7 with the received signal.

Step 3:   Compute the auto-correlation of each of the templates P_1, P_2, P_3, P_4, P_5, P_6 and P_7.

Step 4:   Compare the cross-correlation results from Step 1 with the thresholds as described in the four sets of decision rules, and assign the appropriate indicator for each signal segment.

Step 5:   Recover the baseband data sequence based on the results obtained in Step 4.

Appendix C:

Constants Used for the Common Features Templates for M-ary QAM Signals

Table C1 Constants used for the Common Features Templates for M-ary QAM signals

Variable	Value	Variable	Value
A_1	14	A_2	14
B_1	12	B_2	12
C_1	10	C_2	10
D_1	8	D_2	8
E_1	6	E_2	6
F_1	4	F_2	4
G_1	2	G_2	2

Curriculum Vitae

Ka Mun Ho

Education

May 2000   **Bachelor of Science**, Electrical and Computer Engineering
Rutgers, the State University of New Jersey

May 2003   **Master of Science**, Electrical and Computer Engineering
Rutgers, the State University of New Jersey

January 2010   **Doctor of Philosophy**, Electrical and Computer Engineering
Rutgers, the State University of New Jersey

Employment

2004-2008   **Summer Instructor**
Department of Electrical and Computer Engineering
Rutgers, the State University of New Jersey

2007-2008   **Part-Time Lecturer**
Department of Mathematics
Rutgers, the State University of New Jersey

2003-2007   **Teaching Assistant**
Department of Electrical and Computer Engineering
Rutgers, the State University of New Jersey

Publications

1. Ho, K. M., Vaz, C. and Daut, D. G., "Automatic Classification of Amplitude, Frequency and Phase Shift Keyed Signals in the Wavelet-Domain," *2010 IEEE Sarnoff Symposium,* Princeton, NJ, USA, April 2010. (submitted for publication)

2. Ho, K. M., Vaz, C. and Daut, D. G., "A Wavelet-Based Method for Classification of Binary Digitally Modulated Signals," *2009 IEEE Sarnoff Symposium,* Princeton, NJ, USA, March 2009.

3. Ho, K. M., Vaz, C. and Daut, D. G., "Improved Demodulation of Phase Shift Keyed Signals Using Wavelet Thresholding," *2008 IEEE Sarnoff Symposium,* Princeton, NJ, USA, April 2008.

4. Ho, K. M., Vaz, K. and Caggiano, M., " Scattering Parameter Characterization of Differential Four-Port Networks Using a Two-Port Network Analyzers," *Proc. 55th IEEE Electronic Components and Technology Conference*, Florida, USA, May 2005.

5. Vaz, K., Ho, K. M. and Caggiano, M., "Error Reducing Techniques for the Scattering Parameter Characterization of Differential Networks Using a Two-Port Network Analyzer," *Proc. IEEE International Spring Seminar on Electronics Technology*, Austria, May 2005.

6. Gazula I., Ho, K. M. and Caggiano, M., "Capacitance Extraction of Electronic Package Interconnects of Non-Parallel Configurations," *Proc. 11th International Symposium for Design and Technology of Electronic Packages*, Romania, September 2004.

7. Caggiano, M. and Ho, K. M., "Electronics Packaging - A Course for the Rutgers University School of Electrical and Computer Engineering," *Proc. 54th IEEE Electronic Components and Technology Conference*, Las Vegas, NV, USA, May 2004.

8. Zhang, W., Ho, K. M., Yeh, Y., Vaz, K. and Caggiano, M., "Circuit Modeling: Inductances and Resistances at Radio Frequencies," *Proc. 10th International Symposium for Design and Technology of Electronic Packages*, Romania, September 2003.

9. Caggiano, M. and Ho, K. M., "Electronics Packaging - A Course for the Rutgers University School of Electrical and Computer Engineering," *Proc. 5th International Academic Conference on Electronic Packaging Education and Training*, Dresden, Germany, March 2002.

10. Caggiano, M. and Ho, K. M., "Electronics Packaging - A CD-ROM Course for the Rutgers University School of Electrical and Computer Engineering," *Proc. 25th International Spring Seminar on Electronics Technology*, Prague, Czech Republic, May 2002.

11. Ho, K. M., Rebelo, A. and Caggiano, M., "Electrical Modeling and Measuring Inductance in the Micro Lead Chip Carrier," *Proc. 52nd IEEE Electronic Components and Technology Conference*, California, USA, May 2002, pp.1722-1728.

12. Caggiano, M. and Ho, K. M., "A Web-based Course for the IEEE Community," *Proc. 52nd IEEE Electronics Components and Technology Conference*, California, USA, May 2002.

13. Caggiano, M. and Ho, K. M., "Electronics Packaging – A Course for the Rutgers University School of Electrical and Computer Engineering," *Proc. International Conference on Engineering Education*, Manchester, UK, August 2002.